A STABILITY MONITORING AND ADVISORY SYSTEM FOR SMALL SHIPS

By

Ercan Köse

BSc. , Karadeniz Technical University, Trabzon, Turkey 1983;

MSc. Karadeniz Technical University, Trabzon, Turkey 1985;

M.Phil. University of Newcastle Upon Tyne, U.K. 1991

A THESIS SUBMITTED IN PARTIAL FULFILLMENT OF

THE REQUIREMENTS FOR THE DEGREE OF

DOCTOR OF PHILOSOPHY

in

THE FACULTY OF GRADUATE STUDIES

DEPARTMENT OF MECHANICAL ENGINEERING

We accept this thesis as conforming

to the required standard

THE UNIVERSITY OF BRITISH COLUMBIA

May 1994

In presenting this thesis in partial fulfilment of the requirements for an advanced degree at the University of British Columbia, I agree that the Library shall make it freely available for reference and study. I further agree that permission for extensive copying of this thesis for scholarly purposes may be granted by the head of my department or by his or her representatives. It is understood that copying or publication of this thesis for financial gain shall not be allowed without my written permission.

(Signature)

Department of Mechanical Engineering

The University of British Columbia
Vancouver, Canada

Date 25 - April - 1994

DE-6 (2/88)

Abstract

Considering the loss of lives and money as a result of marine accidents, the importance of reducing or preventing capsizing of small boats is clearly evident.

The research described in this thesis addresses the development of a monitoring and advisory system for the safety of fishing vessels. This system uses environmental information obtained from a number of sensors and proposes corrective action based on a rule-base derived from experiments, theoretical research and human expertise.

Improvements in computer technology and the low prices of measurement equipment facilitates the integration of a system based on off-the-shelf devices and subsystems such as a ship's radar system to measure wave properties.The thesis demonstrates that such off-the-shelf devices and subsystems can be used with special purpose software developed to produce a low cost, intelligent safety monitoring and advisory system.

This monitoring system is designed based on the following requirements :

- The system should measure the minimum amount of data. In order to make system practical and least costly, the equipments already existing onboard should be used.
- The system should not interfere with the operation of the ship, since anything interfering with operation is expected to be discarded by the captain or crew.

In view of the need for the evaluation of wave parameters at a fast rate, in the order of 30 - 60 seconds, for input into the advisory system, two new techniques (*Boxing* and *thinning techniques*) have been developed. Reasonable agreement has been found between these two techniques and conventional techniques, such as Fourier transforms.

A fuzzy expert system has been developed as a decision making process for the monitoring and advisory system. Rules forming the basis for the advisory system are presented. An advantage of this modular structure is that new rules may be easily appended to the existing rule-base in view of further knowledge gained through interviewing experts, experiments or theoretical developments.

Finally, feasibility of this approach has been demonstrated through numerical simulations of various sea conditions on a range of ship forms.

Table of Contents

List of Tables

List of Figures

Acknowledgement

The author wishes first of all to express his sincere thanks to his supervisors, Dr. S. M. Çalışal and Dr. A. B. Dunwoody for the steadfast guidance and encouragement throughout this research, his supervisory committee, Dr. P. LeBlond, Dr. F. Sassani and Dr. R. G. Gosine for many valuable suggestions and comments. Special thanks to Dr. Mehmet Atlar, whose suggestions and guidance aided immeasurably in the development of my thesis.

I would like to thank Karadeniz Technical University, Turkey for sponsoring this research.

I would also like to express my sincere gratitude to the Dynamotive Corporation, especially Mr. Reinhold C. Roth (president & CEO), for their interest, encouragement and financial support for this project.

I am also grateful to my colleagues, Ayhan Akıntürk, Alejandro Allievi, Erhan Budak, Yetvart Hosepyan, and Haw L. Wong for their thorough technical discussions or other social events.

Naturally, the bulk of my gratitude goes to my family for their constant support and encouragement.

Nomenclature

A	: Projected lateral area
A_{cr}	: Critical wave amplitude
A_{44}	: Added mass moment of inertia
B	: Beam
C_B	: Block coefficient
C_u	: Upper deck area coefficient
D	: Damping coefficient
g	: Acceleration due to gravity
G	: Center of gravity
GZ	: Restoring moment arm
H	: Effective depth of the ship superstructure
I	: Mass moment of inertia
k_x, k_y	: Wave numbers in x and y directions
LBP	: Length between perpendiculars
L_x, L_y	: Spatial length
M	: Metacenter
S_ξ	: Sea spectra
s(f)	: MEM spectral density function
T	: Draft
ω_e	: Encounter frequency
ω_n	: Natural frequency

ω_w : Wave frequency

ω_{exp} : Expected number of crossing at any level

U : Ship speed

$\eta(\xi)$: Surface height

θ : Roll angle

ρ_k : Autocorrelation function

ϕ : Angle between ship and wave directions

ϕ_c : Angle of deck immersion

Δ : Displacement

Ω : Nyquist limit

Chapter 1

Introduction

1.1 General remarks

Engineering problems can not be isolated from a question of safety since every human endeavour can not be free of hazards or risks. It is apparent that a need for safety measures will be influenced by an existence of such hazards or risks. In this respect fishing vessels are no exception. Every engineer engaged in marine activities should, to some extent, involve himself in the development of methods aimed at providing the utmost marine safety. Fishing is a difficult and hazardous occupation, a fact that no-one will deny today. This is an occupation that wears and tears hard on body and soul.

In general, the term **safety** implies that no accident is acceptable but this is in contrast to the maritime field where the reality is that a substantial risk of accident is always present.

Safety work is always difficult, as it is difficult to say what is safe and what is not? It is often a question of opinion. Statistics can help to prove a point, but then accidents can be claimed to happen to other people, e.g. those with the careless crew. Improved safety costs money, but on the other hand, it does save lives, reduces injuries and brings peace of mind.

Prevention of accident in the marine industry may be considered in three stages

1. Design stage

2. Construction stage

3. Operation stage

At the design stage, it is important to check whether any safety regulation is violated or not, and to determine what kind of recommendations are provided by the rules of the classification societies. It is also necessary to design an adequate protective system to withstand the effects of accidents. Thus, every possible means of eliminating hazards can be taken into proper consideration.

The next stage is the construction stage. Its function is mostly related to the supervision of whether those safety features considered in the design stage were properly constructed and provided.

The operation stage, " Navigare necesse est, vivere non necesse est ". To sail is compulsory, to live is not compulsory; this ancient saying reveals how the need for an operative merchant marine was evaluated in the past. Fortunately, since then, the evaluation of human life has been considerably upgraded.

Several rules of classification societies are based on the assumption that the ships receive "ordinary seaman-like treatment." This is not necessarily limited to handling in heavy weather and may include other factors, such as those resulting from stability, stowage of heavy cargo, shear forces and bending moments due to cargo and ballast loading and distribution, or collision and grounding avoidance. The captain is expected to exercise good seamanship yet the guidance given to him with regard to the behaviour of the ship in heavy weather and weather conditions is minimal and usually limited to his own experience in general or at best with the specific ship in particular.

1.2 Review of Fishing Vessel Casualties

To understand the current state of marine safety and to make a positive move forward for the promotion of marine safety, a brief review of the historical and technical aspects

of fishing vessel safety is made in this section.

As a result of the trawler losses in 1968 a committee of Enquiry into Trawler safety was set up under the chairmanship of Admiral Sir Deric Holland-Martin in the UK. The final report of the enquiry was published in 1969 and made many recommendations to ensure the safety of fishing vessels. One of the main recommendations on design and construction was that the Board of Trade (currently the Marine Division, Department of Trade) should seek powers to lay down statutory requirements on the stability of newly built trawlers. The committee also considered that the International Maritime Organization's stability criteria would provide a suitable starting point for stability standards in the light of experience.

The recommendations of the committee of Enquiry were adopted by the UK. government and legislation followed which resulted in the Fishing Vessels (Safety Provisions) act 1970 and ultimately the Fishing Vessels (Safety Provisions) Rules 1975. The rules cover most aspects of fishing vessel safety and include requirements for freeboard, stability, fire protection and watertight integrity. Although the recommendations of the Holland-Martin Enquiry were directed primarily to vessels of 24.4 metres in length and above, the 1975 rules require mandatory survey of fishing vessels 12 metres in length and above. In 1977 at the Torremolinos Convention for vessels over 24m in length, guidelines for safety of fishing vessels less than 24m in length were drawn up by joint IMO/FAO working group in 1980.

In September 1976, the Norwegian research vessel M/S Helland Hansen capsized and sank 18 miles north west of Svinoy lighthouse off the west coast of Norway. In 1977, the Norwegian Directorate decided to order model experiments for a further investigation of the accident. The reason was primarily that stability calculations had shown that the vessel fulfilled the requirements of the Torremolinos Conference 1977, as well as the almost corresponding Norwegian requirements [1].

After investigation, the following recommendations were made [2]:

1. Due to the relatively large energy content of moderate waves of 4-6m, small vessels should ideally be self righting. This can often be achieved by constructing the wheel house such that it is weathertight, which implies doors and windows of stronger construction.

2. The GZ curve requirements should in any case be strengthened by requiring positive GZ values up to angles of $80° - 90°$.

3. Openings where water can enter the vessel during heeling to $80° - 90°$ must be closed weathertight, or restricted in size in relation to the size of space to which they lead.

4. Bulwarks, although providing protection in moderate weather, are dangerous in breaking waves. They increase the wave moment and trap water on deck. Rails, combined with low bulwarks, if necessary, should therefore replace high bulwark on small vessels.

In February 1974 the Hull trawler Gaul disappeared in heavy seas off the north cape of Norway. The formal investigation into this disaster concluded that the Gaul capsized and foundered after being overwhelmed by heavy seas. The inquiry considered many possible causes for the disaster and expressed a hope that these would be further investigated by naval architects in the Department of Trade with a view to promoting greater safety. In due course the Department of Trade requested the National Maritime Institute to carry out model experiments on the fishing vessel Gaul to achieve this end [3].

The findings of this investigation are consistent with the view that the Gaul was not lost as a result of inadequate intact stability or poor seakeeping qualities. It would seem most probable that the cause of her loss was due to the severe waves, wind, and the

possibility of encountering a large steep wave at that time in the area of the North Cape bank associated with some other unknown circumstances such as partial flooding from some cause.

The most serious loss of stability considered in this investigation and one that could have been sufficient to cause the Gaul to list heavily and founder is that due to considerable amounts of water present simultaneously on the trawler deck and factory deck, such condition might conceivably arise from the result of a combination of flooding from the salt water supply to the processing pump on the factory deck and water flooding through to an access door on the starboard side of the trawler deck.

M.S.J. Reilly examined fishing vessel loss rates for the period 1961 - 80 and compared the trends of those rates for the period of the committee of inquiry into trawler safety (1971 - 80) with the years preceding the circumstances of that inquiry (1961 - 70). He provided a qualitative evaluation of mortality from occupational accidents sustained by deep sea and inshore fisherman between 1961 and 1980.

In 1985, the Marine Directorate of the Department of Transport considered it appropriate to commission an independent study of "Total Losses" and "Serious casualties" casualty records, after 10 years following the introduction of the fishing vessels (safety provision) rules 1975. This study was done by the Sea Fish Authority. The objective of the investigation was to determine the factors of prime importance in influencing the casualty rate for fishing vessels. This was done by statistical analysis of data obtained from an examination of the Marine Directorate's casualty records. This study was extended in 1986. This analysis also deals with vessels actually fishing or on passage to and from the fishing grounds as a separate group.

The adequacy of the International Maritime Organization (IMO) recommendation A168 for minimum intact stability criteria of fishing vessels has been widely debated since its introduction in 1968. The fact that losses still occur raises questions on the level

of this stability standard and whether it is maintained in practice. This paper discusses the stability and seaworthiness of fishing vessels in the light of recent experience with UK vessels and makes some suggestions for improvement in safety of those vessels[33].

Morrall and MacNaught [4] emphasised that the IMO standards are absolute minima; from research and known casualty evidence, the indications are that when levels of stability are reduced below IMO standards the probability of capsize becomes progressively greater as these criteria are degraded.

Even when IMO stability standards are complied with, safety from capsizing can not be guaranteed. This is because, the required parameter values of the still water statical stability curve are based on a small number of vessels with variability of ship loading and sea conditions at the time of loss. The parameter values selected for this type of stability criteria are independent of vessel size, type, operational and weather conditions and the margin of safety must therefore vary for each vessel and must be unknown.

Ship designers and approving authorities need to have guidance on what are acceptable safe minimum values of the stability properties for the many different types and sizes of ships.

The International Maritime Organization (IMO) has been working towards the development of "physical" criteria which would manifestly enable safety assessment relative to external forces and thus provide indications of safety margins.

H. Bird and A. Morrall [5] introduced the safeship project. The aim of this project was to advance existing knowledge of large amplitude rolling motion and ship capsize mechanisms so as to develop better design criteria and stability regulations.

At the end of this study, the following comment was made on static stability criteria:

"Simple statical righting lever curves will always serve a useful purpose. Because of their relation to the hull form geometry and obvious physical meaning. They are helpful both to naval architects and to ships officers. In the future, they could be more effectively

derived from dynamic criteria."

Y.S. Yang [6] suggested that because so many of the factors influencing the capsizing of ships are essentially probabilistic in nature, it follows that stability assessment must ultimately be based on some form of risk analysis.

Yang explained that the assessment of the risk that a given ship, with a given set of characteristics, will capsize (or reach some other unacceptable condition of stability) during its expected life, must in the end attempt to take account, in a rational and logical way, of the many varying parameters which influence that risk. He devised a practical scheme for the formal assessment of risk of capsize for a given ship. This might initially provide a basis for comparative assessment of ship safety against capsizing and also for exploring the influence of ship design parameters on survivability.

Considering only the loss of lives and money as a result of marine accidents, it is easy to realize the importance of the preventing of capsizing of small boats. The following table shows a summary of marine accidents [7]. As seen from figure 1.1, the most important cause for casualties is operational mistakes.

Year	Collision	Grounding	Striking	Sinking	Foundering	Capsizing	Total
1988	35(3)[1]	190(16)	11(2)	29(21)	14(8)	14(8)	293(58)
1989	45(5)	161(14)	48(14)	5(2)	38(28)	12(4)	309(67)

Table 1.1: Statistics for Fishing Vessel Casualties in Canada

Accidents at sea are rarely the result of a single event; and it is likely that safety assessment must eventually be based on techniques, such as fault tree analysis, which can model the possible sequences of events or malfunctions leading to an accident [8].

[1] Figures in parentheses indicate the total number of vessel lost

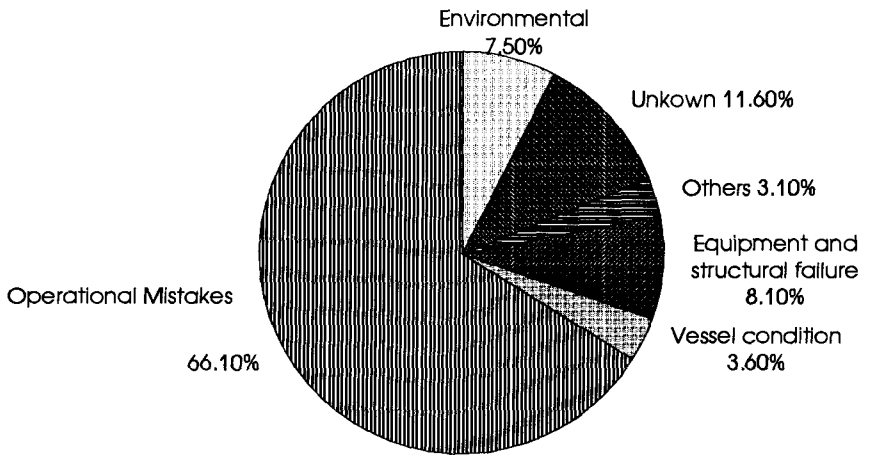

Figure 1.1: Total number of casualties

Köse [8] investigated the accidents of fishing vessels by using the Fault Tree analysis method. The Fault tree analysis is a logical and diagrammatic method used to evaluate the probability of an accident resulting from sequences and combinations of faults and failure events. A fault tree describes an accident - model which interprets the relation between the malfunction of components and observed symptoms. Thus the fault tree is useful for understanding logically the mode of occurrence of an accident. Furthermore, given the failure probabilities of system components, the probability of a top event occurring can be calculated. More explanation of this method can be found in [8].

In this study, the following ranking was found:

- Human Error
- Shift of Cargo and Fish on deck
- Taking Catch and Towing
- Faulty design

- Equipment error

This ranking shows that human error is the most important cause of the loss of vessels. Major human errors are described as [8] :

- Improper lookout
- Misjudged effects (wind, current, speed)
- Failure to ascertain position
- Carelessness / inattention
- Improper corrective procedures
- Failure to determine wave properties
- Crew asleep (present but asleep from fatigue)
- Absorbed in secondary task
- Watch keeper distracted by non-routine event

1.3 Literature Review

The above findings are not very suprisings for a marine researcher. To solve this problem, researchers are working on two different areas ; improvement of vessels seakeeping characteristics and heavy weather damage avoidance systems. The first one is mostly done by doing towing tank experiments or theoretical calculations. The second one is to install a system on board. In this study, we are interested in the development of an onboard system.

In 1975, Lindemann and Nordenstrøm [9] developed a system for ship handling in rough weather. In this system, they measure the accelerations of the ship in six degrees of freedom and stresses at a cross section in the aft quarter length. The main concern of this project was the weather damage on a ship hull and equipment on board.

In 1976, Hoffman [10] analysed the impact of seakeeping on ship operation and discussed considering shipboard guidance as well as shore-based systems. He suggested using charts and ship - shore communications for routing in heavy weather.

In 1979, a catalog for a heavy weather guidance system [11] was developed for FF-1052 class ships. The catalog provides the ship operator with hard copy, quantitative predictions as to how the ship responds in a seaway and some guidance for avoiding excessive ship motions or related events, such as slamming and deck wetness that may cause damage to the ship during heavy weather. This catalog relies on the operator to specify the height, period and directionality characteristics of the seaway.

Hoffman [12, 13] published his results on the integration of shipboard and shore-based system for operation in heavy weather. In this research, they installed the system on board the LASH ITALIA. The system was used by officers on the bridge during heavy weather to evaluate trends of accelerations and bending stresses as well as to provide comparative levels of response evaluation for establishing a performance index for the vessel.

A similar system designed specifically for Great Lake bulk carriers [14] was installed on a 1000 foot ship. Emphasis in this system was on the hull girder response including separation of the signal due to wave-induced and springing components and provision of separate guidance data for each of these responses. Details of the system are given in [14]

In parallel with the above described works, two similar projects were underway in Norway [15, 16] and in Holland in a joint venture with Lloyds [17]. The experience

gathered from these two projects are used to cover the extremely important areas of training and indoctrination of the on-board user to derive maximum benefits out of such a system.

A different type of heavy weather vessel response control system for use in offshore construction was introduced in the early part of 1977 in the North Sea [18]. The system monitors roll, boom tip, absolute and relative motion. The predictive mode of the system provides the operator with the ability to simulate any condition that the vessel is likely to encounter during the operation without having to expose the ship to such hazards as losing the boom due to excessive angular displacement etc.

The above-mentioned studies are mainly for big ships and their structural and equipment safety. None of them dealt specifically with stability of the ships.

In 1982, a microcomputer based capsize alarm system was developed by Koyama [19]. In this system a pendulum was used to measure ship motions; mean period and root mean square of rolling were used to assess the safety of the vessel. As a result of an inadequate pendulum system, the results were not very reliable at high speeds.

1.4 Objective

There is probably no better source of assessment of the seriousness of the situation than the experienced captain on the bridge. However, just as the human "sensor" cannot detect the levels of all responses experienced by the ship, he cannot always know which maneuver to select to alleviate that situation. The monitoring, recording and predictions of response level provide more definite criteria as to when to act. The question of how to act is just as important as when to act. Since in most cases the ship is not provided with any data on its seakeeping characteristics and capabilities, the captain's actions follow his own logic, based ideally on experience with the particular type of ship, loading

condition and weather condition.

The options open to the captain are not always as clean cut as may be implied from the foregoing scenario. If , for example, the excessive roll is a result of quartering seas approaching the ship from the port side, the decision whether to seek a change by decreasing the angle, that is to more beam seas, or increasing the angle to somewhere close to following seas, is not so obvious since it depends to a large extent on the size of the ship, its speed of advance and wave properties. In such a case some guidance in the decision-making process could be useful.

The aim of this study is to develop a reliable monitoring of vessels and environmental parameters playing an important role in the capsizing of vessels and establishment of corrective action to increase the reliability of the vessel or to avoid capsizing.

There are two main considerations ;

- The system should measure a minimum amount of data. In order to make this system practical and least costly, the equipment that already exists on board such as radar should be used.

- The system should not interfere with the operation of the ship. This is specially important for fishing vessels. Since the vessel is their working environment, it is feared that anything interfering with fishing operation would be removed.

It should also be noted that the system developed in this research is a monitoring and advisory system, not a control system. The aim of the system is to help the captain to decide on an appropriate course of action based on information derived from basic ship-based sensors. The suggested action also includes feedback regarding the conditions that makes the vessel unsafe.

Chapter 2

An Overview of a Monitoring and Advisory System

2.1 Analysis of Capsizing Modes

As a basis for deciding on the appropriate parameters and general layout of the monitoring and advisory system, capsizing modes and statistics are examined.

Experimental and theoretical calculations show that capsizing modes can be divided into 6 categories [20, 21]

1. Low cycle resonance
2. Pure loss of stability
3. Resonant excitation
4. Broaching
5. Loss of transverse stability in beam to quartering seas
6. Impact excitation due to a steep wave

Low cycle resonance can be recognized by the frequency of the roll motion. The essential prerequisite for this to occur is an encounter frequency (see Appendix B) nearly equal to the twice the roll natural frequency. Figure 2.2 shows this phenomenon in terms of roll angle and changes in stability (restoring moment) of the ship. The phenomenon appears to occur approximately in the following sequence [22]. As an initial condition, assume that the ship has an initial roll angle θ_0 to port side (Figure 2.2), when the wave

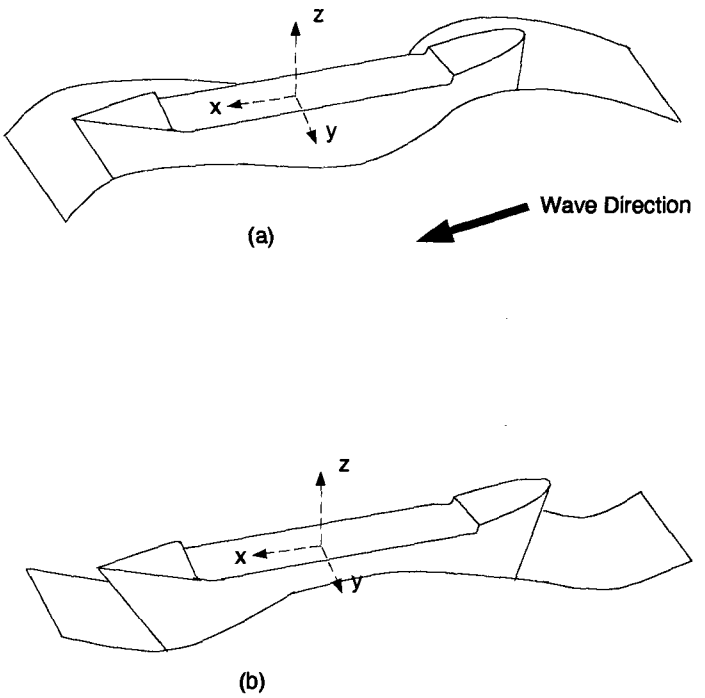

Figure 2.1: Two critical conditions for a ship in following waves

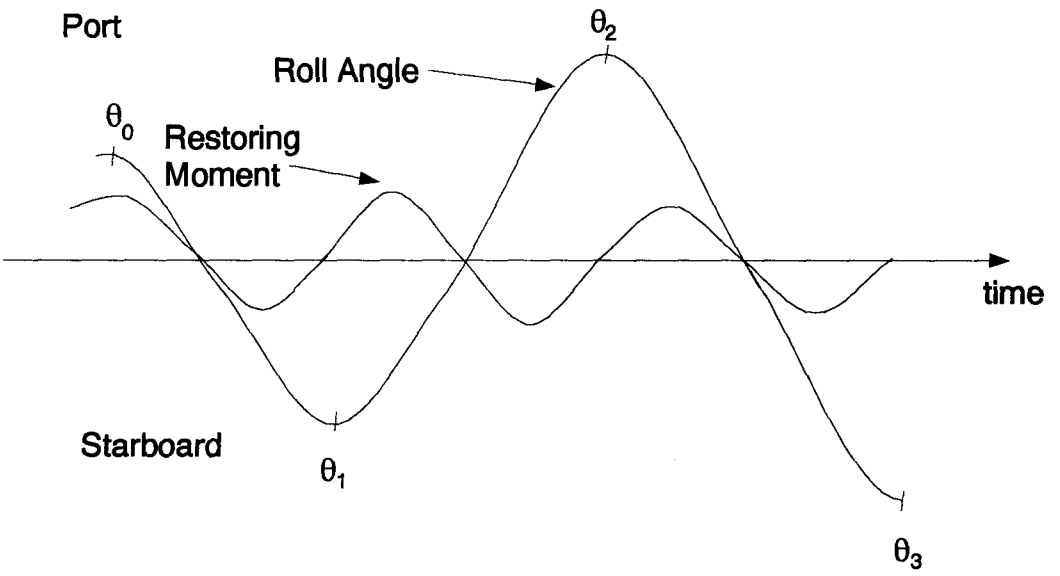

Figure 2.2: Fluctuations in ship stability

trough is at midship (Figure 2.1 a.). While the ship is rolling to the starboard side, the crest of a wave moves to amidships (Figure 2.1 b.) , reducing the stability of the ship (Figure 2.3) and it takes a large roll (θ_1 in Figure 2.2). This wave moves past the ship and a trough comes into the midship position (Figure 2.1 a.) while the ship is rolled over to port side, resulting in increased restoring moment (Figure 2.3). This causes the ship to roll back upright, acquiring a high roll angular velocity by the time it reaches the upright position. Another wave crest, meanwhile, moves into the amidship position, resulting in diminished stability once again as the ship starts rolling past upright and to the starboard side (θ_2 in Figure 2.2). The ship then rolls over to the starboard against a diminished restoring moment (θ_3 and Restoring moment Figure 2.2). This process continues until either the ship capsizes or it moves out the wave group and the roll motion dies down.

Pure loss of stability occurs when the righting arm (GZ) decreases to the point that there is not sufficient restoring energy in the vessel to upright itself. The essential prerequisite for this to occur is a ship speed nearly equal to the wave phase velocity so that the ship remains almost stationary relative to wave crest for a sufficient length of time to capsize (Figure 2.1 b. and Figure 2.3). This usually occurs in a following sea at high speed. The ship simply loses all stability when the crest of a high, steep wave moves into the amidship position.

Broaching implies the loss of directional control. A vessel may broach in two ways.

1. When the vessel speed is close to the phase speed of the wave, it is forced to move along with the wave so that it becomes directionally very unstable and broaching may occur in a relatively short time span (eg. 50 to 150 seconds).

2. When the vessel is hit from astern by sufficiently steep waves in a successive manner, it can be yawed to such an extent that rudder action cannot rectify the situation before the next wave yaws the vessel even further.

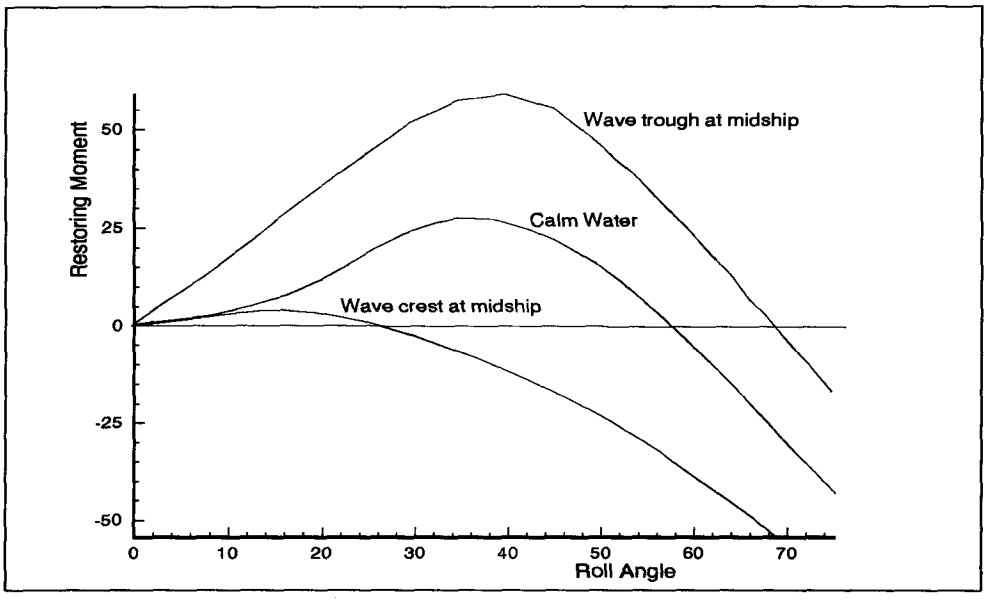

Figure 2.3: GZ curve of American Challenger for two extreme wave positions

Resonant excitation refers to the condition where the vessel is excited at its natural roll frequency by beam to stern quartering seas (Figure 2.4), very large roll angles may result, if the wave amplitude is sufficiently large.

Loss of transverse stability in beam seas to quartering seas (Figure 2.4) refers to the same phenomenon as pure loss of stability. There is however a significant speed dependence for pure loss of stability, while loss of transverse stability may occur at any speed [21].

Impact excitation due to steep, possibly breaking waves from a beam causing the vessel to heel to a large angle [21].

In addition to the above, two different modes can occur in a combined fashion, for example, broaching may be followed by pure loss of transverse stability, or resonant excitation may be followed by loss of transverse stability.

As seen from the above capsizing modes, there are three critical conditions for inducing ship instabilities:

- wave speed equals ship speed in following seas
- encounter frequency equal to twice the roll natural frequency
- encounter frequency equals roll natural frequency.

Equation 2.1 shows that encounter frequency is a function of wave frequencies, ship speed and the angle between ship and wave directions.

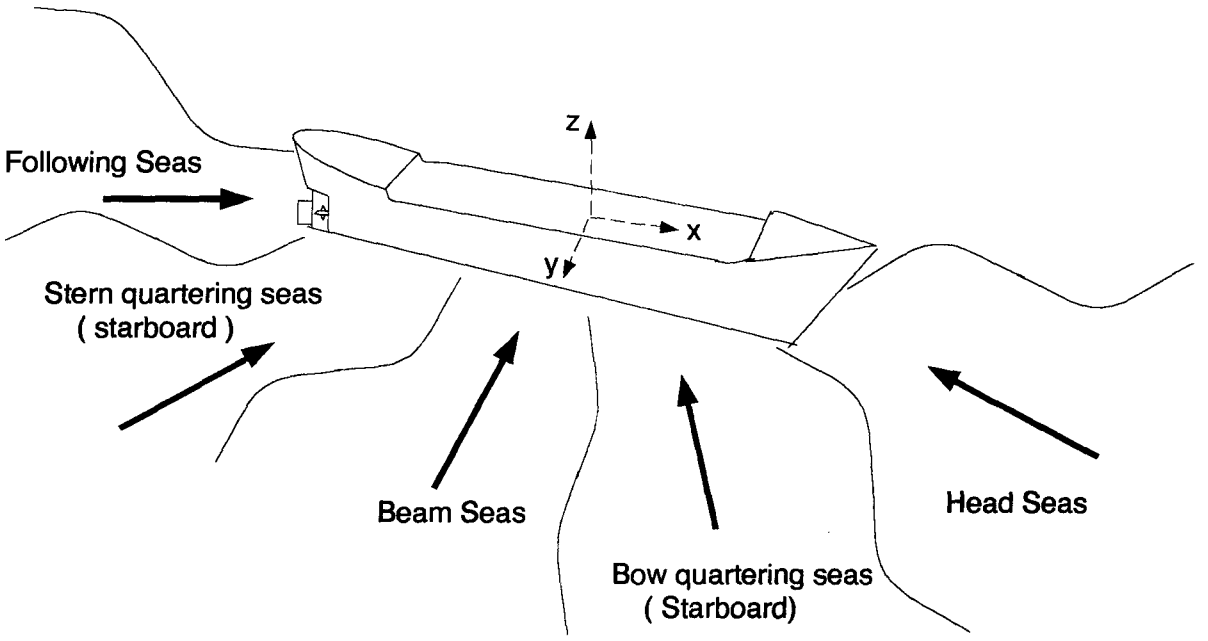

Figure 2.4: Wave directions with respect to the ship

2.2 General Layout of the Monitoring and Advisory System

The following parameters need to be measured to identify the capsizing modes explained above.

1. Wave properties : Encounter frequency is shown to be very important factor in ship capsizing. Encounter frequency is given by :

$$\omega_e = \omega_w - \frac{\omega_w^2 U}{g} \cos(\phi) \tag{2.1}$$

where

ω_e : Encounter Frequency

ω_w : Wave frequency

U : Ship speed

ϕ : Angle between wave direction and ship direction

g : Acceleration due to gravity

As seen from equation 2.1, encounter frequency is a function of wave frequency and direction. Therefore, these wave properties are needed to decide the reliability of a vessel.

2. Vessel speed : It is shown that capsizing modes 1, 2, 3, 4 have a strong dependency on ship speed, that is why, this information is necessary for the advisory system to make a decision.

3. Responses of vessel (heave, roll)

The above mentioned capsizing modes are for heavy weather conditions. Unfortunately, this is not the case always, there are some examples in the statistics [7] that vessels were lost when the weather was relatively calm. Investigations [23] on these accidents show that these accidents occured because of free surface effects, overloading or going from sea to river (density change). Therefore, the monitoring system should also

monitor static stability characteristics of the vessel. The following parameters need to be measured to monitor static stability.

1. Draft and trim : These are used in static stability calculations to find the displacement of the ship. Since the body plan of the vessel is assumed to be known from the design stage, displacement of the ship can be calculated by integrating up to the draft at each station.

2. Levels of water and fuel tanks : This information is used to make free surface corrections. This correction is detailed in chapter 3.

A general layout of the monitoring and advisory system is given in Figure 2.5. As seen from Figure 2.5, this system consists of three subsystems:

- Measurement sub-system
- Calculation sub-system
- Advisory sub-system

Measurement sub-system is divided into 4 sub-systems:

1. Radar - Frame grabber : This sub-system provides the necessary information to the advisory sub-system for wave parameter calculations. This system uses the ship radar as an environment monitoring system and obtains radar images, then information about waves is extracted from these images. A detailed explanation of this procedure is contained in chapter 4.

2. Loran-C and ship's log: Provides position of the vessel with respect to ground so, speed of the vessel.

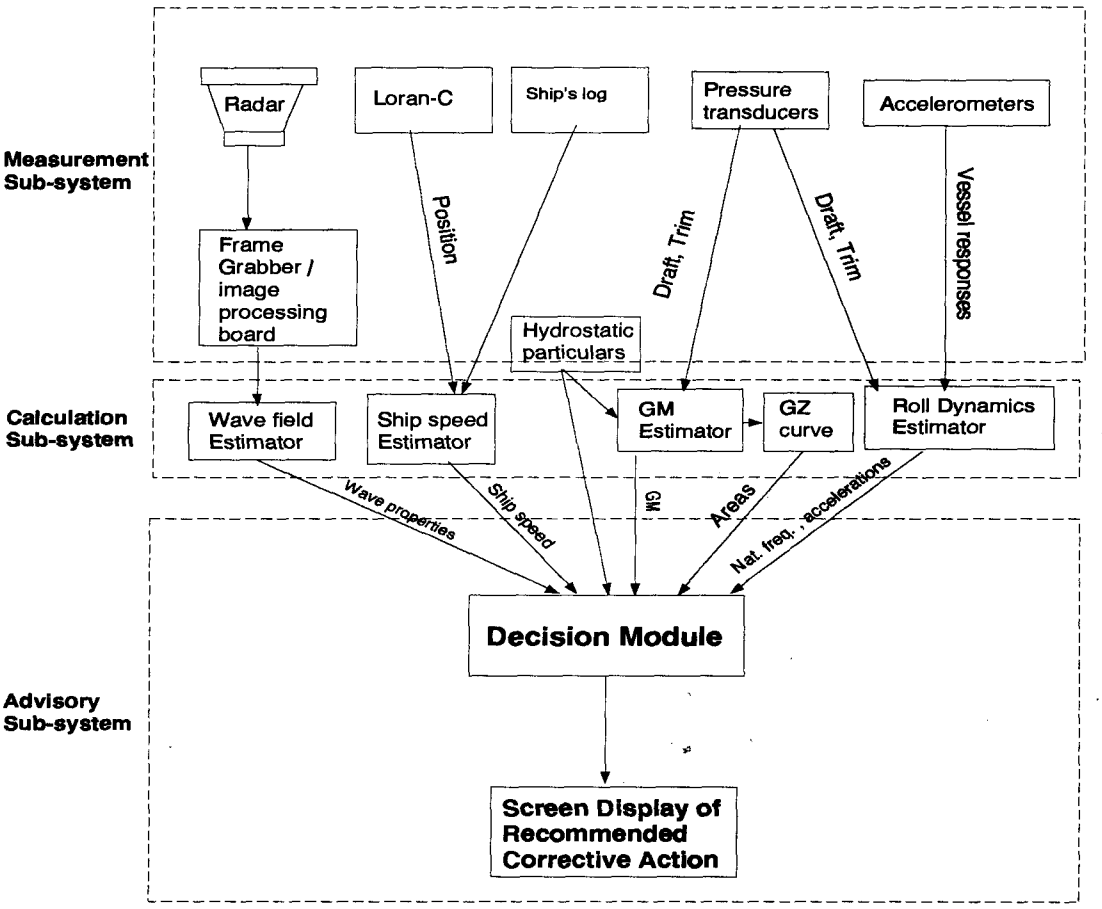

Figure 2.5: General layout for monitoring and advisory system

3. Pressure transducers : Provide necessary information such as draft trim and levels of each tank for static stability calculation.

   Pressure transducers can be used to measure draft and trim. An example of transducers locations are shown in Figure 2.6.

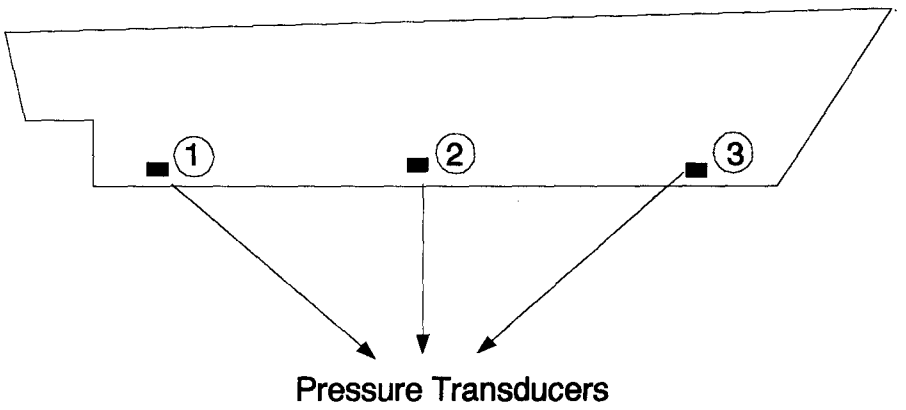

Figure 2.6: An example for Transducer locations

Pressures need to be measured at least at four different locations. Three of those say on starboard side of the ship (as shown in Figure 2.6). The fourth one is port side of the amidship.

Sensors 1,2 and 3 can be used to calculate static draft and trim. Sensors 2 and 4 may be used to find heeling angle.

4. Accelerometers :Accelerometers can be used to measure vessel responses for dynamic stability of the vessel.

Calculation sub-system consists of 6 categories (see Figure 2.5).

1. Wave field estimator : The wave properties such as frequency and direction are found from radar images by using image processing techniques. A detailed explanation of this can be found in Chapter 4.

2. Ship speed estimator : Position of the ship at any time can be obtained from Loran-c and this can be used to estimate ship speed.

3. Hydrostatic particulars : These are physical parameters of the ship such as length beam, draft, curves of form which are known after construction.

4. Metacentric height : The position of the center of gravity is also necessary for static stability calculations. Estimation of metacentric height is explained in detail in section 3.3.

5. Restoring arm (GZ) curve : In order to decide initial stability of the vessel, this curve is needed. International Maritime Organization (IMO) and most countries have some rules regarding area under this curve to be met. This concept will be explained in Chapter 3.

6. Roll dynamics estimator: There are three different calculations in this section :

   - To calculate the probability of the roll angle exceeding a limit value in a certain time
   - Expected maximum roll angle
   - Natural roll frequencies.

   Detailed explanations of these three method is given in chapter 5.

7. Heave motion : This can be used to estimate wave height. Explanation for this methodology can be found in chapter 5.

Advisory System (also known as Decision Module) uses the data from calculations and applies rule of thumb in order to identify corrective action that should be taken by the captain of the vessel. A general layout of Decision Module is given in Figure 2.7

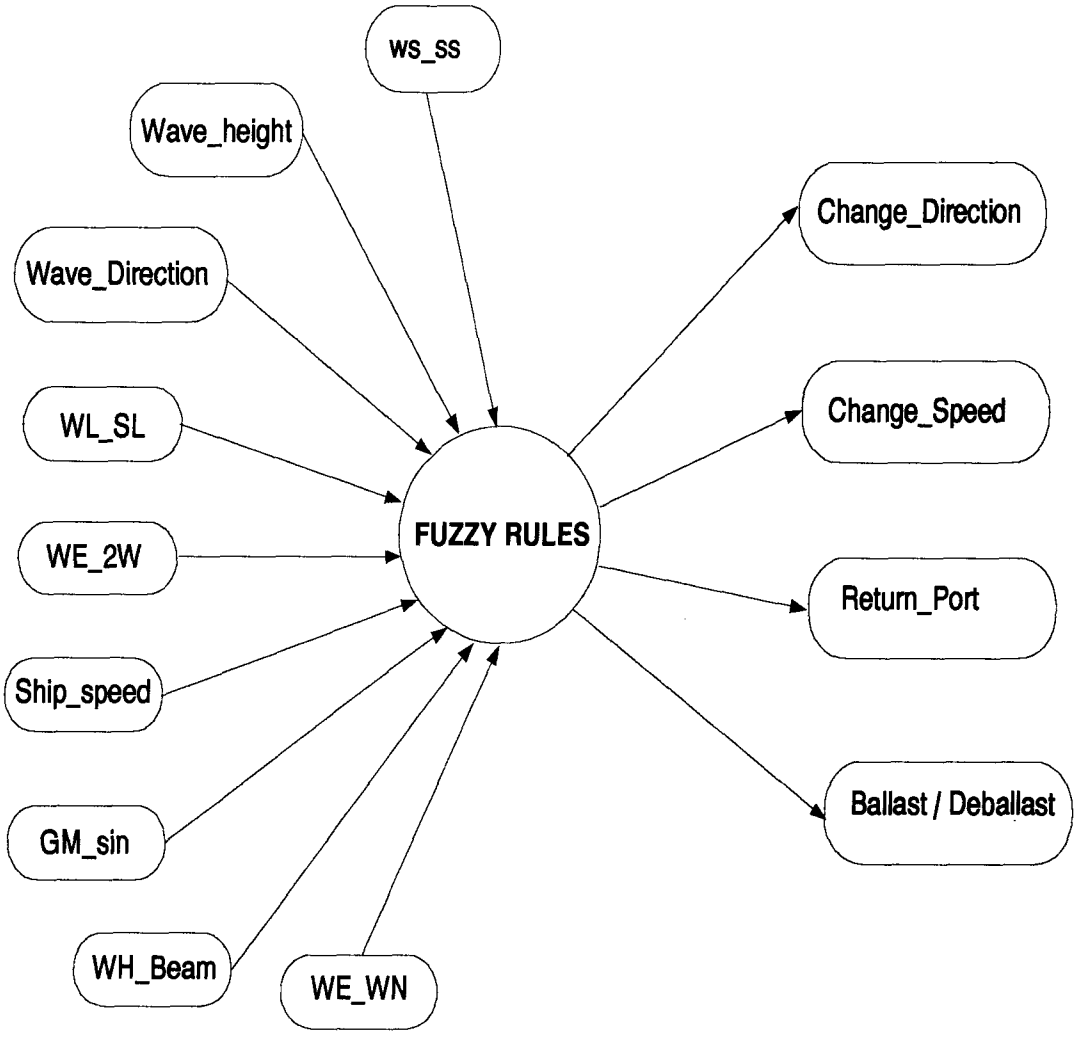

Figure 2.7: General layout of Decision Module

Suggestions : Display the suggested action by a fuzzy expert system on a monitor or alarm from a speaker.

Chapter 3

Static Stability

3.1 Background

Although, stability criteria for a vessel in relatively calm waters (rolling angle less then 15°) are well established, still accidents occur in these conditions. For example, an accident happened in British Columbia in July 1992. The skipper of the fishing vessel said that

> I feel disappointed it happened in my own back yard. I have been fishing these waters 43 years and I have never seen anything like it. ... We were just coming through the narrows and the catch shifted. She rolled on us really slowly. .... The Province newspaper July 1992.

Investigation on this accident by Marine Casualty Investigation Division shows that the vessel did not have enough stability to upright herself even under small external forces. This was caused by the free surface effects of the fuel tanks and liquid in the holds. Even though captain knew the effects of free surface on ships stability, he had no way of measuring or monitoring water levels in the tanks. If he had had this information, this accident may have been prevented.

Another interesting example was told by Ian Bayly of Transport Canada.

> This was during one of the training courses for captains of fishing vessels. An Instructor was teaching the static stability of the vessels, and explaining the

> importance of GM (metacentric height), after 10 minutes, a captain stood up and said that you are talking about GM, but I have a Caterpillar engine in my vessel, what am I doing here ?

Unfortunately, there are more examples like this in the statistics.(see [7]). That is why, it is decided to include the static stability monitoring part in this system. In order to calculate the static stability, the draft, trim and body plan of the vessel have to be known.

3.2 Static Stability Criteria

Consider a ship floating upright on the surface of a motionless water. In order to be at rest or in equilibrium, there must be no unbalanced forces or moments acting on it. There are two forces that maintain this equilibrium: the force of gravity and force of buoyancy. When a ship is at rest, these two forces are acting in the same vertical line, and in order for the ship to float in equilibrium, they must be exactly equal numerically as well as opposite in direction.

When the ship is heeled by an external inclining force, the center of buoyancy is moved from the centerline plane of the ship. There will usually be a separation between the lines of action of the force of gravity and the force of buoyancy. This separation of lines of action of the equal forces, which act in opposite directions, forms a couple whose magnitude is equal to the product of one of these forces (displacement) and distance separating them (GZ). In Figure 3.1 (a), where this moment tends to restore the ship to the upright position, the moment is called a positive righting moment and the perpendicular distance between the two lines of action is the righting arm (GZ).

Suppose that the center of gravity is moved upward to such a position that when the ship is heeled slightly, the buoyancy force acts in a line through the center of gravity. In

the new position, there are no unbalanced forces, or in other words, the ship has a zero moment arm and a zero moment. In figure 3.1 (b), the ship is in neutral equilibrium, with both righting moment and the righting arm equal to zero.

If one moves the center of gravity even higher, as in Figure 3.1 (c), the separation between the lines of action of the two forces as the ship inclines slightly, is in the opposite direction from that in Figure 3.1 (a). In this case, the moment does not act in the direction that will restore the ship to the upright, but rather will cause it to incline further (negative stability).

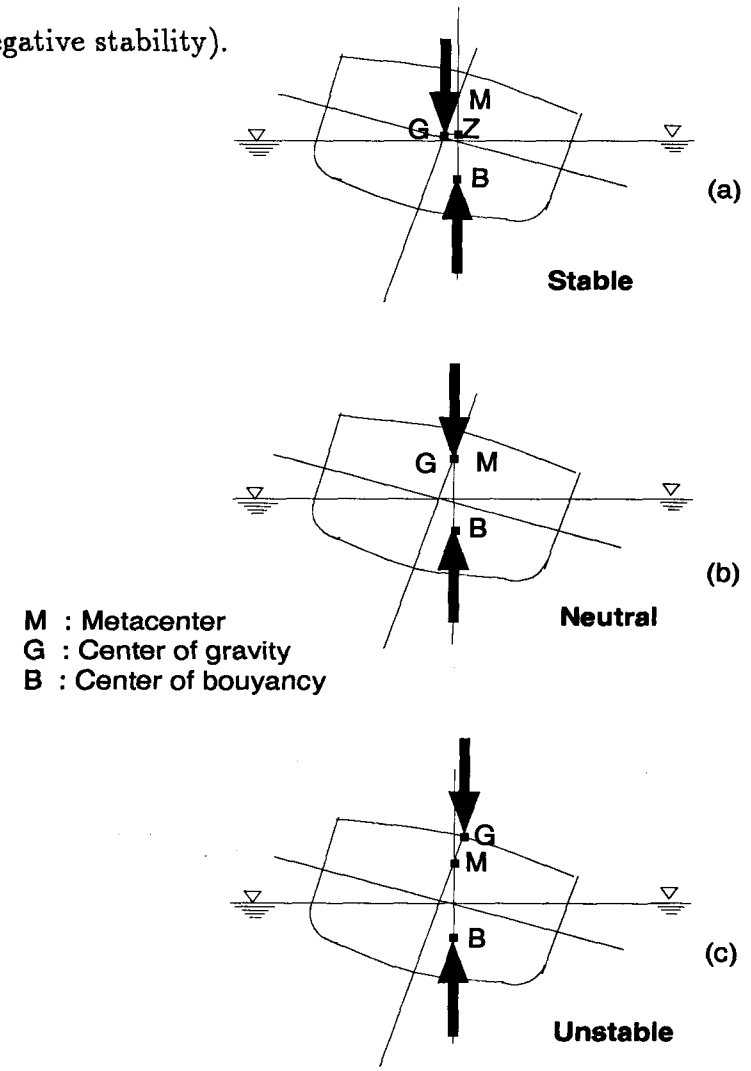

Figure 3.1: Possible stability conditions

The most satisfactory means of presenting a complete picture of stability is a plot of righting arm with its angle of inclination which is called a static stability curve. Such a curve may be used to determine several important characteristics which are:

- The righting arm at any inclination
- Metacentric height (GM) (see Appendix I)
- The angle of maximum righting moment
- The range of stability
- Dynamic stability (related to the area under the GZ curve).

The righting arm moment equals the righting lever times displacement. An example GZ curve is given in Figure 3.2 where ϕ_c is the angle of deck edge immersion. The area under the curve represents the ability of the ship to absorb energy imparted to it by wind or any other external force.

The recommendations of the International Maritime organization (IMO) with regard to intact stability standards are:

- Area under GZ curve up to 30° should not be less than 0.05 rad-m
- Area under GZ curve between 30° and 40° should not be less then 0.030 rad-m
- Area under GZ curve up to 40° should not be less then 0.09 rad-m
- Minimum initial GM should not be less then 0.35 m
- The maximum righting lever should occur at an angle of heel equal to or greater than 30°.

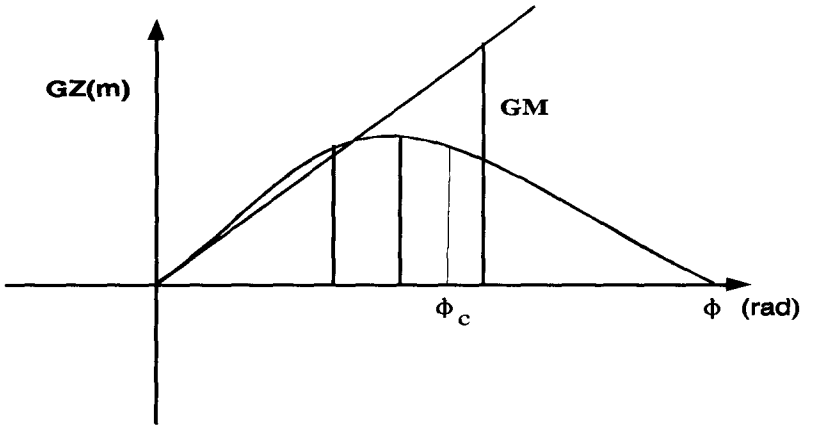

Figure 3.2: An example of GZ curve

In order to calculate the GZ curve, the position of center of gravity, body plan of the vessel and displacement need to be known. It is assumed that body plan of the vessel is given. The displacement can be found from draft and trim measurements and the body plan of the vessel. The only unknown to estimate the GZ curve is the location of the center of gravity.

3.3 Estimation of Metacentric Height

Metacentric height (GM) is estimated by using two different methods;

3.3.1 Estimating the Coefficient of GZ curve

In order to identify the stability conditions of the vessel defined by the GZ curve, the location of the center of gravity must be determined. The ship's rudder can be used to create free rolling by turning it to one side and back [24, 25].

The equation of the motion for a ship freely rolling may be written as :

$$(I + A_{44})\ddot{\phi} + D\dot{\phi} + R\phi = 0 \tag{3.1}$$

where I : Mass moment of inertia

A_{44} : Added mass moment of inertia

$D\dot{\phi}$: Damping moment

$R\phi$: Restoring moment

rearranging equation 3.1, one obtains

$$R\phi = -(I + A_{44})\ddot{\phi} - D\dot{\phi} \tag{3.2}$$

In order to decide the general form of the GZ curve, polynomial of different orders are fitted to some known GZ curves. The 9th order polynomial is found to be the best fit to different GZ curves (Figure 3.3).

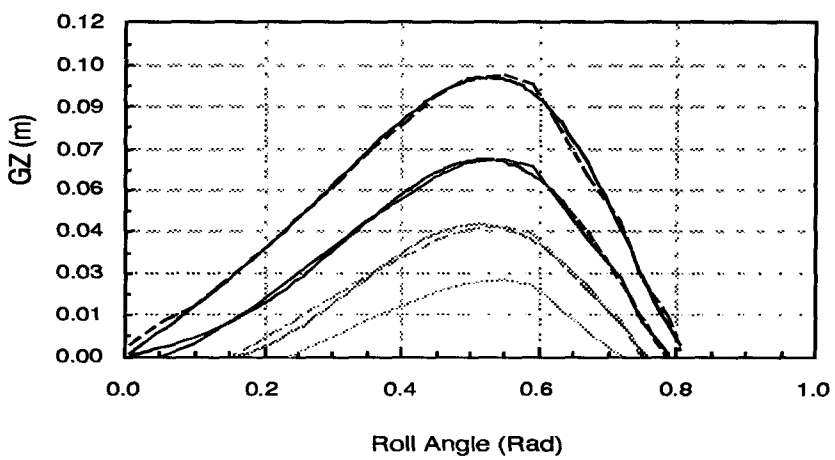

Figure 3.3: 9th order polynomial fit

then, the general form for the GZ curve is assumed as:

$$R\phi = a_o\phi + a_1\phi^2 + a_2\phi^3 + a_3\phi^4 + a_4\phi^5 + a_5\phi^6 + a_6\phi^7 + a_7\phi^8 + a_8\phi^9 \tag{3.3}$$

Since the equation of motion must be satisfied at any point on the rolling curve, there are more equations than unknowns. These equations can be solved by using a least square method.

The above explained method is applied to a fishing boat studied at UBC. For this calculation, a single chine model was used. Hydrostatic particulars and body plan of the model are given below.

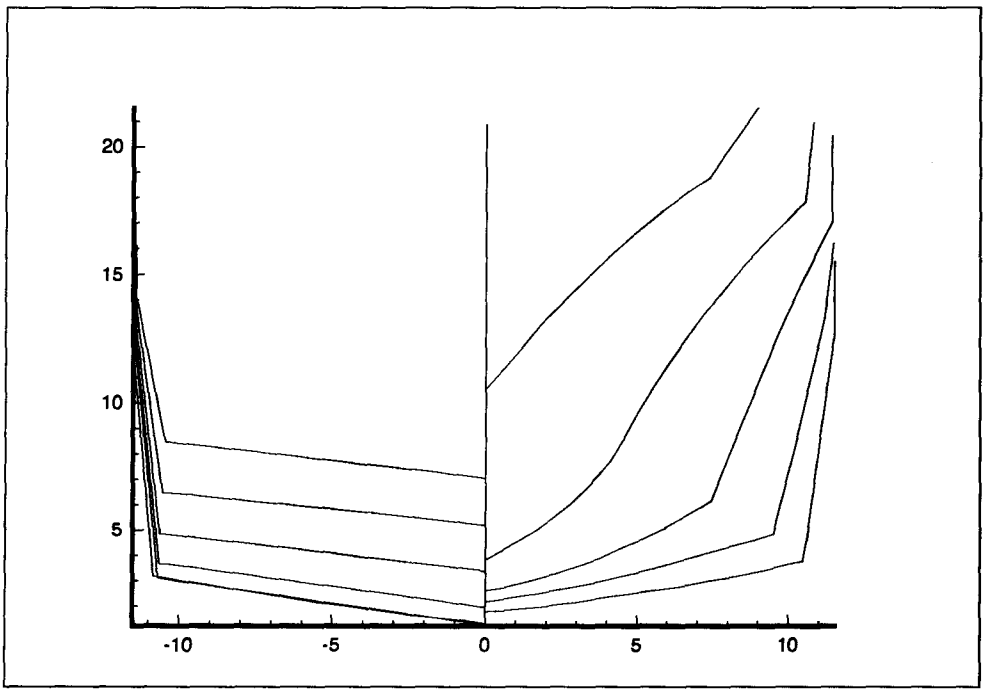

Figure 3.4: Body plan of single chine vessel

Length (LBP)	1.805 m	Displacement	115.4 kg
Beam	0.539 m	Block Coeff. (CB)	0.531
Depth	0.352	KM	0.3 m
Draft	0.246	GM	0.05 m

The damping coefficient was estimated by using Himeno's method [26]. In this

method, total roll damping is estimated as the sum of equivalent linear damping coefficients. That is :

$$B_R = B_F + B_E + B_L + B_W + B_{BK} \tag{3.4}$$

where B_R : Equivalent linear roll damping

B_F : Frictional damping

B_E : Eddy damping

B_L : Lift damping

B_W : Wave damping

B_{BK} : Bilge keel damping

a more detailed explanation of this method can be found in [26].

The following GZ curve was found using this method.

As seen from Figure 3.5, for small angles, the fit is good, but it is not good for large angles as there is very limited information at large angles. Therefore, this estimated curve is used to calculate GM only. Since GZ = GM $\sin(\phi)$ (for small angles), GM can be found from this curve. By combining this GM information and the informations given (body plan, draft, trim), a better estimation of the GZ curve is found [24, 27] (see Figure 3.6).

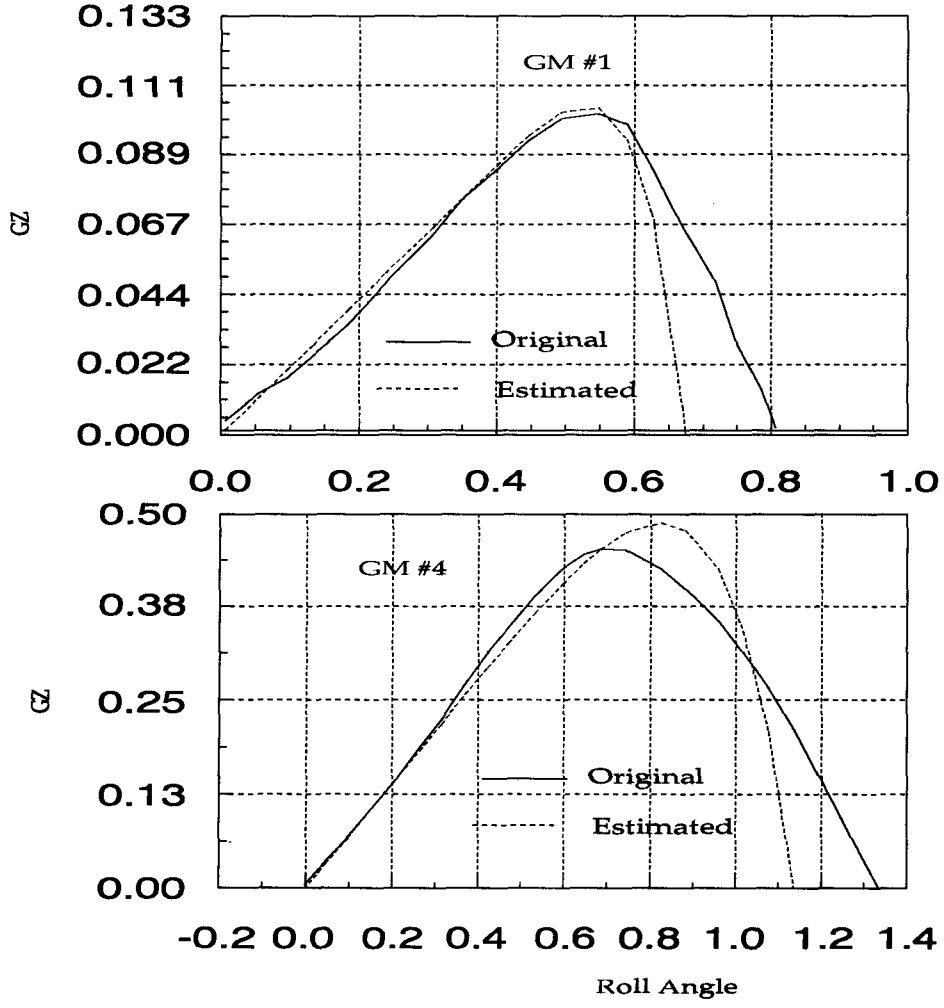

Figure 3.5: Estimated GZ for single chine vessel

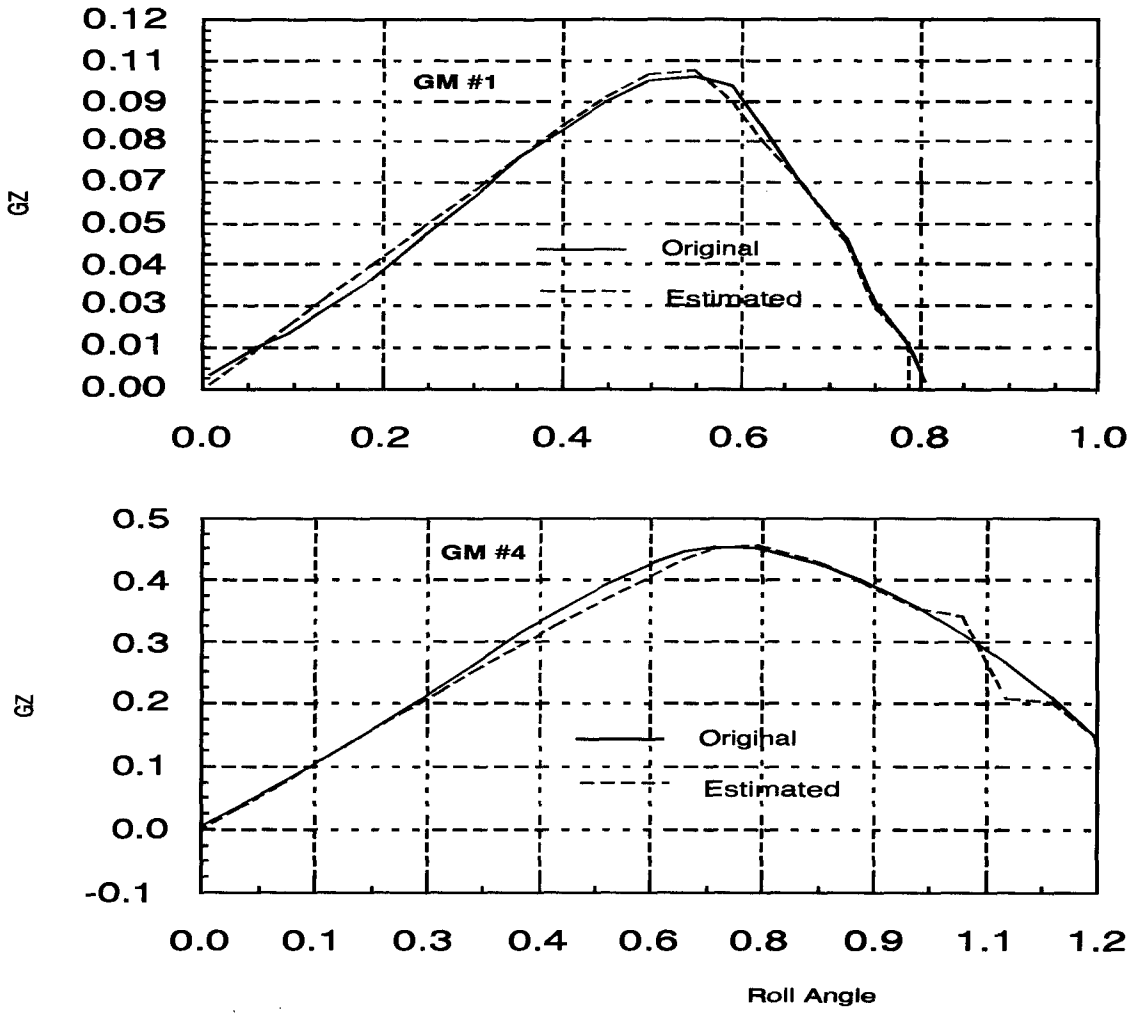

Figure 3.6: Final estimation of GZ curve

Then, by using Canadian Coast Guard rules (or International Maritime Organization's rules), a decisions about the stability (safety) of the vessel can be made.

3.3.2 Spectral Analysis

It is assumed that the mean period of roll decay curve is very close to the natural frequency. Then, if the mean period of roll is known, the location of the center of gravity can be obtained by using the following equation.

$$GM = \frac{(I_4 + A_{44})\omega_n^2}{\rho g \Delta} \tag{3.5}$$

where $(I_4 + A_{44})$: Virtual mass moment of inertia

ω_n : Natural frequency

Δ : Displacement

Thus, the accuracy to which GM can be determined is dependent upon the knowledge of $(I_4 + A_{44})$ and Δ as well as ω_n.

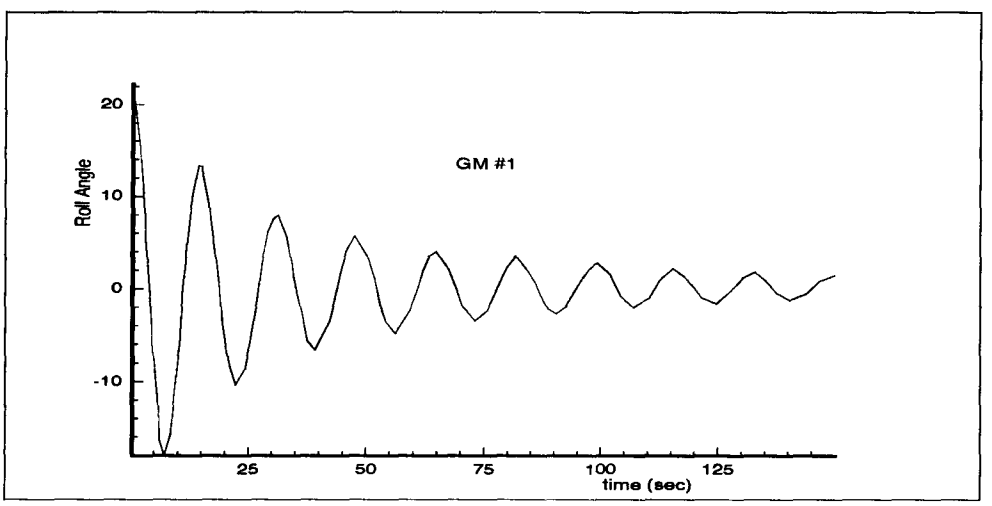

Figure 3.7: Roll decay curve for GM #1

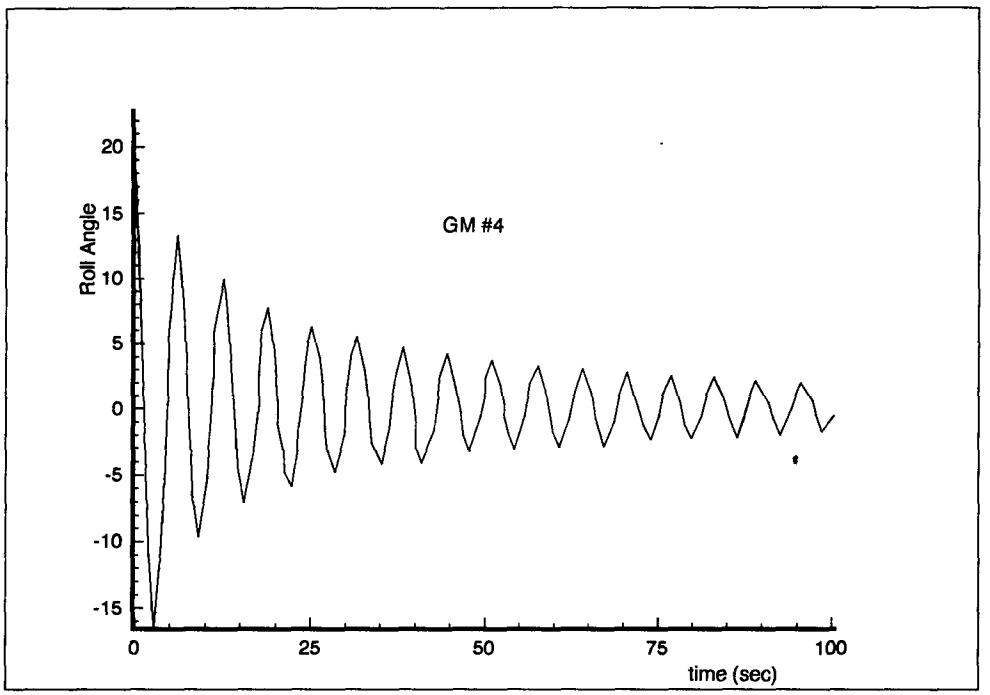

Figure 3.8: Roll decay curve for GM #4

This method is used to estimate the GM of the single chine vessel mentioned above. Free roll decay data is used to find the natural frequencies of the vessel. Figures 3.7 and 3.8 show roll decay curves of the vessel for two different loading conditions [28].

The following equation is used to estimate $(I_4 + A_{44})$ [29, 30].

$$(\frac{k_{xx}}{B})^2 = f[C_b C_u + 1.10 c_u (1 - c_b)(\frac{H_e}{T} - 2.0) + \frac{H_e^2}{B^2}] \tag{3.6}$$

where f = 0.177 - 0.2 for fishing vessels

C_B : Block coefficients

C_u : Upper deck area coefficient

C_u = Area / (Length x Beam)

H_e : Effective depth of the ship structures

H_e = D + (A / LBP)

D : Molded depth

A : Projected lateral area of superstructures

LBP : Length between perpendicular (see Appendix I)

T : Draft (see Appendix I)

B : Beam

From the above equation, the value of k_{xx} for the heavy condition is found as;

$$k_{xx} = 0.3668B \tag{3.7}$$

The Table 3.3.2 shows the results found from this method.

	Original (in)	Estimated (in)
GM #1	0.256	0.286
GM #4	1.969	1.78

Table 3.1: Comparison between original and estimated GM values

An error analysis is done to check dependence of the estimation of GM on k_{xx}, Δ and ω_n. In the first step, k_{xx} is increased 10%, this affected estimation of GM $\approx$ 10%, which corresponds 0.0078m (GM #1) and 0.065 (GM #4). Then, ω_n is decreased 10%, this corresponds 10% correction to the estimation of GM.

By assuming that the above errors all act in the same direction, the overall error in the estimation of GM will be less than 20%. This estimate is on the conservative side, since at times errors may act in opposite directions, thus in practice the prediction errors will be between 5 and 20%. This result can be improved by using a better method to estimate k_{xx} such as experiments and keeping a log of weight added to the vessel.

Chapter 4

Measurements of Wave Properties

4.1 Introduction

Measuring wave properties has been a challenge for researchers for some times. There have been some attempts to solve this problem. Most of these studies focused on three different areas:

1. Shipboard Observation
2. Floating buoy
3. Remote sensing

Tucker[1956] developed an instrument that measures waves from a ship. In principle, the instrument measures the height of the water surface relative to a point on the ship's hull and adds this to the height of the point relative to an imaginary reference surface, thus giving the height of the water surface independent of the position of the ship. While in such an instrument there is a frequency attenuation effect for the shorter wavelengths, the spectrum can be partially corrected for the error introduced. Certain of the British weather ships have been fitted with Tucker meters, and wave height records have been collected on a routine basis while on station, although these strip chart records have not been routinely used to calculate the point spectra.

Deleonibus and et al. [31] observed wave height spectra from the USNS Kane with a semiportable bow-mounted wave system. Distance from the sea surface to a transducer

at the bow of the Kane was measured with an infrared height sensor. Displacement of the bow associated with surface wave motion was obtained with a static pressure measuring device. Wave height spectra were estimated by cross-spectrum analysis of signals from these two devices.

Voronovich and at al. [32] investigated the possibility of using a wire wave-gauge to measure wave parameters from a ship at drift. Waves were measured by a resistance string wave recorder whose sensor was hung out at the bow or stern of the ship. The effect of rolling was taken into account by synchronous recording for an accelerometer that records the vertical acceleration of the suspension point for the wave gauge.

An alternative approach has been to fit a buoy with an inertial measurement system. The quantities recorded are wave slope in two perpendicular, known compass directions and surface displacement (by double integration of the measured vertical acceleration). From records of these quantities against time, it is possible to estimate the distribution of variance with respect to direction in any frequency band [Longuet-Higgins, Cartwright and Smith 1963]. If assumptions are made as to the nature of the spreading function, it is possible to generate a simplified directional spectrum estimate from these data. This technique has been used primarily for special situations such as full scale trials and no large collections are available for more general application.

The use of HF radar to measure various parameters characterizing sea state was suggested by Crombie [33] over four decades ago. He correctly deduced from measured echo spectra that the dominant (first order) return was explained by the simple Bragg or diffraction-grating mechanism. Since then, considerable interest has been shown in the application of remote sensing techniques to the measurement of ocean waves and currents.

These studies have largely dealt with the use of three forms of radar systems: SAR (synthetic aperture radar), SLAR (side-looking aperture radar), and HF (high frequency

radar). Because of the size of the antennas required, HF radar has only been deployed as a land-based system. SAR and SLAR systems, however have been successfully used in aircraft and orbiting satellites, thus allowing large areas of the oceans to be scanned.

In addition to these widely reported remote sensing techniques, some limited interest has also been shown in the use of conventional marine radar imaging for the collection of the ocean data.

Ijima and at al. [34] and Wright [35] were among the first to report the use of such radar for imaging ocean waves. Oudshoorn [36], Willis and Beaumont [37], Evmenov et al. [38] and Mattie and Harris [39] have also reported wave images obtained by radar. These researchers visually inspected the radar images to obtain estimates of the mean wave direction, wave length and period.

Recently, it has been proposed that digitized pictures of ship radar images of ocean waves be processed in order to obtain the spectral characteristics of the surface wave field. The corresponding scheme (backscattered microwave power $\rightarrow$ light intensity of the radar screen $\rightarrow$ gray level density on a film $\rightarrow$ numerical gray level $\rightarrow$ two-dimensional Fourier transform) is considered by Hoogeboom and Rosenthal [40]. The imaging takes place owing to the modulation of the backscattered microwave power by the long ocean waves through short wavelength Bragg-scattering waves as well as effects of shadowing by the wave crests (important at low grazing angles). The preliminary studies [41] show by calculating two-dimensional power spectra that the spectral properties of such images are similar to those obtained from the conventional pitch- and-roll buoy measurements. The spectral value of each wave number seems to be a well defined function of the corresponding value of the directional surface wave spectrum, depending smoothly on the environmental and radar parameters.

Hence two-dimensional power spectra obtained by processing ship radar images contain useful information about the wave directionality. But, uncertainty of 180° (ambiguity) remains in the determination of the wave propagation direction. It is hardly possible to remove this ambiguity simply by looking at the image of an irregular wave field. This disadvantage is usually overcome by assuming that waves travel inshore [42] or downwind which require additional information and leaves aside the possible detection of upwind traveling [43], wave reflection from obstacles [44], or backscatter caused by bottom irregularities [45]. In the last two cases the power spectra of the main and reflected wave trains usually occupy the same region of the wave number plane and hence remain indistinguishable.

A major problem exists in the interpretation of two dimensional wave number spectra, whether they are obtained from ship radar or any other imaging system, since 180° directional ambiguity exists in the resulting spectra. For relatively simple wave spectra, this ambiguity can be removed by assuming that the mean wave direction will be closely related to the wind direction. For more complex sea conditions, where there may be waves propagating at large angles to the wind, or if the wind direction is unknown, such a method is no longer applicable.

Atanosov and et al. [46] suggested a possible solution of the ambiguity problem for spatial power spectra of arbitrary wave fields by processing two images in the spectral domain, the second obtained shortly after the first one, making use of the known dispersion relation.

This ambiguity appears if the "frozen" surface at one specific time is used for the derivation of the power spectrum. By using two successive images it is possible to generate unique two dimensional power spectra, which may be useful in many situations to determine the actual direction of wave propagation.

Young et al. [47] developed an analysis technique for a full time series of radar images; each taken at successive revolution of the radar antenna. They concluded that the introduction of the third time dimension in the analysis has the advantages of providing information on the wave phase speed and hence the magnitude and direction of the near surface currents, removing the directional ambiguity inherent in the two dimensional analysis and providing an extremely high signal to noise ratio.

Ziemer and Rosental [48] looked at the transfer function from the wave field to the PPI-image. They investigated behavior of the image transfer function by measurement and computer simulations.

4.2 Analysis of Radar Images

The fact that marine radars give returns from ocean waves has been known for many years. Indeed, such returns (sea clutter) can pose serious problem in marine navigation [49], as they can obscure echoes from small objects such as buoys. In fact, special sea clutter controls are fitted to most commercial radar systems to facilitate the suppression of the returns from waves. Figure 4.1 shows a photograph of the radar screen (plan position indicator or PPI) in which wave images are clearly visible.

Interpretation of coherent radar signals often involves the calculation of a power spectrum or a periodogram that describes the frequency content of the data. The conventional Fourier approach, based on the work of Wiener and of Blackman and Tukey [50], relates the autocorrelation function of a signal and its power spectrum through the Fourier transform. Cooley and Tukey popularized the Fourier approach with the computationally efficient fast Fourier transform (FFT) which has dominated the analysis of radar data.

4.3 Data collection

Image data used in this study was collected by M. Allingham [51] and J. Buckley [52], throughout the Grand Banks ERS-1 SAR Wave Spectrum Validation Experiment cruise [53].

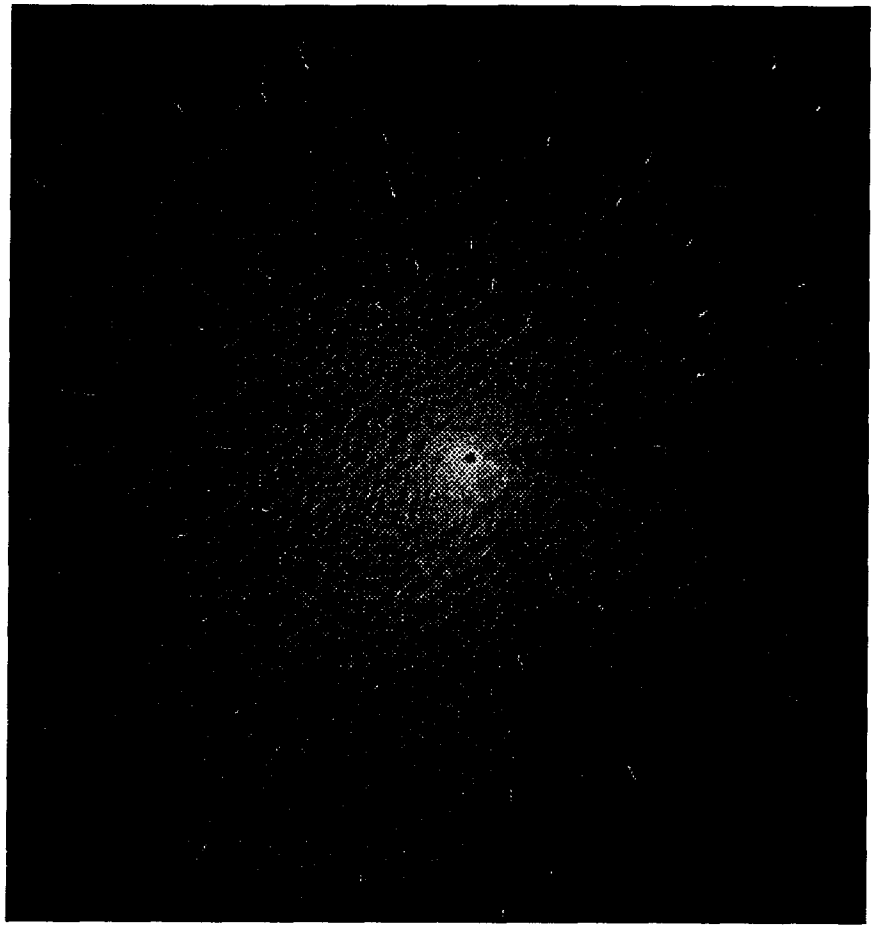

Figure 4.1: An example of radar screen

Sea surface radar backscatter data was collected by an Integrad RSC-20 radar digitizer and scan converter connected to a Racal-Decca BT362 standard ship's radar. The radar unit transmitted either 0.05μs or 0.25μs long pulses at a peak power of 25 kW and a frequency of 9.80 GHz. The antenna rotation was approximately 25 rotations per minute at a pulse repetition frequency of 1200 [52].

4.3.1 Application of Fourier Analysis to Image Spectra

Young et al.[1983] present a concise explanation of how a time series of two dimensional maps of sea surface height (or radar backscatter) can be transformed into a directionally unambiguous wave spectrum (or radar images spectrum).

M. Allingham and J. Buckley [51, 52] extracted twenty-four sub-arrays of data at 15° intervals around the ship Hudson. Each 'data cube' had dimensions of 64 by 64 pixel by 16 images, corresponding to a physical dimension of 1327 by 1327 m. The center of each sub-array lay at a distance of 64 pixels (1327 m) from the center of the main array (the ship Hudson). This distance of 64 pixels corresponds to a depression angle of about 0.7°.

Then, each array was passed to a three dimensional fast Fourier transform (FFT) routine. The output array from the FFT was then formed into a periodogram estimate of the radar determined wave spectrum by adding the squares of the real and complex transform coefficients and then summing over the positive frequency ranges (following Equation B.11). More detailed explanation of this method can be found in [51].

In Figures 4.2,4.3,4.4, an example image , its spectrum and contour plot found from 3-D FFT developed by M. Allingham [51] and J. Buckley [52] are shown. In the figures, peaks show the dominant wave frequencies and wave direction is from small peak to big peak in Figure 4.2.

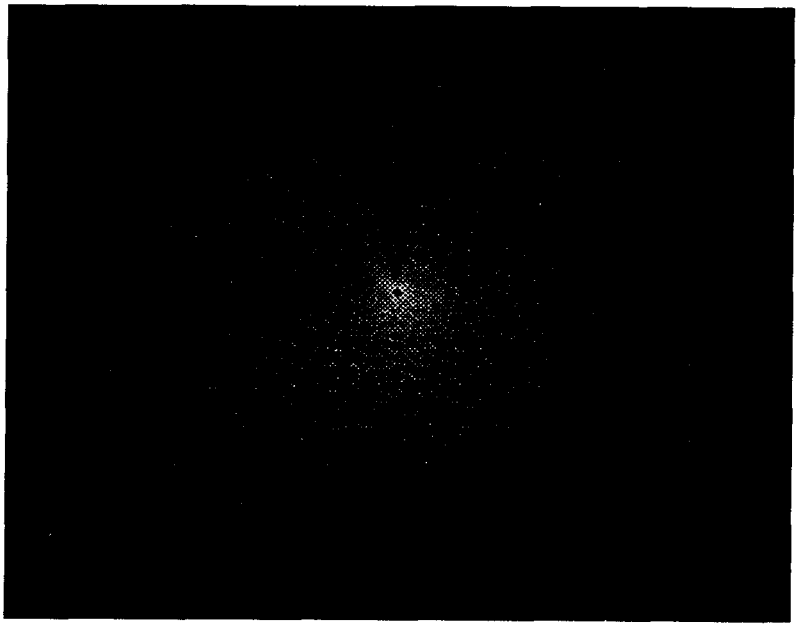

Figure 4.2: Radar image from 1130 November 23

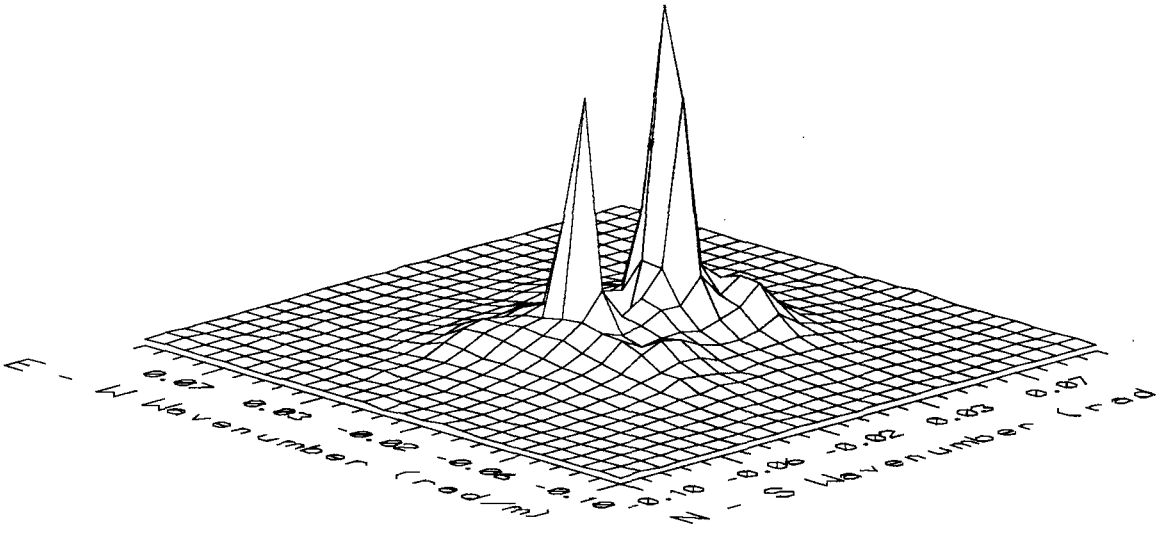

Figure 4.3: Spectrum of Radar image from 1130 November 23 (FFT)

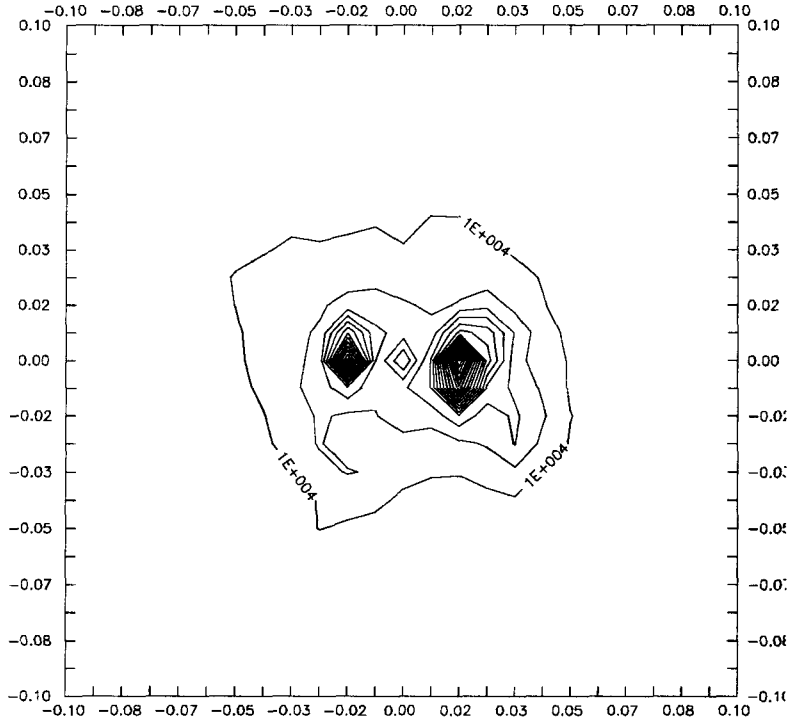

Figure 4.4: Contour plot of Radar image from 1130 November 23 (FFT)

In Figures 4.2 and 4.4, an example image , its spectrum calculated by a 3 - D. FFT technique based on Young et al [47] developed by Allingham and Buckley [51, 52] is shown. In the figures, peaks show the dominant wave frequencies and wave direction is from small peak to big peak.

Calculation of this spectrum required approximately 12 minutes on an HP 720 workstation and is therefore computationally too intensive to be operationally useful for a vessel at sea (see Appendix F). In view of the need for the wave parameters in 30 to 60 seconds, for input into the intelligent advisory system, two alternative techniques have been developed. The *boxing technique* is based on fitting a rectangle to the wave pattern on the image, while the *thinning technique* derives the wave properties from a skeleton image of the radar.

4.3.2 Boxing Technique

The stages in the *boxing technique* include those shown in Figure 4.5,

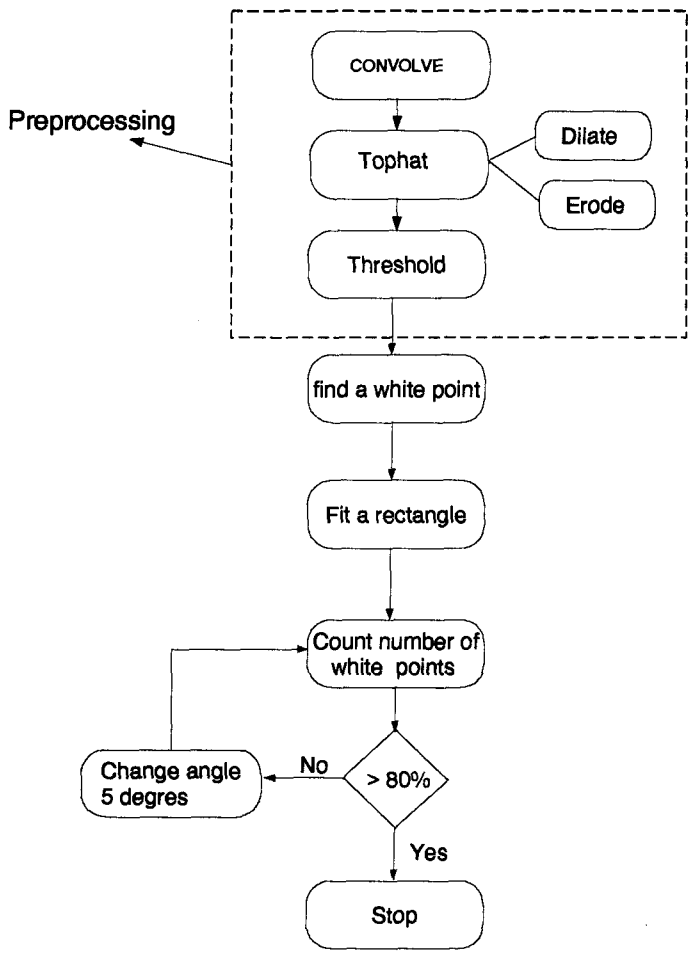

Figure 4.5: Steps for *Boxing Technique*

1. **Preprocessing** : Original images used in this analysis are in gray scale. In order to facilitate segmentation of the wave crests, a gray scale tophat process is applied to the original image in order to enhance the contrast between the crest and the trough and to merge the wave segments along the wave axis. The Tophat process consists of two different steps : Dilation and Erosion. Dilation is an operation which adds pixels to the boundary. It increases the size of the object. Erosion removes pixels from boundary. In

general, erosion and dilation are not inverses of one another. Therefore, using erosion after dilation smoothes away imperfections in wave crest boundaries.

The crests are segmented by threshold, based on a statistical analysis of the gray-level histogram of the preprocessed radar (figure 4.6). The histogram is bi-modal with modes corresponding to the crests and troughs of the wave, and the threshold is selected to minimize the within-mode/between-mode variance ratio.

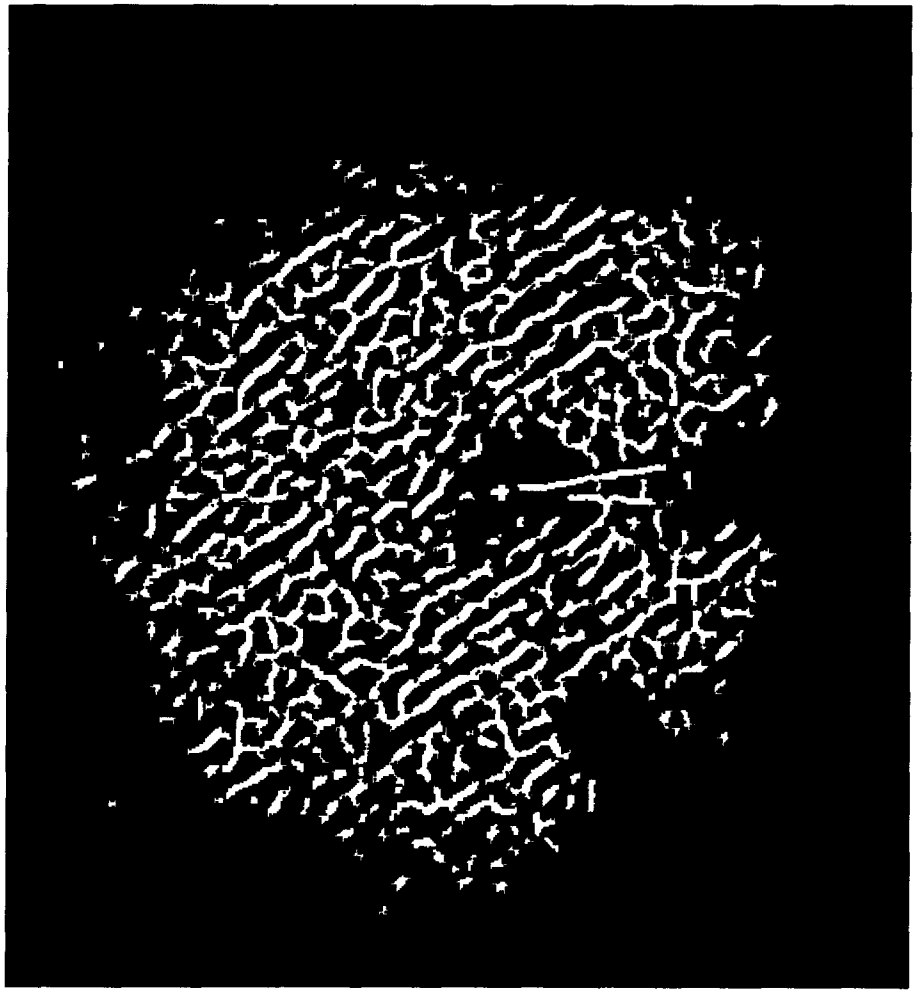

Figure 4.6: An example preprocessed image

2. **Wave Crest Orientation** : In order to find the wave orientation a white point at the border of a wave crest (binary configuration) is selected. Next, the width of the configuration is checked, and a horizontal rectangular box (11 x 50 pixels) is established around the pattern, and the number of white points in this rectangle are counted. This process is repeated as the box is rotated by 5 degree increments through an angle of 180°. The fullness of the box is used to assess the goodness of the fit between the box and the wave, and the box orientation corresponding to the best-fit between the box and the wave is selected as the wave orientation. The boxing technique is carried out at four locations in each image and the average orientation is selected.

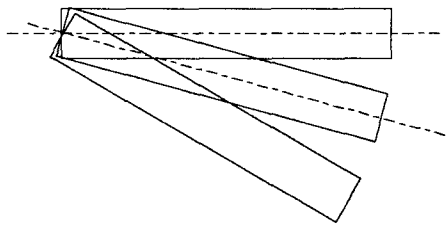

Figure 4.7: Boxing Technique

3. **Wave motion** : The wave propagation direction is found by estimating the shift between a known wave in two consecutive images. In this method, a wave pattern (a 11 x 50 window) from the first image is convolved with the second image along a line normal to the wave orientation. In this process, fit between actual image points are considered rather than comparing the fit of the chosen rectangle. An error function calculated in least squares sense is given as,

$$\text{ErrorFunction} = \sum_{1}^{n}(x_i - x_j)^2 \tag{4.1}$$

where x_i and x_j are pixel values in the first image and second image, respectively.

The shift in window position between successive images that corresponds to the minimum error gives the wave motion direction.

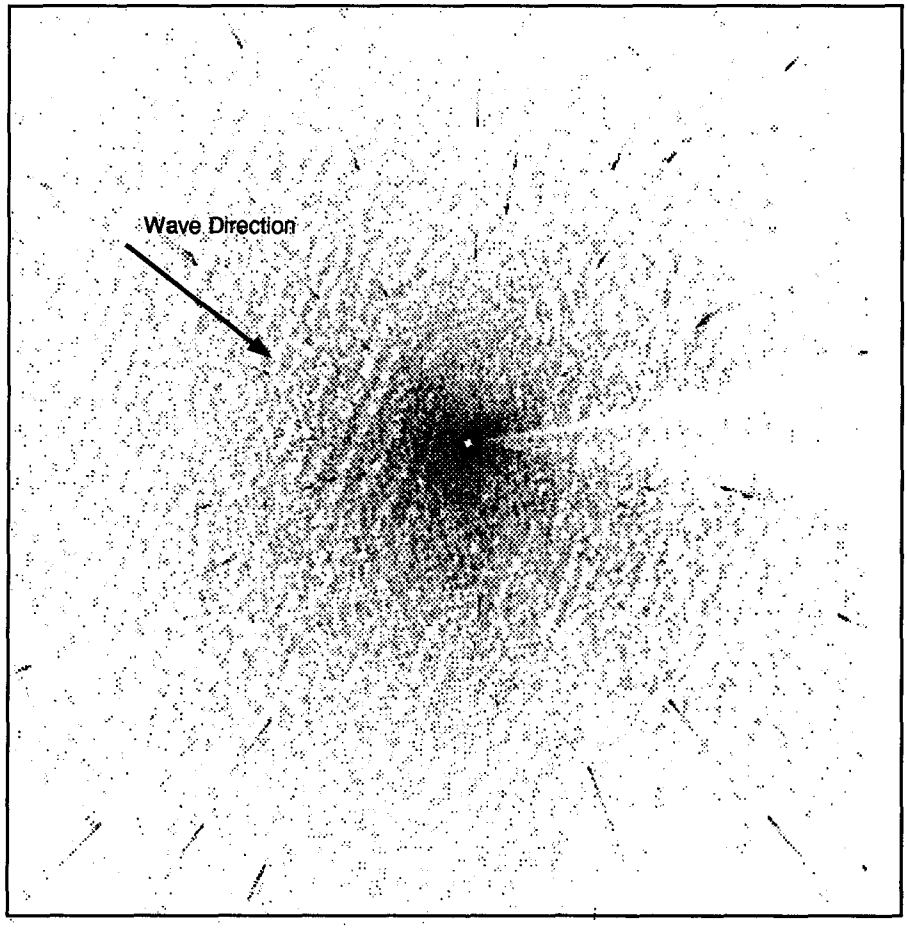

Figure 4.8: Wave direction calculated using ***boxing technique.***

4. **Wave Frequency** : The unprocessed gray-level radar image is used to calculate the frequency of the dominant wave. Wave frequencies are found based on the selected wave orientation, the image points along a line that is orthogonal to the wave orientation are extracted from the image for spectral analysis. The FFT technique is used to calculate the wave numbers . Then frequencies are found by using dispersion relation.

$$\omega = \sqrt{gk \tanh(kd)} \tag{4.2}$$

where k is wave number and d is water depth.

The success of the boxing technique depends on the initial placement of the rectangular box. The radar images tend to have limited regions in which the wave directions are obvious since there is considerable noise in the images and much of the wave information is obscured. The *boxing technique* works well if the box is placed in the vicinity of an obvious wave, although reliable automatic placement of the box remains as a problem. To improve the above procedure, a more global *thinning technique* has been developed.

4.3.3 Thinning Technique

The stages involved in the *thinning technique* include (Figure 4.9),

1. **Preprocessing** : This process is as described for the *boxing technique.*

2. **Wave Crest Orientation** : The binary radar image is transformed by the thinning process. In this process, boundary pixels are removed from the wave patterns whilst retaining connectivity. Thinning stops when no further pixels can be removed without causing loss of continuity. Consequently, the thinning algorithm needs to traverse the entire object boundary, marking pixels which are candidates for removal and remembering how many times each has been visited. Those candidates which have been visited only once are then removed. This process continues until only the skeleton or spine of each

object remains.

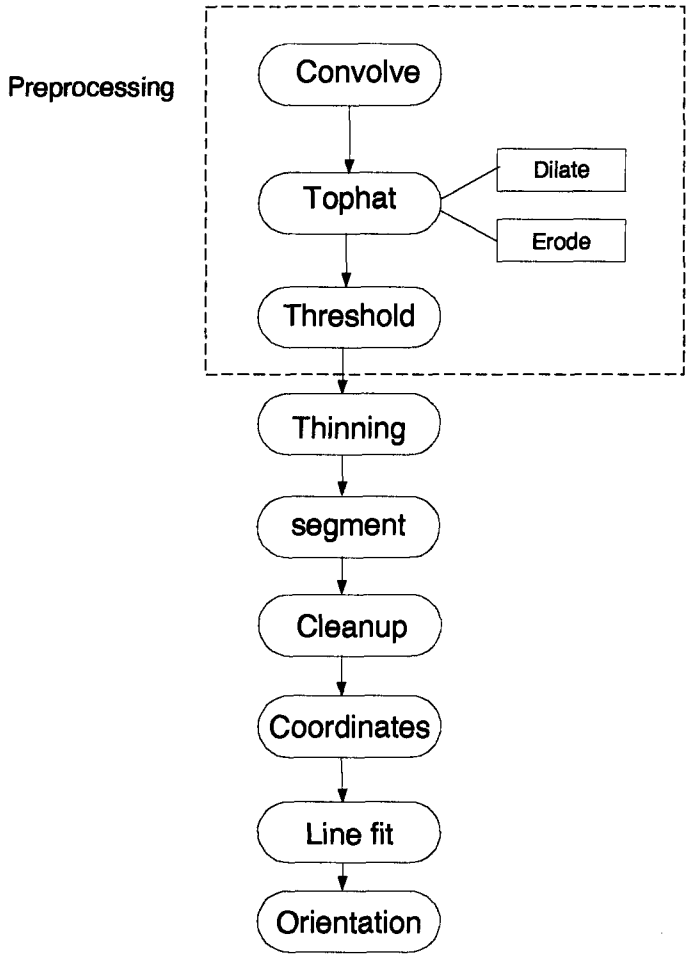

Figure 4.9: Steps for *thinning technique*

The thinned image for the radar image of Figure 4.8 is illustrated in Figure 4.11.

The skeletons run along the length of the objects corresponding to waves. Since there is considerable cross-linkage between waves in the binary image because of noise, shorter skeleton segments are evident in a direction normal to the wave. The skeleton of the entire radar image is then decomposed into distinct unconnected segments by removing all branch-points on the skeleton and all the small segments (less than 20 pixels) are removed. These individual segments are assessed in order to determine the

dominant wave orientation. The complexity of each segment is considered by measuring the curvature of the individual segments. Each segment that is sufficiently linear is fit with a a straight-line using the points on the segment.

The following images (Figures 4.10, 4.11, 4.12) show the intermediate steps for the same radar image for the *thinning technique* .

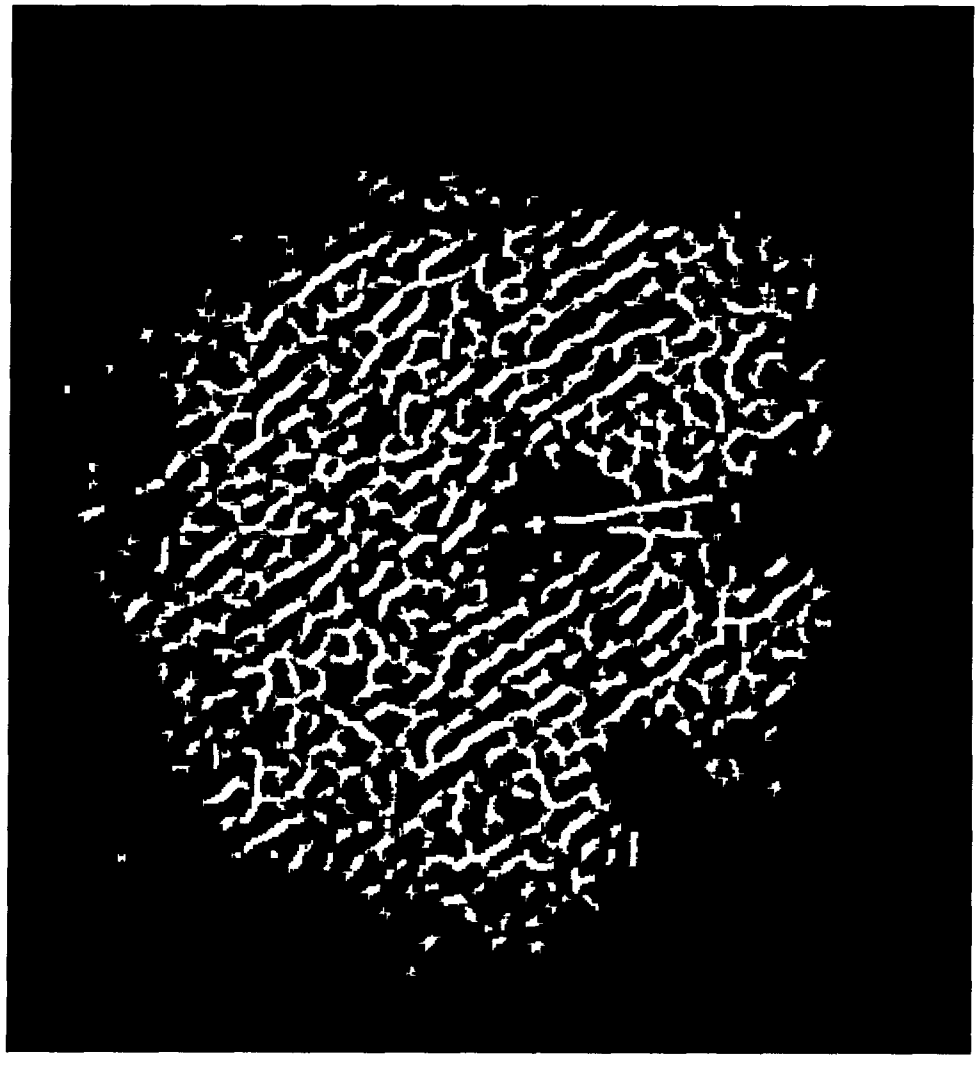

Figure 4.10: An example image after thresholding

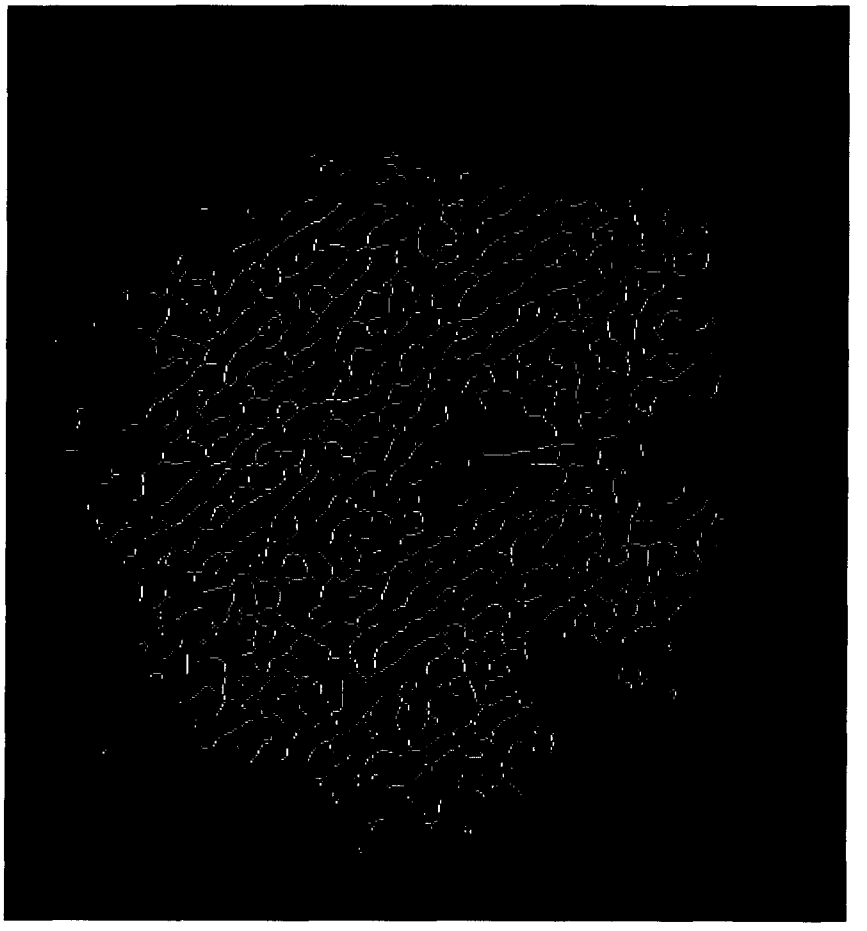

Figure 4.11: An example image after thinning and segmentation

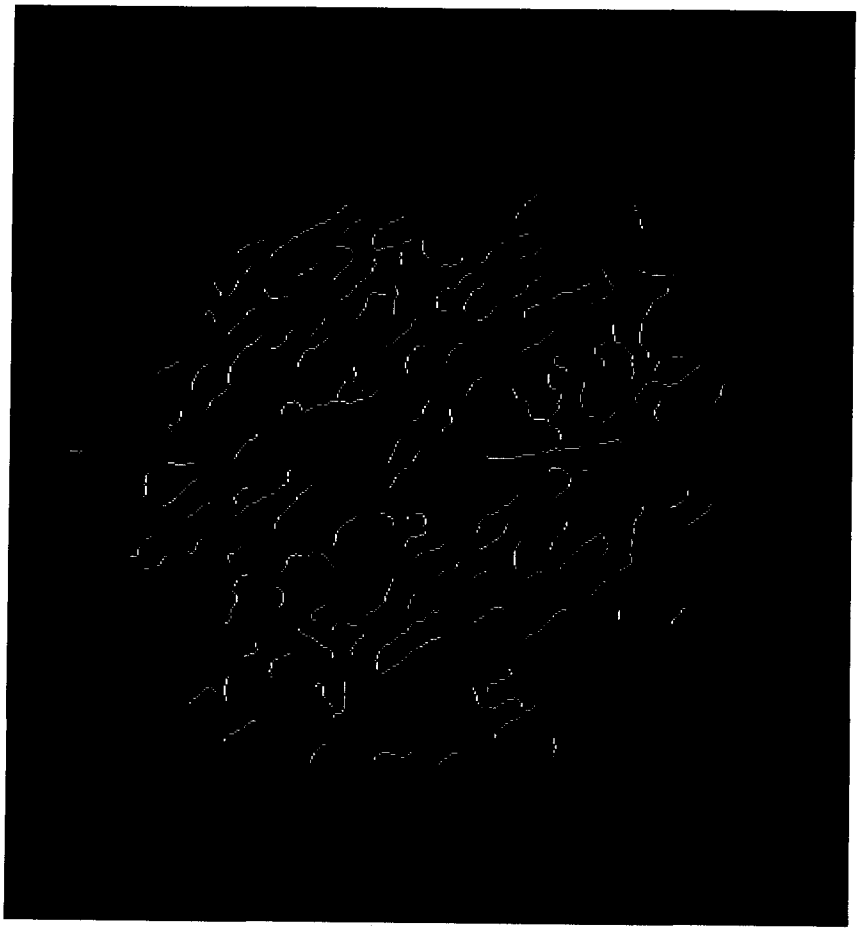

Figure 4.12: An example image after the cleaning process

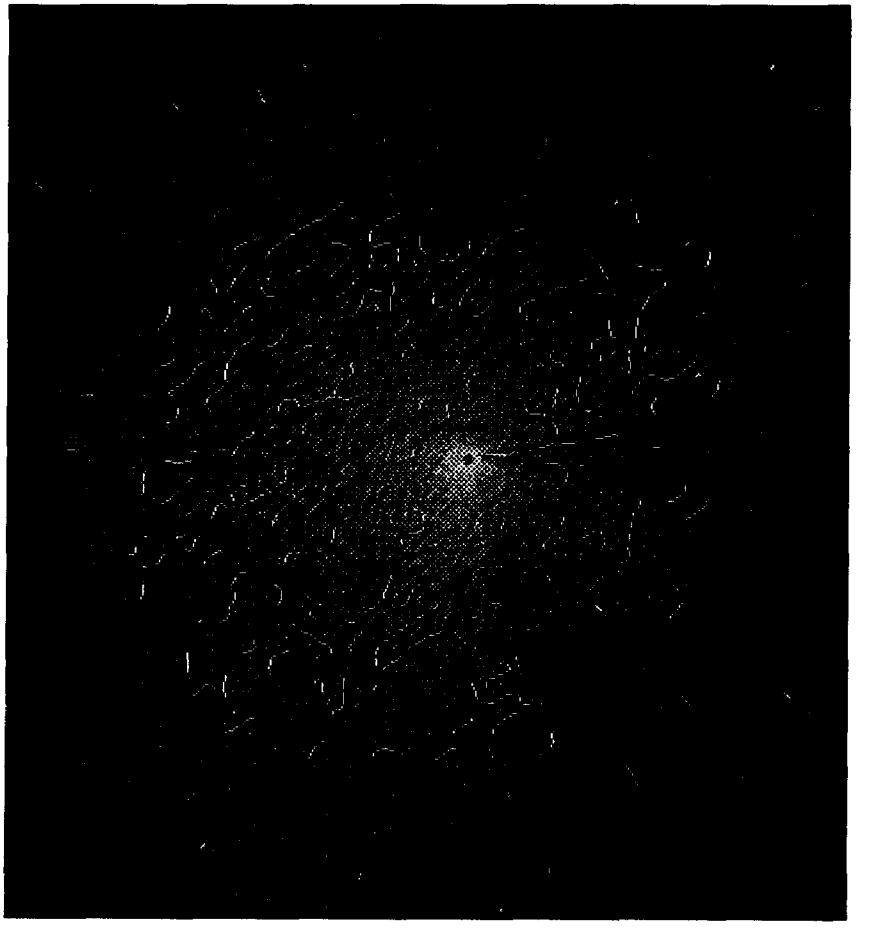

Figure 4.13: An example wave segments with original image

As seen from Figure 4.13, the lines selected correspond to the wave troughs not wave crests. In order to find wave crest, we needed to get rid of the center white blob caused by the ship, this increased the processing time. But finding wave troughs solved this problem completely.

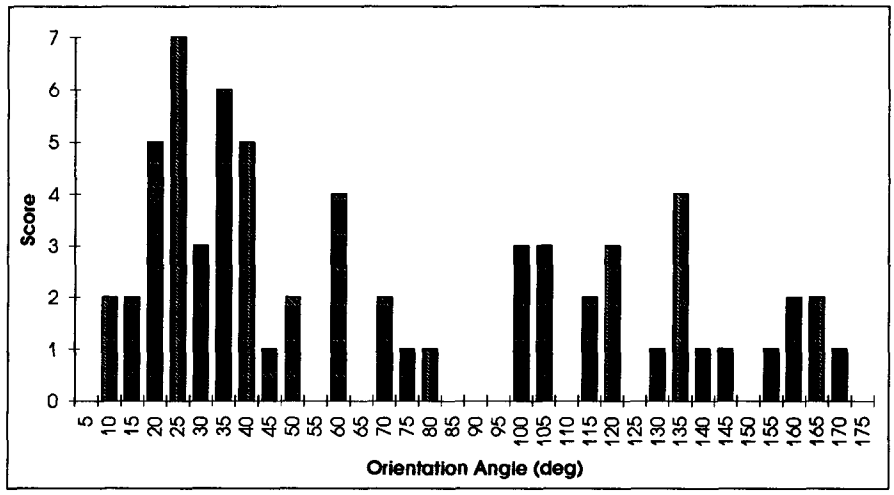

Figure 4.14: A histogram of wave orientation

As seen from Figure 4.14, a histogram of wave orientations is maintained, and the goodness-of-fit and the length of each segment are used to bias the histogram entries. The wave orientation corresponding to the peak in the histogram is selected as the dominant wave direction.

3.Wave Motion :

Once the dominant wave orientation for a set of successive images has been determined, a small region of an image in the vicinity of the dominant waves is compared with neighboring regions in successive image.

This process is illustrated in Figure 4.15. Since the wave orientation is known from stage 2, comparisons between the initial image region and regions in successive images are restricted to shifts along the line normal to the wave orientation. The least-squares error between the regions is used as the basis for selecting the wave direction.

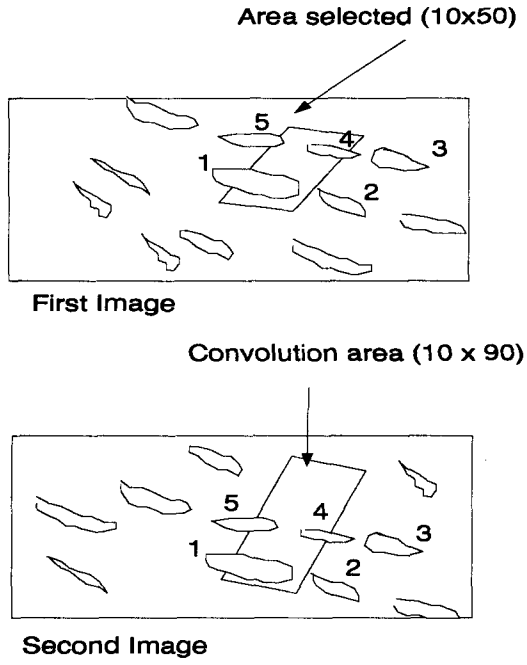

Figure 4.15: Finding wave direction

4.**Finding the Wave Frequency** : This step is as described for the *boxing technique.*

4.3.4 Comparison of Image Processing Techniques

It is important to clarify what each type of spectrum represents. A two dimensional ocean surface elevation spectrum (wave spectrum) contains information regarding the frequency / wave number distribution of the ocean wave potential energy and its direction of propagation. The analysis of pitch/roll/heave buoy measurements give such a two dimensional wave spectrum. On the other hand, a radar image spectrum found from FFT, *boxing* or *thinning techniques* is a two dimensional spectrum of the radar image of the sea surface, not a spectrum of the actual sea surface energy. Radar image spectra represent the square of the backscattered radar energy.

Thirty radar image sequences are used to compare these techniques. The list of these images can be found in appendix E.

As seen from Table 4.3.4, the frequencies and direction found from the *thinning technique* are very close to those found from conventional methods such as Fourier Transform (FFT), wave buoy (Wavec) and satellite (ERS-1). Table 4.3.4 also shows the required computation time. Fourier transforms are computationally expensive methods. For example, analysing an image data (usually 512 x 512 X 16) can take about an hour, the FFT based method developed by Allingham and Buckley takes about 12 min to find wave direction and frequencies. But these methods are not fast enough to use in a monitoring system that is developed in this study. The two techniques developed take about 30 - 60 seconds.

Time	Wavec [1]		ERS-1		FFT		*Thinning*	
	Freq.	Dir.	Freq.	Dir.	Freq.	Dir.	Freq.	Dir.
	(Hz)	(Deg.)	(Hz)	(Deg.)	(Hz)	(Deg.)	(Hz)	(Deg.)
1112 Nov. 12	0.084	201	-	-	0.067	180	0.070	175
	0.110	159	-	-	0.106	157	0.108	160
1128 Nov. 20	0.168	80	0.12	86	0.124	71	0.110	70
	0.094	215	0.084	244	0.083	225	0.811	215
1130 Nov. 23	0.139	160	0.107	122	0.110	139	0.120	120
	0.120	71	0.108	76	0.107	43	0.110	35
Computation Time	-	-	-	-	12 min[2]		30 - 60	sec

Table 4.1: An comparison of the present methods with other conventional methods

[1] Wavec , ERS-1 and FFT values are taken from [51]

[2] This time is for the FFT method explained in [51], [52], other methods would take about an hour

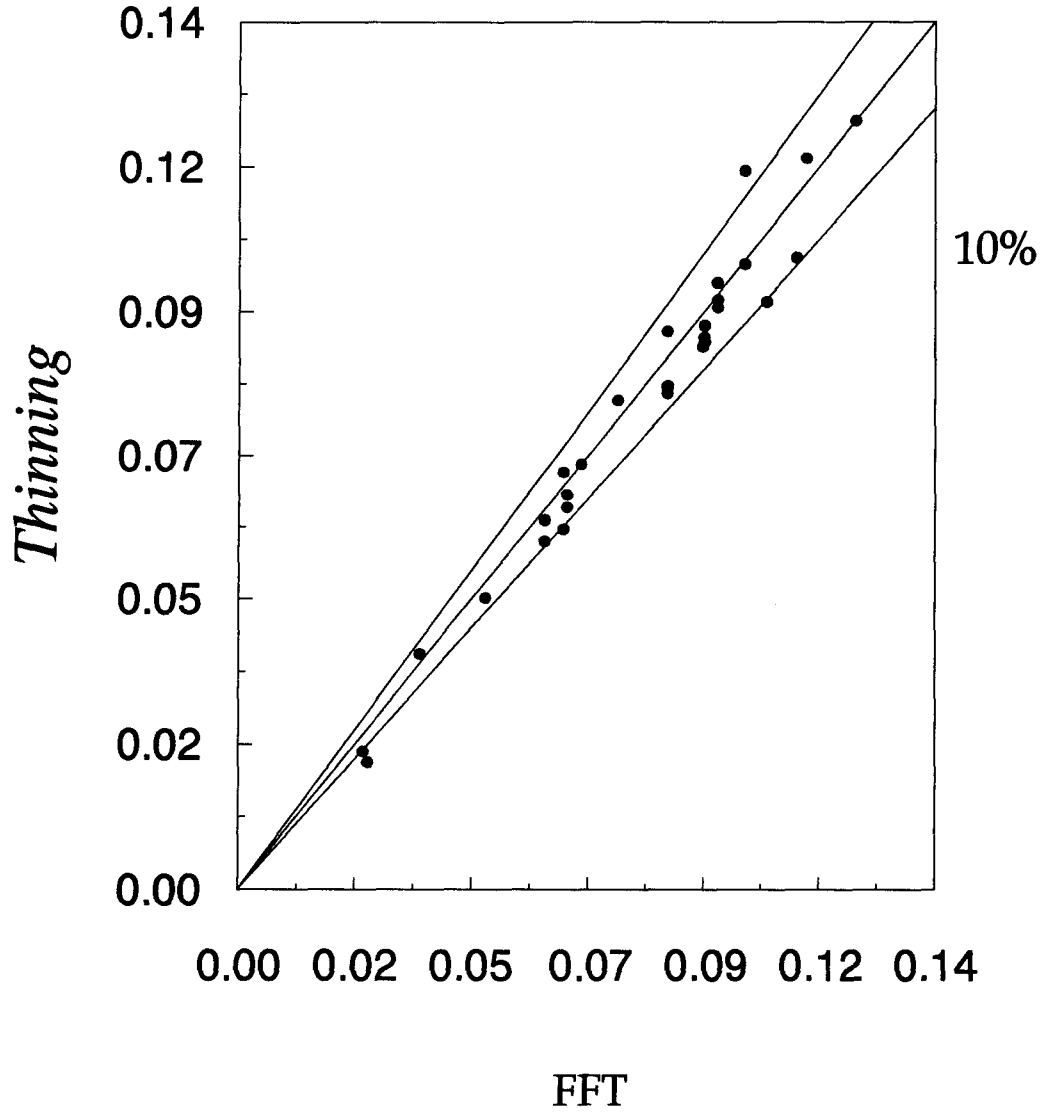

Figure 4.16: Difference in calculation of frequencies between FFT and Present method

4.3.5 Conclusion of Measurement of Wave Properties

In this chapter, as a part of the monitoring system, two new techniques (*boxing* and *thinning techniques* were developed to find wave direction and frequencies from ship radar. Although the *boxing technique* is easy to implement, it has limitation of being

local. That is, the accuracy of the method depends on the selected position of the box. The *thinning technique* is more global and captures more of the overall variations in the wave patterns.

The histogram found from the *thinning technique* is suitable for the Fuzzy Expert System used in this study. The peaks of the histogram found from the *thinning technique* are used as membership functions of wave parameters

The primary advantages the *boxing* and *thinning techniques* have over 3-D FFT is the reduced computational time of operation. Finding wave parameters with the 3-D FFT method can take about 12 min[3] on an HP 720 work station. But the techniques developed take about 30-60 seconds on a 486-50 based PC.

[3]If the FFT method developed by Allingham and Buckley is used, otherwise it would take about an hour

Chapter 5

Ship Dynamics

5.1 Estimation of Wave Height

This section discusses wave height calculations for usage in the monitoring and Advisory system.

There are three common ways of estimating wave height from a ship.

1. Visual observation
2. Ship-shore communication
3. Onboard system

1. Visual observation :

   The most basic and ancient source of data on waves is the visual observations made on board ships. The accuracy of these observations may vary from officer to officer depending on his relative experience.

   Observers tend to underestimate the heights of following seas and overestimate head seas because of the difference in ship behavior, and the periods reported are often influenced by the ship's natural pitch period [13].

   Although this method of observation is subjective and crude, when data are collected over a wide area by radio and redistributed to all participating ships, the data do have a limited usefulness in establishing seastate conditions and in short range storm avoidance.

2. Ship-shore communications :

   The transmission of weather conditions and gale warning bulletins, using conventional communication channels available on board have, for many years, been major means of advising the captain of the expected weather conditions ahead.

   A typical example of a facsimile recorder output, giving wave height contours over the Atlantic, is shown in Figure 5.1. Though the picture is of a rather general nature, it does indicate expected wave heights of a storm advance. Such information is, in most cases, better than none; however it can also lead to wrong interpretations since the chart is limited to the wave height and does not provide any information with regard to the period of the wave, which is a major factor affecting the response of the ship. In spite of the explained disadvantages, this informations can be useful for routing or avoiding storm.

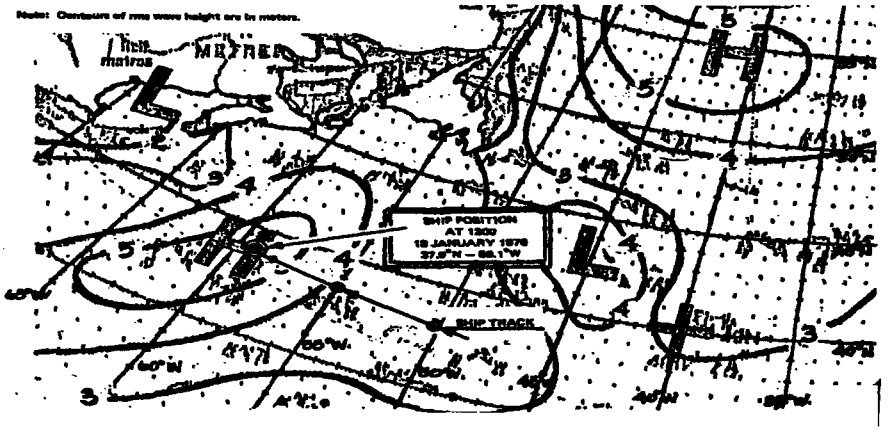

Figure 5.1: An facsimile recorder output printed onboard Lash Italia

3. Onboard systems

The use of the ship itself, as a means of measuring the encountered wave system, is not necessarily new and the Ship Board Wave Recorder (SBWR), otherwise known as Tucker wave meter [54], has been in use for the past 30 years. The data obtained from these ships, after some additional processing, constitutes the backbone of design wave data available today [13].

A similar approach for using the ship responses as a means of determining the encountered wave system is by way of utilizing the response spectra obtained from measurements on board and the response amplitude operator (RAO) of that specific response to obtain the wave spectra. The method is refered to as a "reverse procedure".

The response of a ship at 0 speed to a given sea spectrum and heading is:

$$\mathrm{RES}^2 = \int_0^\infty \int_\chi \mathrm{RAO}^2(\omega,\chi) S_\xi(\omega,\chi_i) d\chi d\omega \tag{5.1}$$

where RAO (ω,χ) is the response amplitude operator as a function of frequency (ω) and heading (χ) to the component wave, and $S_\xi(\omega,\chi_i)$ is the spectral ordinate as a function of frequency and component direction.

At a specific frequency, equation 5.1 reduces to :

$$\mathrm{RES}^2 = \int_\chi \mathrm{RAO}^2(\omega,\chi) S_\xi(\omega,\chi_i) d\chi \tag{5.2}$$

where RES is the response of the vessel. The short-crested spectrum may be represented as the product of a point spectrum and a spreading function $\mathrm{SF}(\chi_i)$:

$$S_\xi(\omega,\chi_i) = S_\xi(\omega)\mathrm{SF}(\chi_i) \tag{5.3}$$

If the above representation of a short-crested spectra is assumed, equation 5.2 can be written as:

$$\mathrm{RES}^2(\omega) = \int_\chi \mathrm{RAO}^2(\omega,\chi) S_\xi(\omega) \mathrm{SF}(\chi_i) d\chi \tag{5.4}$$

Since the point spectrum is independent of χ, the expression becomes

$$\mathrm{RES}^2(\omega) = S_\xi(\omega) \int_\chi \mathrm{RAO}^2(\omega,\chi) \mathrm{SF}(\chi_i) d\chi \tag{5.5}$$

Solving for the spectral ordinate :

$$S_\xi(\omega) = \frac{\mathrm{RES}^2(\omega)}{\int_\chi \mathrm{RAO}^2(\omega,\chi)\mathrm{SF}(\chi_i) d\chi} \tag{5.6}$$

The derivation for the forward speed case is similar, with equation 5.6, becoming :

$$S_\xi(\omega) = \frac{1}{J} \frac{\mathrm{RES}^2(\omega_e)}{\int_\chi \mathrm{RAO}^2(\omega,\chi)\mathrm{SF}(\chi_i) d\chi} \tag{5.7}$$

where

$$\begin{aligned} J &= (1 - 4V\cos(\chi)\omega_e/g)^{\frac{1}{2}} \\ \omega_e &= \omega - \frac{\omega^2 V \cos(\chi)}{g} \end{aligned} \tag{5.8}$$

where V is forward speed.

This equation offers the principle of a method for estimating the sea spectrum from a ship's response to waves. Since finding motion spectra requires a long time, the RAO is used to estimate wave height from the estimated heave amplitude ($Z_{1/3}$).

The RAO (response amplitude operator) of a ship for each wave direction and speed can be obtained from either experiments or ship motion programs. In this study shipmo.for [55] was used to obtain RAO. An example RAO is given in Figure 5.1.

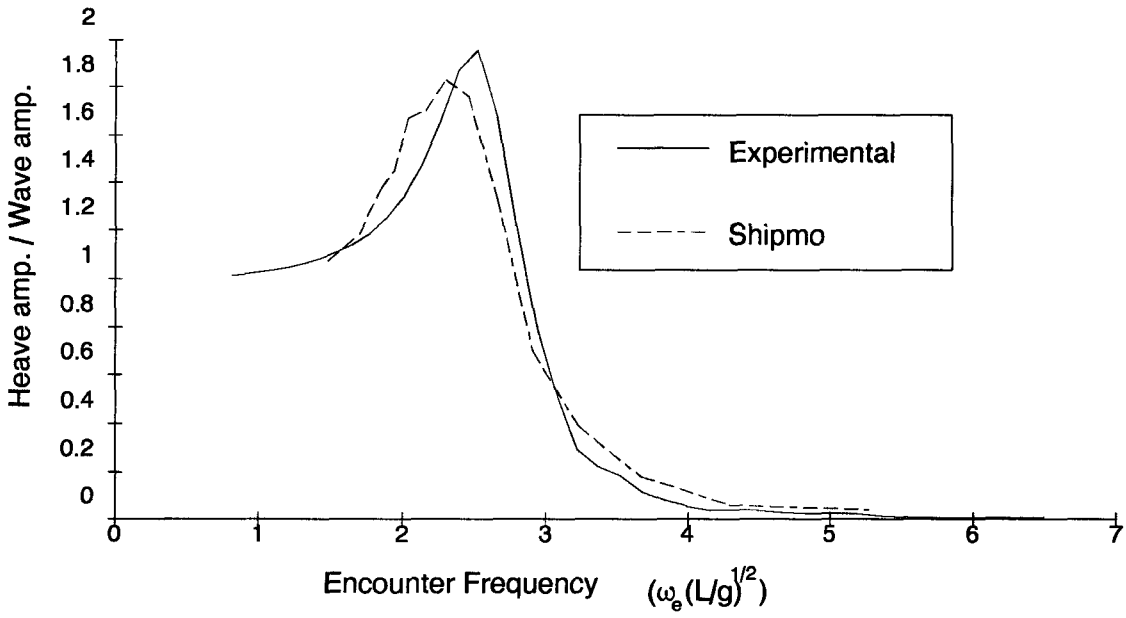

Figure 5.2: An example RAO for heave motion of UBC series model #2

Figure 5.1 shows a general comparison of estimated and experimentally found RAOs for 12 UBC series. As seen from this figure, estimated results are within %10 of experimentally found results. Therefore, for such a ship, theoretical RAO's can be used to estimate wave height.

As seen from Figure 5.1, this operator gives relative ship motion with respect to non-dimensional encounter frequency. Since encounter frequency can be found from radar image processing (see in Chapter 4), the only unknown in this equation 5.7 to find wave height is heave amplitude.

Heave motion data (Figure 5.4) is used to find estimated heave amplitude ($Z_{1/3}$). To

find ($Z_{1/3}$), heave amplitudes are put in descending order. The average of 1/3 of the maximum heave amplitudes is used as the estimated significant heave amplitude.

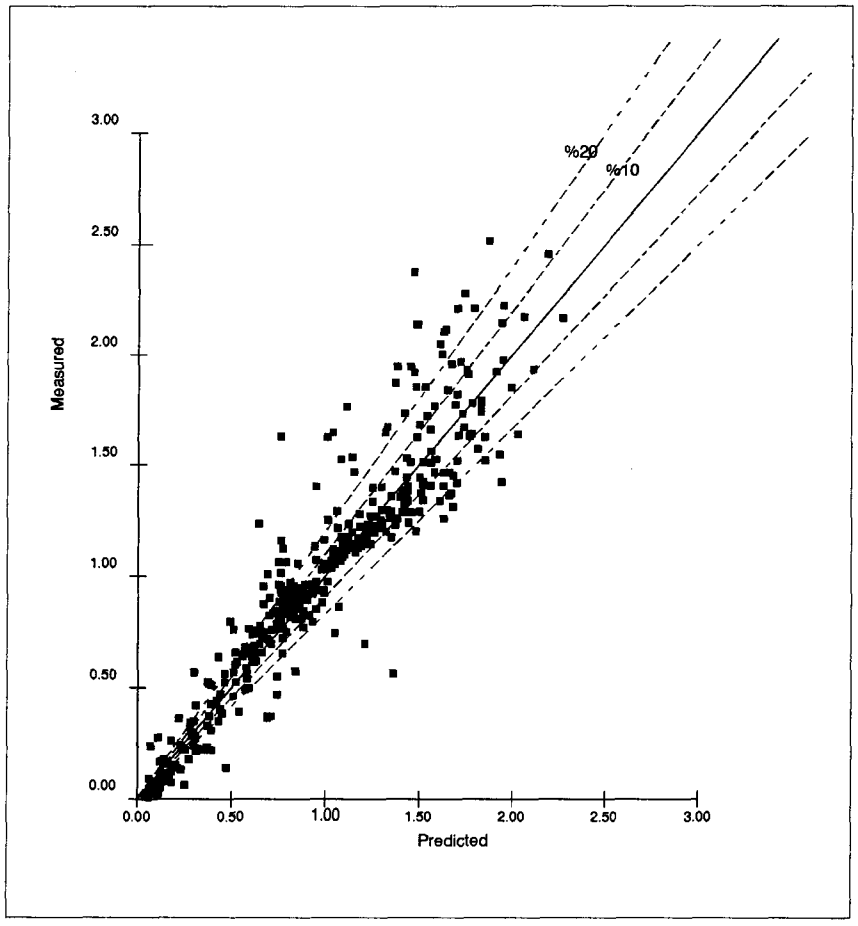

Figure 5.3: Comparison of experimental and estimated RAOs for UBC series

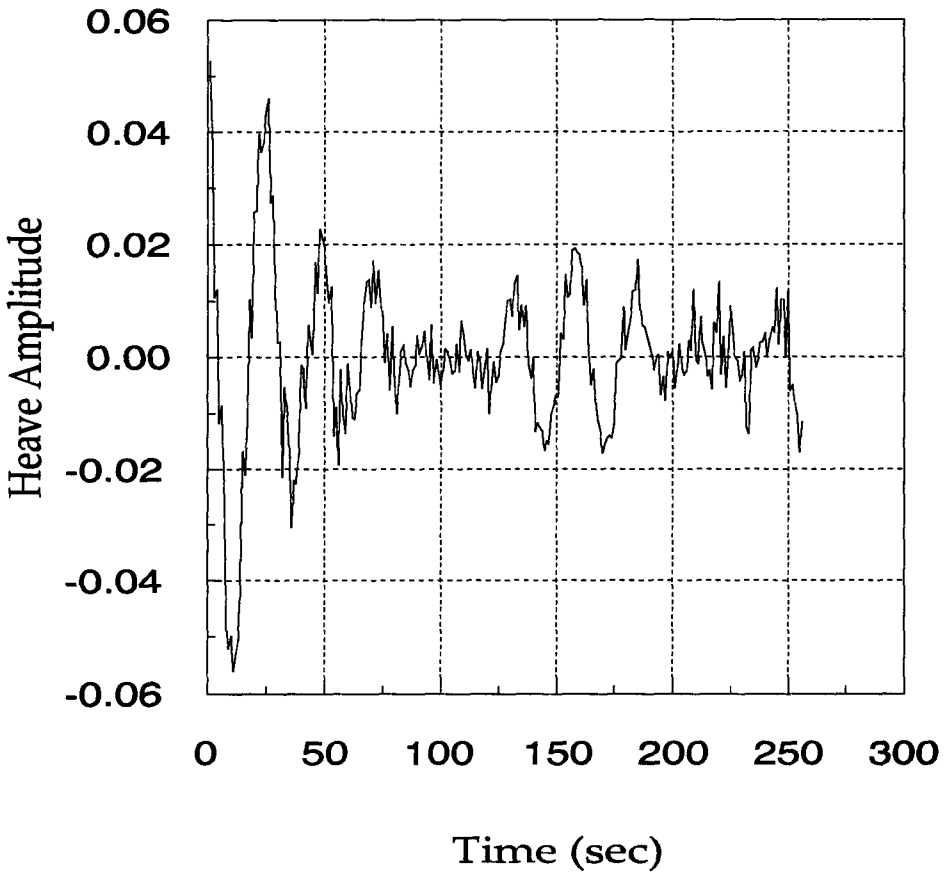

Figure 5.4: Typical recorded heave motion data for UBC #2

Estimated wave heights by using the above explained technique are given in Figure 5.5 and Table 5.1. It can be seen from Figure 5.5, that the error in estimation of wave height is less then %10.

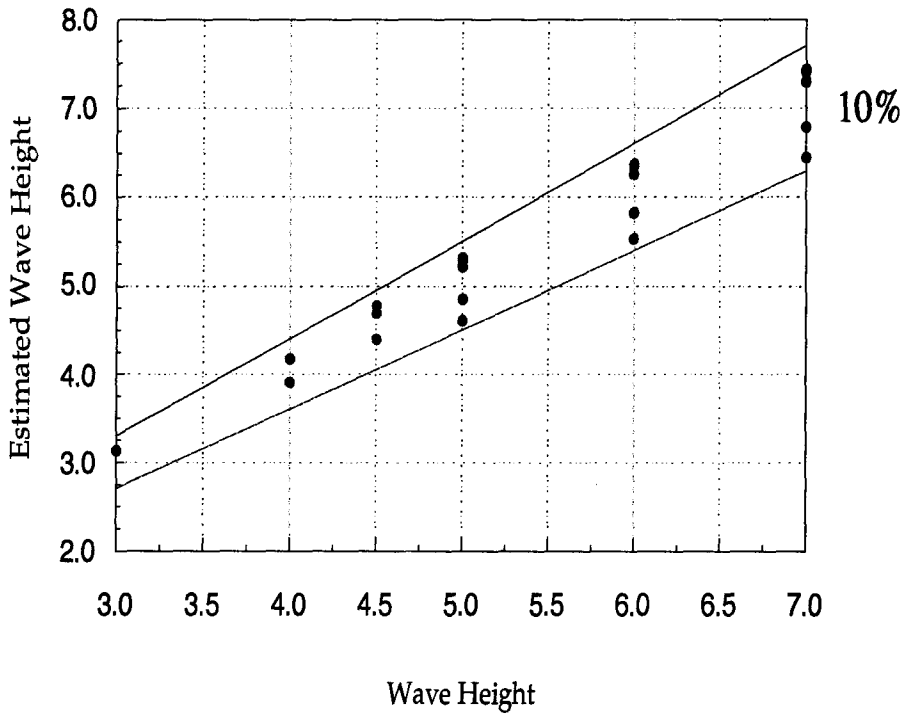

Figure 5.5: Estimation of wave height

Sig. Wave Height (m)	Wave Period	Estimated wave height (m)	error (%)
2	7	1.842	7.9
2	9	1.940	3.0
2	11	2.085	4.3
3	8	3.128	4.2
3	11	3.128	4.2
4	8	3.907	4.3
4	11	4.171	2.3
4.5	8	4.396	2.3
4.5	11	4.692	4.2
4.5	15	4.779	6.2
5	7	4.607	7.8
5	9	4.851	2.9
5	11	5.214	4.27
5	13	5.288	4.27
5	15	5.310	6.21
6	7	5.527	7.876
6	9	5.822	2.97
6	11	6.256	4.27
6	13	6.346	6.21
6	15	6.372	6.21
7	7	6.448	7.87
7	9	6.792	2.97
7	11	7.299	4.27
7	13	7.403	5.76
7	15	7.434	6.21

Table 5.1: Estimated wave heights

5.2 Roll Natural Frequency

It is assumed that the vessel rolls at its natural frequency when excited by random waves. Therefore, the peak in the spectrum of roll motion corresponds to the roll natural frequency.

The two most popular ways of finding spectrum of a time series are Fourier Transforms and Maximum Entropy method. Comparison of these two methods is given in Table 5.2.

Feature	Fourier Transfoms	Maximum Entropy method
Spectral window effets	Convolution of window spectrum with true signal spectrum reduces resolution and allows leakage through window sidelobes	No window effect since autocorrelation function is estimated for all lags
Linearity of spectrum	Spectral estimation is linear	Estimation is nonlinear
Accuracy of frequency estimation	To within $\pm 1/2N\Delta t$	Not easily defined, but can be estimated very closely
Resolution of closely spaced frequencies	Propotional to $1/N$	Data dependent, but resolution approximately proportional to $1/N^2$

Table 5.2: Comparision of Maximum Entropy method and Fourier transforms

As seen from the above table, the Maximum entropy method (MEM) can estimate natural frequencies accurately and distinguish closely spaced frequencies. Therefore, this method is used to find the natural roll frequency of a ship.

5.2.1 Maximum Entropy Method

Choosing the best spectral-domain representation of a truncated discrete time series, for which only an imperfectly determined autocorrelation function can be calculated, is a major problem in signal analysis. Among the countless spectra that may be consistent with a given autocorrelation function, only one spectrum can be optimal. A set of rules governing that choice must be established.

Jaynes [56] introduced a method of statistical inference called the " maximum entropy estimate". He showed that information theory (Shannon and Weaver, 1949) provides a criterion for selecting the best statistical description of a process when only a partial knowledge of that process is available. The optimal choice is the only one which is maximally non-committal with regard to any missing data, and which is simultaneously constrained to be consistent with all available data. The result is the best estimate that

could have been made on the basis of the data at hand.

The application of maximum entropy spectral analysis has met with considerable success in geophysics. Burg [57, 58] presented the formulation resulting from the application of entropy consideration to spectral determinations and also a method of computing the required prediction error coefficients. The maximum entropy method (MEM) using the Burg algorithm was applied by Ulrych [59], who showed the resolution properties of this approach.

Theoretical considerations concerning the development of MEM have been presented by Barnard [60], Edward and Fitelson [61], Smylie et al. [62].

The maximum entropy MEM spectrum of a stationary, random, uniformly sampled process is found as the spectrum that results from maximizing the entropy of that process.

In applying the concept of maximum entropy to spectral analysis we begin with the relationship between the entropy (strictly speaking, the entropy rate for an infinite process) and the spectral density S(f) of a stationary Gaussian process.

$$H = \frac{1}{4f_N} \int_{-f_N}^{f_N} logS(f)df \tag{5.9}$$

where f_N is the Nyquist frequency. The derivation of equation (5.9) is shown in detail in [62] . Rewriting (5.9) in terms of the autocorelation $\phi(k)$ of the process gives

$$H = \frac{1}{4f_N} \int_{-f_N}^{f_N} log[\sum_{-\infty}^{\infty} \phi(k)exp(-i2\pi fk\Delta t)]df \tag{5.10}$$

where Δt is the uniform sampling rate. Maximizing equation (5.10) with respect to the unknown $\phi(k)$ with the constraint that S(f) must also be consistent with the known autocorrelation $\phi(k), \ldots, \phi(M-1)$ results in the MEM spectral estimate. This estimate expresses maximum uncertainty with respect to the unknown but is consistent with the known information.

The variational procedure leads to the well known expression for the MEM spectral density [62] and [61], which for a linear process x_t is

$$S(f) = \frac{2\sigma^2}{\left|1 - \sum_{k=1}^{P} A_k exp(-i2\pi k f_0 \Delta)\right|^2} \tag{5.11}$$

In (5.11), P_M is a constant and the α_i are prediction error coefficients that are determined from data. Estimations of the A_k and M are given in Appendix C.

Assuming for the moment that parameters A_k and σ^2 are known, it is found that equation 5.11 is actually a closed-form analytic equation for the response spectrum. Consequently, the search for relative maxima of the spectrum can be accomplished with the aid of a classical result from calculus which states that the derivative of a function is zero at an extremum. Since the spectrum is available in function form, one can locate any relative extrema of the power spectrum (i.e. relative maxima or minima) by solving

$$\frac{dS(f)}{df} = 0 \tag{5.12}$$

All frequencies which form the solution set of equation 5.12 must corresponds to extrema of the spectrum. Thus, this set of frequencies, which will be known as the set of critical frequencies, contains the natural frequency estimates.

Before substituting the equation for MEM spectrum into equation 5.12, it is convenient to recast equation 5.11 in to a form more easily manipulated.

$$|1 - \sum_{k=0}^{p} A_k e^{-j2\pi k f \Delta}|^2 = \rho_0 + 2\sum_{k=1}^{p} \rho_k \cos(2\pi k f \Delta) \tag{5.13}$$

where :

$$A_0 = 1 \tag{5.14}$$

$$\rho_k = \sum_{i=0}^{p-k} A_i A_{i+k}$$

The accuracy of this identity can be demonstrated by a straight forward manipulation involving an interchange of summation order. Alternatively, if the coefficients A_k are viewed as a time series, the ρ_k can be interpreted as an autocorrelation function of the A_k's. Thus equation 5.13 is simply a restatement of the well known relationship between the Fourier Transform of a time series (ie.$A_0, A_1, \ldots, A_\rho$) and the Fourier Transform of its autocorrelation function (ie. ρ_k). Utilizing the identity of equation 5.13, the pth order MEM spectrum can be written as:

$$S(f) = \frac{\sigma_p^2 \Delta}{\rho + 2\sum_{k=1}^{p} \rho_k \cos(2\pi k f \Delta)} \tag{5.15}$$

After substituting equation 5.15 into equation 5.12 and evaluating the derivative, the following result is obtained

$$\frac{\sum_{k=1}^{p} k\rho_k \sin(2\pi k f \Delta)}{|\rho_0 + 2\sum_{k=1}^{p} \rho_k \cos(2\pi k f \Delta)|^2} = 0 \tag{5.16}$$

One set of solutions for equation 5.16 is obtained by finding all frequencies that cause the denominator to become infinite. However, comparing the denominators of equation 5.16 and 5.11, it is found that any solution, f_0, obtained from the denominator of equation 5.16 becoming infinite, corresponds to a zero in the spectrum (ie. S(f) =0). Since this condition is of no value in estimating peaks of the spectrum, the numerator of equation 5.16 must include all solutions which corresponds to maxima of the spectrum. Thus any frequency which corresponds to a relative maximum of the spectrum must also be a solution of equation 5.17.

$$\sum_{k=1}^{p} k\rho_k \sin(2\rho k f \Delta) = 0 \tag{5.17}$$

Conversely, any frequency which is a solution of equation 5.17 must corresponds to an extremum of the spectrum.

While the solution set of equation 5.17 includes both maxima and minima (excluding zeros of the spectrum) it is a relatively simple task to determine which type of extrema a given solution corresponds to. One way of checking the solution type is to simply plot the spectrum and verify the extrema graphically. Since, this method is not suitable for this study, another method which uses second derivatives employed for determining the solution types. This method identifies maxima and minima of a function with positive and negative second derivatives of the function respectively. Accordingly, the second derivative of the pth order MEM spectrum evaluated at f_0, a solution of equation 5.17, is given by

$$\frac{d^2 S(f)}{df^2}\Big|_{f=f_0} = \frac{4\pi\sigma_p^2\Delta^3 \sum_{k=1}^{p} k^2\rho_k \cos(2\pi k f_0 \Delta)}{[\rho_0 + 2\sum_{k=1}^{p} \rho_k \cos(2\pi k f_0 \Delta)]^2} \tag{5.18}$$

Since the denominator of equation 5.18 is always positive, the sign of the second derivative is decided by the numerator. Consequently, the second derivative test can be written as

$$\sum_{k=1}^{p} k^2\rho_k \cos(2\pi f_0 \Delta) \begin{cases} < 0 & \rightarrow \text{relative maxima at } f_0 \\ = 0 & \rightarrow \text{indetermined with this test} \\ > 0 & \rightarrow \text{relative minima at } f_0 \end{cases} \tag{5.19}$$

This test has proved very useful in the estimation of natural frequencies in that solutions of equation 5.17 can be quickly and easily verified as a maxima without the use of graphics or interaction with the analyst.

This above procedure is used in the estimation of roll natural frequency. In order to check the convergence and to find the optimum number of data points needed, the above explained methodology is applied to the single degree of fredom roll motion. It is assumed that the roll motion of a ship, when subject to a pure rolling moment, M(t), may be modelled by second order differential equation of the form :

$$I\ddot{\phi} + B\dot{\phi} + C\phi = M(t) \tag{5.20}$$

where, I is the roll mass moment of inertia of the ship (including added mass moment of inertia), ϕ is the roll angle, $B\dot{\phi}$ and $C\phi$ damping and restoring moments respectively.

In these simulations, the roll moment was chosen as

$$M(t) = A\text{rand}() + B\sin(wt) \tag{5.21}$$

where, rand() is a random number generator, A and B are constants.

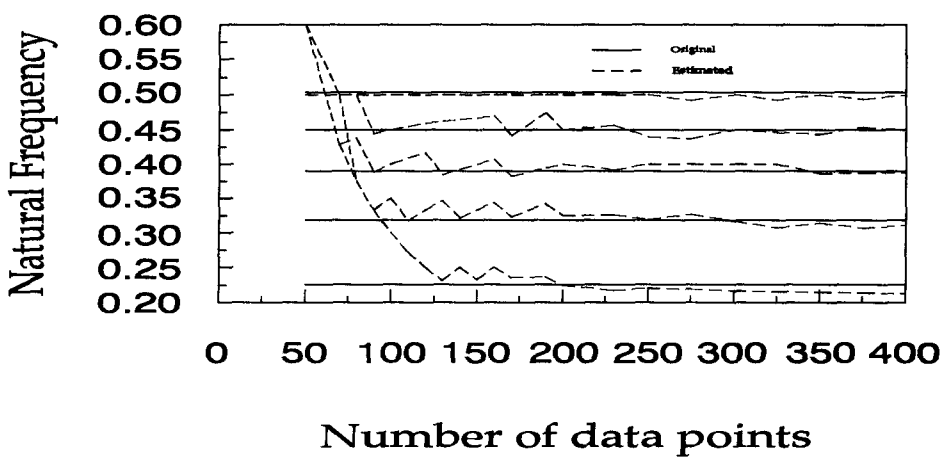

Figure 5.6: Convergence of MEM natural frequency estimator

As seen from, Figure 5.6, estimations yield to the correct answer after 150 measurement points. Figure 5.7 shows the accuracy of the estimations for different natural

frequencies.

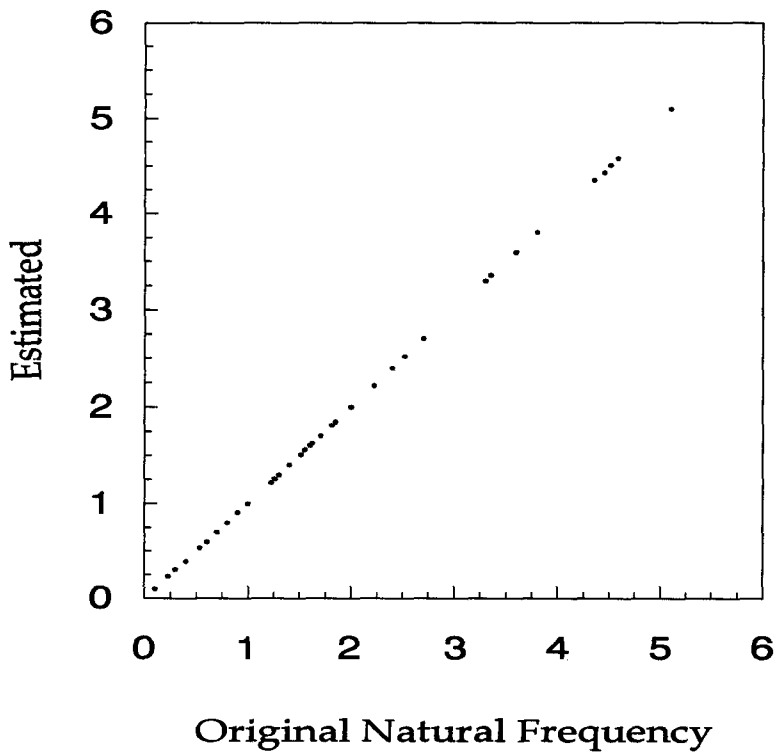

Figure 5.7: Results of MEM natural frequency estimator for single degree of freedom system

As the next step, the above method is applied to the single chine vessel (see Chapter 2.). Firstly, an experimentally obtained roll decay curve [28] (Figure 3.7) is used to estimate the roll natural frequency. In this step, it is assumed that the ship rolls at its natural frequency, when its freely rolling. Secondly, a ship motion program (Roll_dyn.C) [63] was run to obtain roll motion data in following seas. In this run, a Bretschneider spectrum (see Appendix D) is used to simulate incoming waves.

Results of this simulation for different significant wave heights are shown in Table 5.3 and Figure 5.8.

Sig. Wave Height (m)	Original (rad/s)	Estimated (rad/s)
0.8	0.408	0.382
0.9	0.408	0.38
1.2	0.408	0.383
1.5	0.408	0.385

Table 5.3: Results from MEM natural frequency estimator

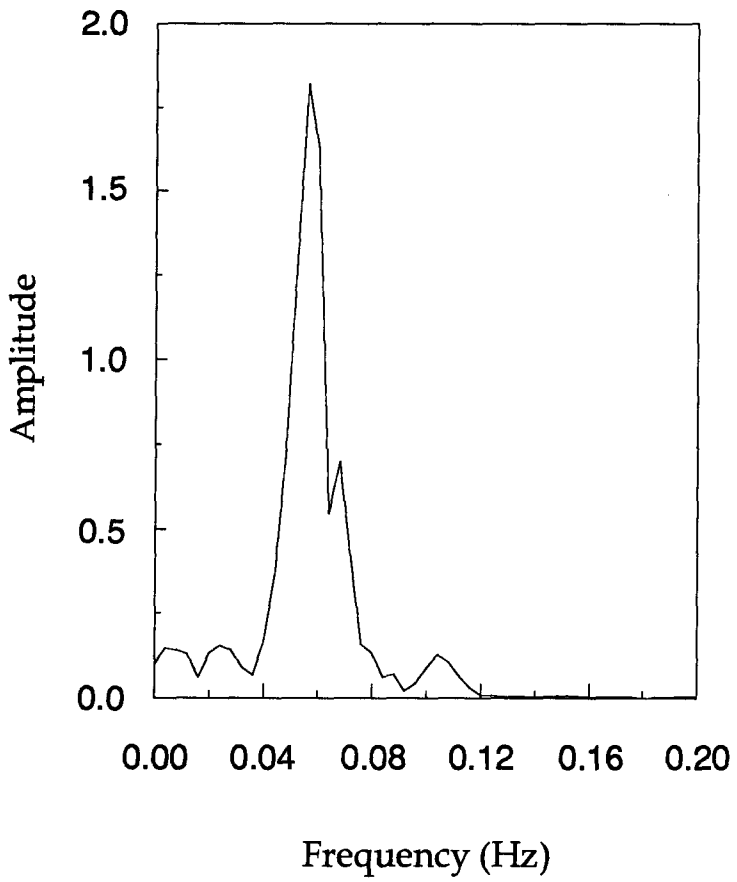

Figure 5.8: Spectrum of roll motion

The same methodology is also applied to find the natural frequency of the American Challenger vessel. For this analysis, experimental results from reference [64] are used.

Figure 5.9 shows a time series of roll motion of American Challanger.

Results of MEM analysis of this data is shown in Figure 5.10. As seen from 5.10 and Table 5.4, the results are very close.

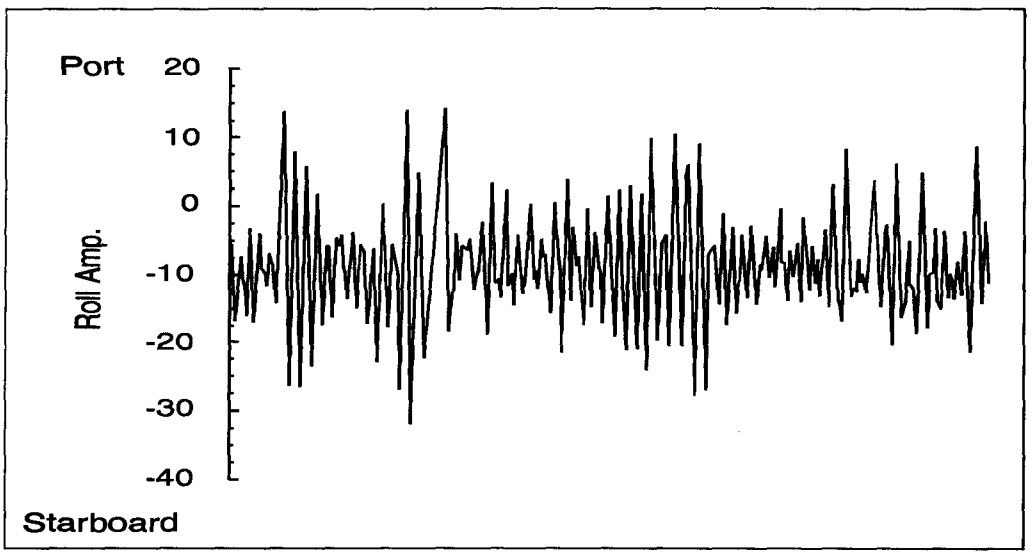

Figure 5.9: Roll motion data for American Challenger

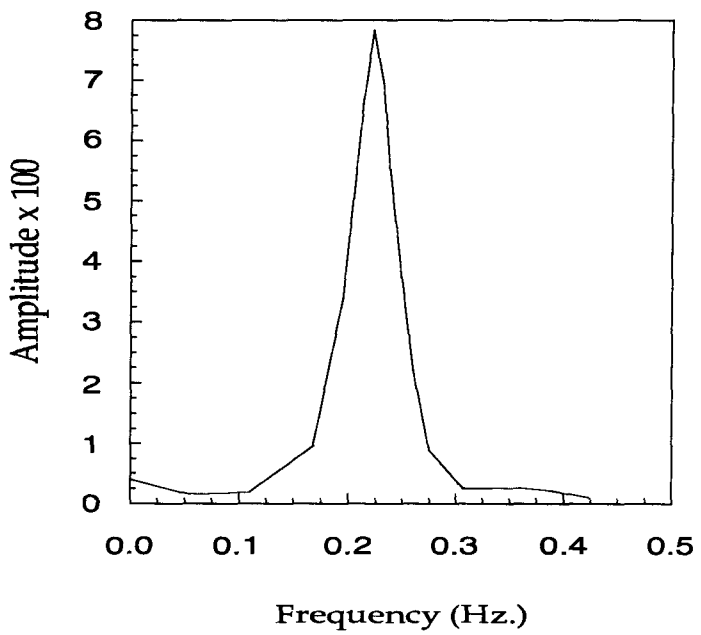

Figure 5.10: Roll motion spectra for American Challenger

Actual (given)	Estimated by MEM
0.7	0.69

Table 5.4: Comparison of natural frequencies

5.3 Estimation of Probabilities

It is well known that vessels are not designed to withstand all weather conditions. Vessels are supposed to seek a shelter under some conditions. These conditions are usually different than explained in previous chapters. For example, assume that wave height is increasing gradually, but frequencies are not in the resonance range and wave direction is beam seas. This condition does not satisfy any capsizing modes mentioned earlier. In order to identify these sort of conditions, the following two probabilistic approaches are used.

5.3.1 Probability of Roll Angle passing a limit value in time T

Let $x(t)$ be the roll response of a vessel. Assume that $x(t)$ is a stationary, random process, and $\overline{\omega}_{exp}$ is the expected frequency of crossing the limit level x = a with positive slope [65].

Figure 5.11 considers the geometry involved in a function crossing the level x = a during particular time interval dt. All functions cross the line t=t (Figure 5.11, but only a small fraction of these cross the line x = a with positive slope $\dot{x} > 0$ during the interval dt. Two such samples are indicated in Figure 5.11. Suppose that dt is so small that the samples can be treated as straight lines in the interval. If a function crosses the line at t=t with an x value less then a, it will also cross x = a, if its slope $\dot{x}$ at t = t has any value from infinity down to the limiting value (a - x) / dt [65]. Using this statement, any

function can be examined to determine whether or not its combination of x and $\dot{x}$ values will yield a crossing of x = a (Figure 5.12).

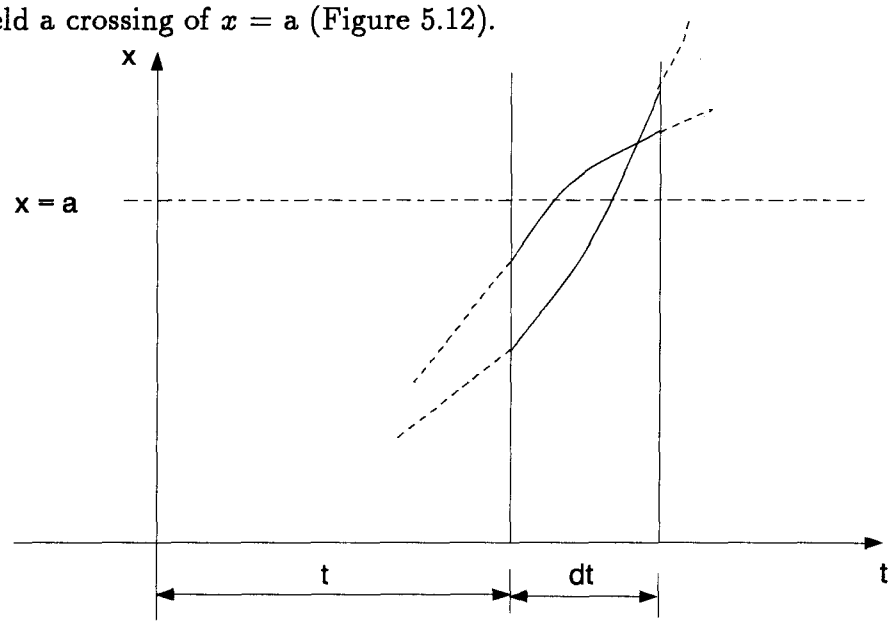

Figure 5.11: Sample functions crossing level x = a with positive slope

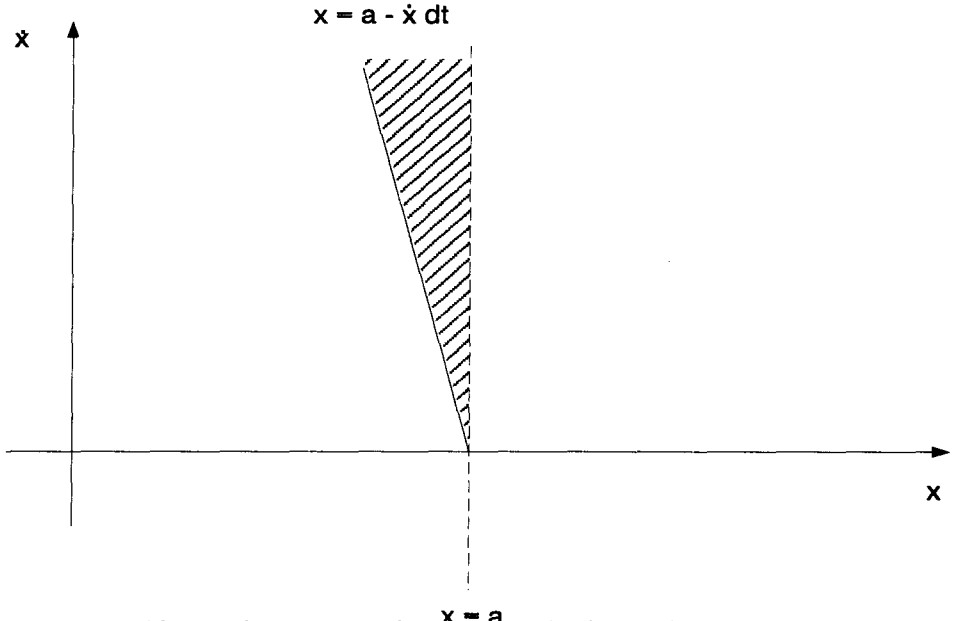

Figure 5.12: *Favorable* combinations of x and $\dot{x}$ which results in crossing of x = a during dt interval

An analytical method of examining combinations of x and $\dot{x}$ values is provided by the

joint probability distribution of x and $\dot{x}$ for stationary processes [65]. The probability of a sample having x between x and $x + dx$ and having $\dot{x}$ between $\dot{x}$ and d$\dot{x}$ is p(x,$\dot{x}$)dxd$\dot{x}$. In the (x,$\dot{x}$) plane the *favorable* combinations of x and $\dot{x}$ values are shown in the shaded area of Figure 5.12 between the line x = a and line where $\dot{x}$ equals the limiting value (a - x) / dt.

Now the expected number of crossing of x = a during the dt is just the same as the fraction of *favorable* combinations out of all possible combinations, since *favorable* combinations will yield exactly one crossing while unfavorable combinations gives no crossing. Finally the expected number of such crossing per unit time can be written as [65]:

$$\overline{\omega}_{exp} = \frac{1}{dt}\int_0^{\infty} dx \int_{a-\dot{x}dt}^{a} p(x,\dot{x})dx \tag{5.22}$$

where the integration limits have been chosen to cover the shaded area in Figure 5.12. For small values of dt, the x variable is substantially equal to a in the x integration so that, one obtains, by letting dt $\rightarrow$ 0 [66]

$$\overline{\omega}_{exp} = \int_0^{\infty} \dot{x}p(a,\dot{x})d\dot{x} \tag{5.23}$$

This result for the expected number of crossing of the level x = a, with positive slope, per unit time, applies to any stationary process not neccesarily normal [65].

In order to evaluate Equation 5.23, the following assumptions are made. Roll motion ($x(t)$) is an ergodic, stationary Gaussian (normal) random process with zero mean. This requires that the joint density takes the following form.

$$p(x,\dot{x}) = \frac{1}{2\pi\sigma_x\sigma_{\dot{x}}} exp\left[-\frac{1}{2}\left(\frac{x^2}{\sigma_x^2} + \frac{\dot{x}^2}{\sigma_{\dot{x}}^2}\right)\right] \tag{5.24}$$

Note that Equation 5.24 implies that x and $\dot{x}$ are uncorrelated. Substituting in Equation 5.23 and evaluating the integral, one finds

$$\overline{\omega}_{exp} = \frac{1}{2\pi}\frac{\sigma_{\dot{x}}}{\sigma_x} exp\left(\frac{-a^2}{2\sigma_x^2}\right) \tag{5.25}$$

This equation gives the probability of crossing at any level of a in a unit time. On the other hand, if one wants to find in time T,

$$\overline{\omega}_{exp} = \frac{T}{2\pi}\frac{\sigma_{\dot{x}}}{\sigma_x} exp\left(\frac{-a^2}{2\sigma_x^2}\right) \tag{5.26}$$

Similarly, expected maximum roll angle can be found as [67]:

$$E[X_{max}] = \int_0^{\infty} 1 - exp\left(\frac{-T}{2\pi}\frac{\sigma_{\dot{x}}}{\sigma_x} exp\left(\frac{-x^2}{2\sigma_x^2}\right)\right) dx \tag{5.27}$$

In the evaluation of the above method, use can be made of results from the San Francisco Bay experiments, reported by Haddara et al. [64, 21] to calculate the probabilities of capsizing. A typical motion time series of a model run that ended with capsize is shown in Figure 5.13 [64, 21].

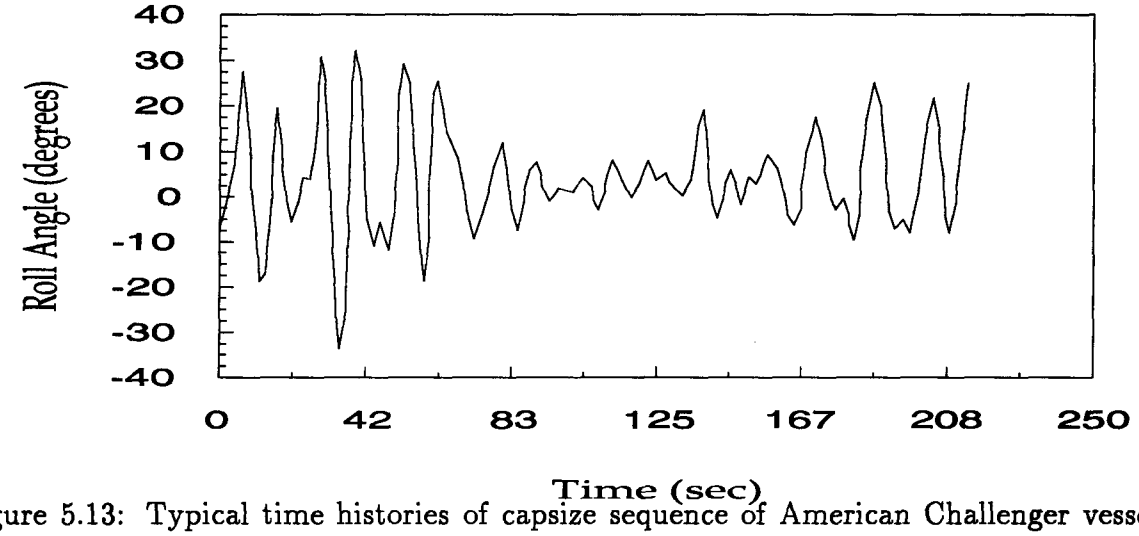

Figure 5.13: Typical time histories of capsize sequence of American Challenger vessel recorded on San Francisco Bay

The following results were found by using statistical analysis :

Variance	124.946670
Standard deviation	11.1779547
Absolute deviation	8.42763428
Standard error	0.790400753

Table 5.5: Result of statistical analysis for time histories of capsizing

Substituting these results into Equation 5.26, and using a time limit as 30 minutes gives

Expected Frequency of Roll angle crossing 60° in 30 minutes is 4.3 times

In this study, the limit for expected frequency is set as 1, that is, if the expected frequency is bigger than 1, a warning will be issued. In this case warning is **return to port**. The limit for roll angle is set at either 60° or the angle of deck immersion whichever is less.

Similarly, the expected maximum roll angle in 30 minutes was found as 100°. The limit is 60°.

Chapter 6

Development of A Fuzzy Expert System

6.1 Introduction

In recent years, expert systems have received increased attention as practical applications of artificial intelligence to solve real problems. In traditional rule - based approaches, knowledge is encoded in the form of antecedent - consequent structures; when new data is encountered, it is matched to the antecedent clauses of each rule, and those rules where antecedents match the data exactly are fired, establishing the consequent clauses. This process continues until a desired conclusion is reached, or no new rules can be fired.

This forward propagation scheme for logical inference assumes that all facts are known precisely, a constraint which is rarely satisfied in the marine field. There is almost always uncertainty present; uncertainty in the facts, and uncertainty in the rules describing casual relationships among facts. Results of radar image processing techniques can be used as an example of uncertainties in measurements. As seen from Figure 4.14, wave direction is not clear. Therefore, in order to handle this uncertainty, a triangular membership function between 15° and 40° is used as a wave direction.

The following rule shows the uncertainties in the rules. " If the wave direction is following seas (Figure 2.4), and the encounter frequency is close to twice the natural roll frequency, then the ship is in danger ". In this rule, there are two elements of fuzzyness:

- Definition of wave direction : Following seas can be considered as fuzzy input, because the boundaries of following seas could be ±20° of wave direction exactly

from behind.

- Relationship between frequencies : The relation between encounter and natural roll frequency is given as "close or equal". This description is a fuzzy description.

To consider these uncertainties, a fuzzy expert system is used in the decision making step.

A general introduction to fuzzy logic is necessary to explain the methodology which is used by a fuzzy expert system.

6.2 Introduction to Fuzzy Logic

Fuzzy logic is a superset of conventional (Boolean) logic, that has been extended to handle the concept of partial truth, truth values between "completely true" and "completely false". It was introduced by Lotfi Zadeh [68] in the 1960's as a means of modelling the uncertainty of natural language.

Fuzzy Subsets

There is a strong relation between Boolean logic and the concept of a subset, there is also a similar relationship between fuzzy logic and fuzzy subset theory.

In classical set theory, a subset U of a set S can be defined as a mapping from the elements of S to the elements of the set {0,1},

$$U : S \rightarrow \{0, 1\}$$

This mapping may be represented as a set of ordered pairs, with exactly one ordered pair present for each element of S, and the second element is an element of the set { 0,1}. The value zero is used to represent non-membership and the value one is used to represent membership. The truth or falsity of the statement:

X is in U

is determined by finding the ordered pair whose first element is X. The statement is true if the second element of the ordered pair is one, and the statement is false if it is zero.

Similarly, a fuzzy subset F of a set S can be defined as a set of ordered pairs, each with the first element from S, and second element from the interval [0,1], with exactly one ordered pair present for each element of S. This defines a mapping between elements of the set S and values in the interval [0,1]. The value zero is used to represent complete non-membership, the value one used to represent complete membership, and values in between are used to represent intermediate degrees of membership. The set S is referred to as the universe of discourse for the fuzzy subset F. Frequently, the mapping is described as a function, the membership function of F. The degree to which the statement

X is in F

is true is determined by finding the ordered pair whose first element is X. The degree of the truth of the statement is the second element of pair.

Logic Operation

The standard definitions in fuzzy logic are :

$$\begin{aligned} \text{truth (not x)} &= 1.0 - \text{truth (x)} \\ \text{truth (x and y)} &= \text{minimum(truth(x) , truth(y))} \\ \text{truth (x or y)} &= \text{maximum(truth(x) , truth(y))} \end{aligned}$$

It should be noted that if just the value zero and one were used in these definitions, the truth table obtained would be same as the one expected from conventional Boolean logic. This is known as the *extension principle*, which states that classical results of Boolean logic are recovered from fuzzy logic operations when all fuzzy membership grades are restricted to the traditional set 0,1. This effectively establishes fuzzy set and logic as a true generalization of classical set theory and logic. In fact, by this reasoning all crisp

(traditional) subsets are fuzzy subsets of this very special type.

6.3 Fuzzy Expert System

Fuzzy expert systems deal with uncertainty in their knowledge base and the information supplied, in a rational and understandable way, based on the use of fuzzy logic. They use a collection of fuzzy membership functions and rules, instead of Boolean logic, to reason about data. The rules in a fuzzy expert system are usually of a form similar to general If - Then rules. As an example we can study the following rule which says that if waves are coming from behind (following seas) and the difference between wave speed and ship speed is small and the speed of the ship is high then reduce speed.

IF wave_direction IS *follow*
AND (DW_speed_SSpeed) IS *Zero*
AND Ship_speed IS *high*
THEN DShip_speed IS *moderate_negative*

where wave_direction, (DW_speed_SSpeed), and Ship_speed are input variables, and DShip_speed is an output variable, *moderate_negative* is a membership function (fuzzy subset) defined on wave_direction, *Zero* is a membership function defined on (DW_speed_SSpeed) and so on. The antecedent (the rule's premise) describes to what degree the rule applies, while the conclusion (the rule's consequent) assigns a membership function to each of one or more output variables. Figure 6.1 shows a general layout for the fuzzy expert system. Left hand sides are the input variables, available to the fuzzy rules and the right hand sides are the possible outputs desired from fuzzy rules.

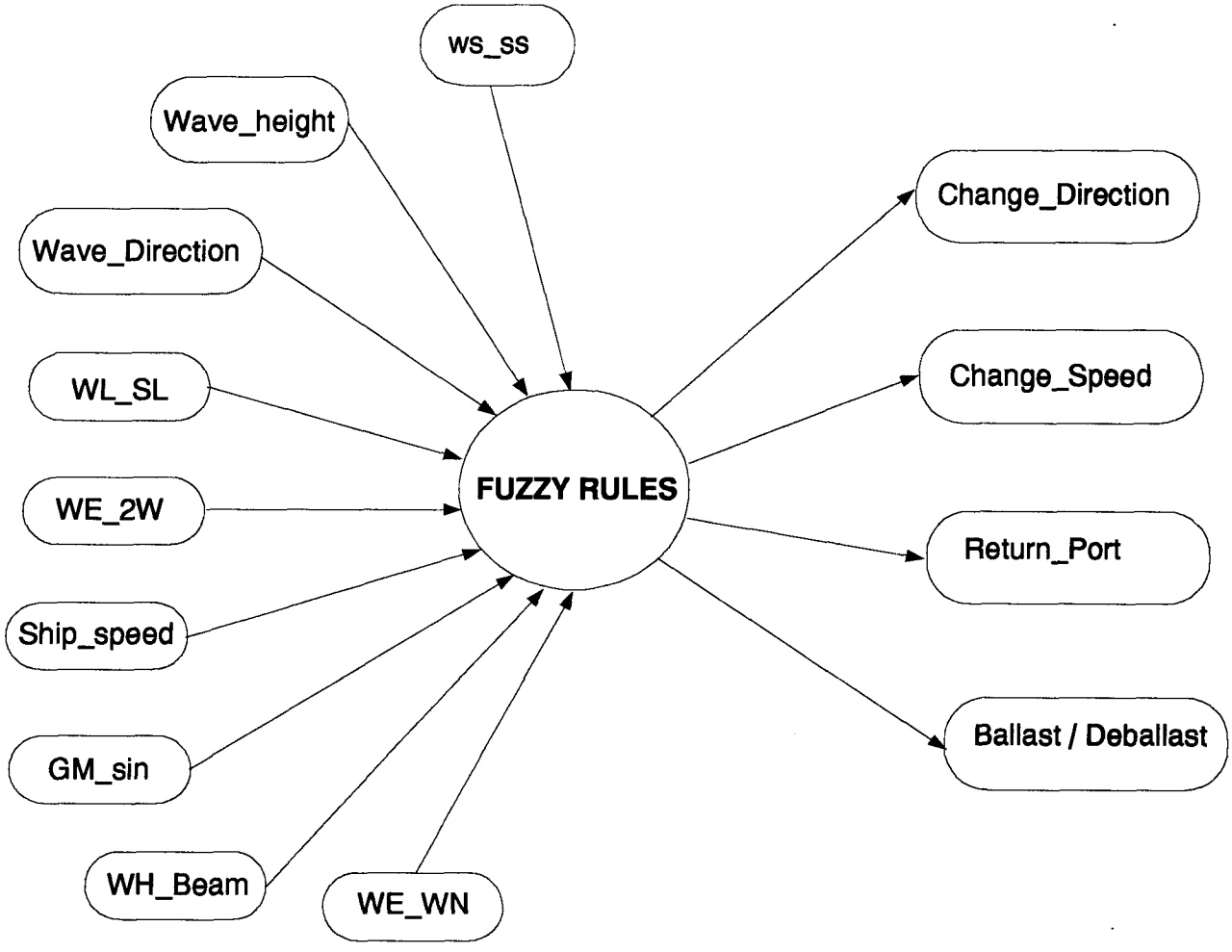

Figure 6.1: A general layout for Fuzzy Expert System

6.3.1 Determination of Membership functions

A fundamental tenet of fuzzy set theory is that observations can partially belong to predefined sets. This is in sharp contrast to the traditional Boolean logic, in which membership in a set is an all or nothing proposition. Suppose that we have measured

ship's speed and have sets called slow, medium, and high. Boolean logic would dictate that memberships are determined by means of fixed cut off points, say at 5 and 10 m/s. Speed which is at least equal to 10 would be a member of the high set, while all others would be in either the medium or slow set. This is illustrated in the upper part of Figure 6.2. On the other hand, fuzzy definitions of this set allow for partial membership. A ship speed slightly higher than 4 m/s would be almost a full member of the slow set and only trivially a member of the medium set. 5m/s would be a half-member of each set.

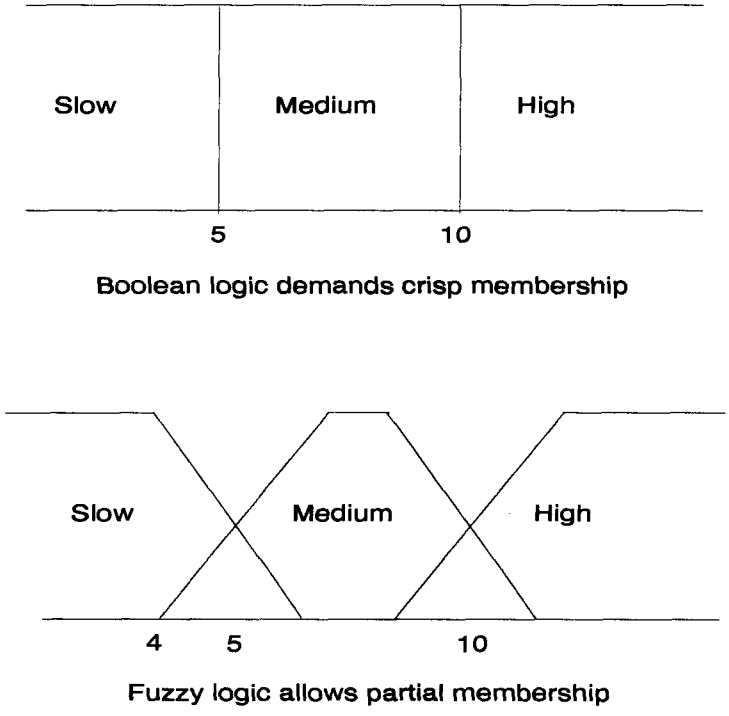

Figure 6.2: Membership functions

Limits of each member of membership functions of input variables used in this study are obtained from experimental and theoretical calculations.

6.3.2 Input Output Forms and Interpretation

Expert systems used are capable of dealing with incoming and computed information in two different forms: crisp or fuzzy. Crisp data consist of single values. Most real world devices, such as accelerometers generate crisp data. Fuzzy data consists of an array of believability values each between zero and one such as wave directions found from radar images.

The degree to which a data value belongs to a fuzzy subset (its membership in the fuzzy subset) is computed somewhat differently depending on whether the data value is crisp or fuzzy. When data is crisp, the degree of membership is the value of the fuzzy subset's membership function at that data value, as shown in Figure 6.3.

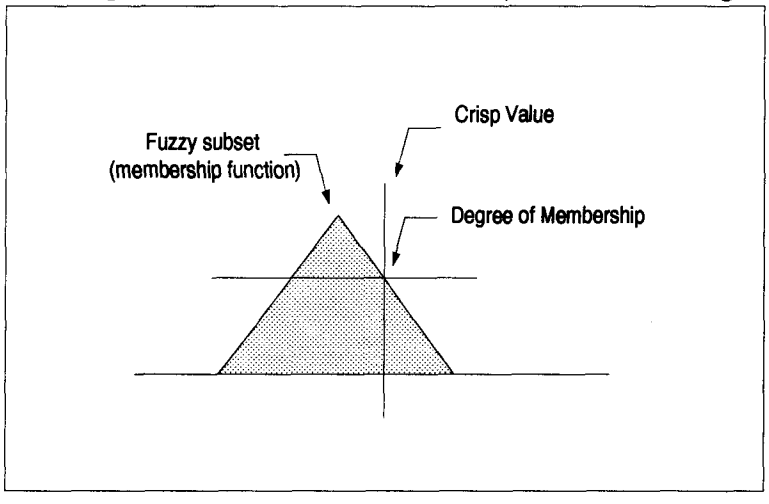

Figure 6.3: Degree of membership for a crisp data value

When the data value is fuzzy, the degree of membership is determined as the maximum degree of membership value for the intersection of the membership functions for the fuzzy data value and fuzzy set as shown in Figure 6.4

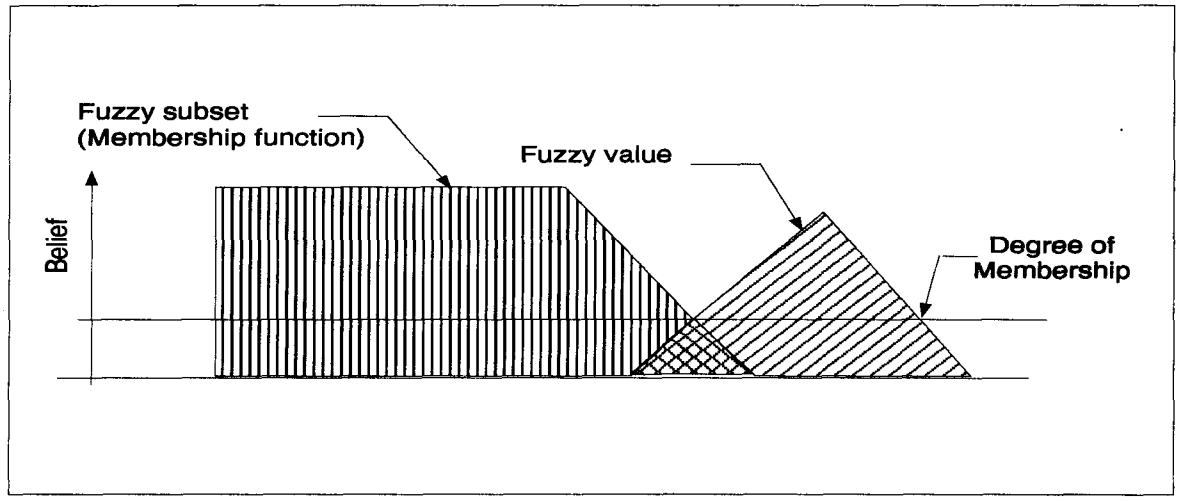

Figure 6.4: Degree of membership for a fuzzy data value

6.3.3 Inference Method

The process of applying the degree of membership computed for a production rule premise to the rule's conclusion to determine the actions to be performed is called performing an inference, one is inferring the actions to be performed from the premise. There are several methods for performing fuzzy logic inferences. Two of the most common methods are the max-min and max-dot (also known as the max - product) method.

In either inference method, the basic concept is that a value (set) to be assigned to the output is scaled by or clipped to the degree of membership for the premise, and that

all of the scaled or clipped sets for all of the rules that set this output unionized together to form the final membership function. In reality, in most cases the two methods give similar results.

The Max - Min Inference Method

In the max - min inference method, the final output membership function for each output is the union of the fuzzy sets assigned to that output in a conclusion after clipping their degree of membership values at the degree of membership for the corresponding premise, as shown in Figure 6.5. In Figure 6.5, PM and PS are positive medium and positive small respectively.

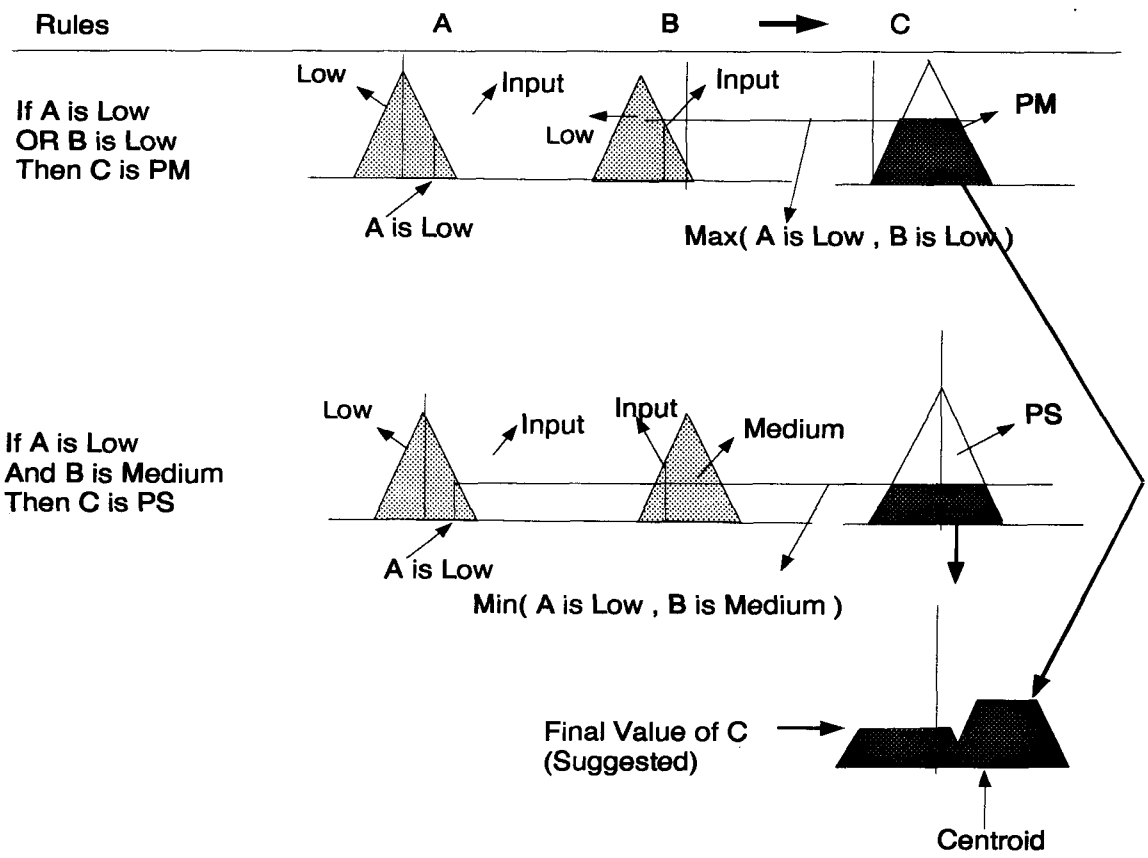

Figure 6.5: The max - min inference method

As seen from the first rule in Figure 6.5, the conclusion is assigned after the following steps:

- Find the corresponding belief values for inputs A and B
- Find the maximum of these corresponding values, since relationship is given by "OR".
- Clip the membership function of C from the maximum value found at step 2.

The resulting membership function (PM) from the above steps is the result of rule 1. The results for rule 2. is found by similar steps. Then, these two resulting membership functions are used to find the final value (suggestion) by a defuzzyfication method (see section 6.3.4).

The Max - Dot Inference Method

In the max - dot or max - product inference method, the final membership function for each output is the union of the fuzzy sets assigned to that output in a conclusion after scaling their degree of membership values to the peak at the degree of membership for the corresponding premise, as shown in Figure 6.6.

The conclusion is assigned by using similar steps as explained in "max - min inference method". The only difference here is that the maximum point is used as the tip of triangular membership function.

The max - min inference method is used in this study to find the final decision.

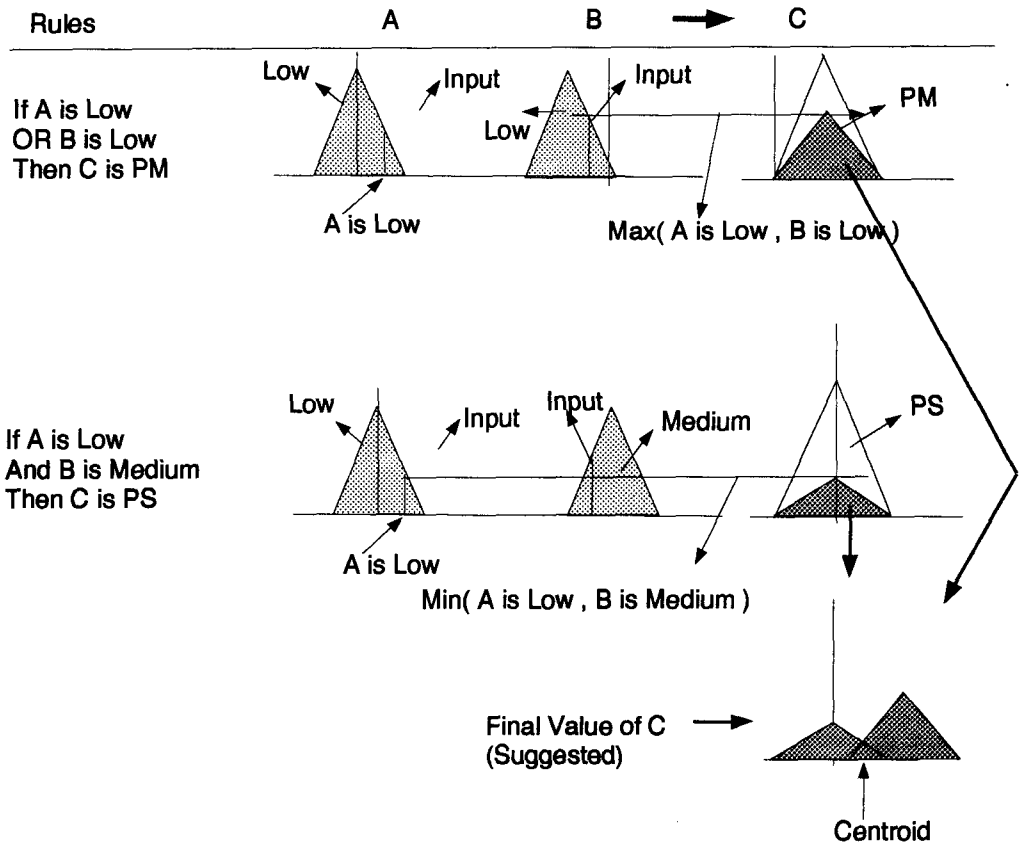

Figure 6.6: The max - dot inference method

6.3.4 Defuzzification

All fuzzy logic inference methods result in fuzzy values for all output information. In order to generate a single crisp value, a method is needed to pick a value that represents the membership function in the best possible way. These methods are called defuzzifications. There are several methods of performing this defuzzification. Two of the most commonly used ones are the height and the centroid method.

The height defuzzification method picks an average of the output values corresponding to the centroid of the scaled or clipped output membership functions as the crisp value for an output, weighted by the heights of the clipped or scaled output membership function.

This method could give misleading results, when it is used in those cases where the membership function graphs are not symmetrical [68]. Therefore, the centroid method is used in this study for defuzzification, as seen from Figure 6.7

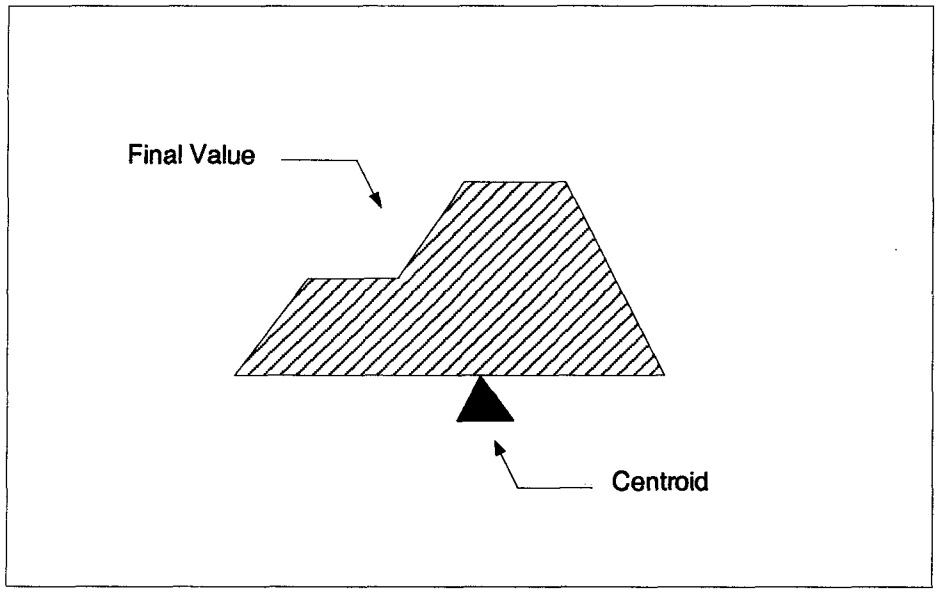

Figure 6.7: The centroid defuzzification methods

6.4 Explanation of the Rules Used by the Expert System

This section explains the general rules used by the fuzzy expert system. In the rule base developed, there are different rules for different situations. For example, for the same rule, there are different solutions for say different ship speeds, such as when it is high reduce speed, or when it is medium change direction. In this section, instead of giving all these combinations of the rules, a general explanation of a rule is given and how

and where it is obtained is explained. The expert system has 36 rules to cover possible combinations of the rules explained in this section.

Rule 1 :

This rule is extracted from theoretical and experimental studies.

If wave length **is** equal to ship length

and encounter frequency **is** twice the natural roll frequency

and wave direction **is** following to quartering seas

then a) Reduce speed until wave speed is more than 20% of the ship speed.

b) Change Direction.

Two extreme positions of the wave, namely, with a crest at the ends and with a crest amidship are shown in Figure 6.8.

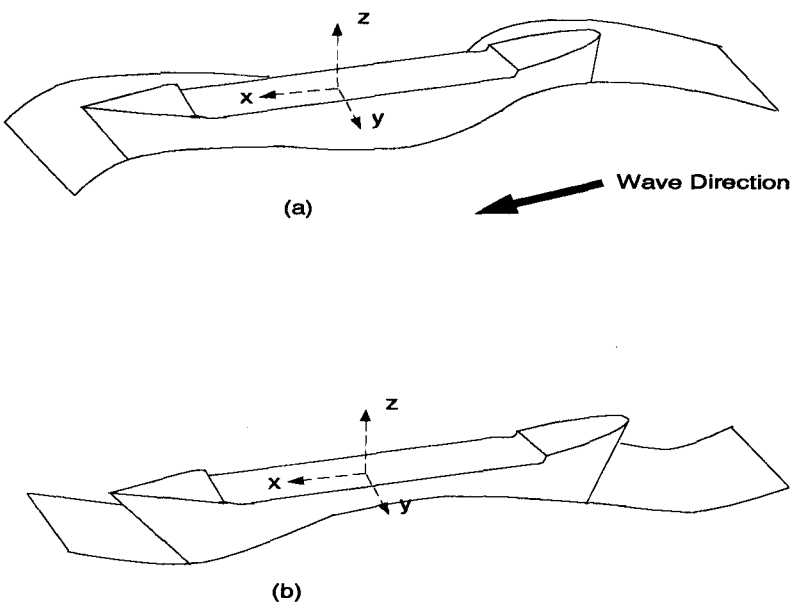

Figure 6.8: Two extreme positions of the wave

For a normal ship form with flared sections at the ends and wall sided sections amidships, it can be seen that the inertia of the waterplane is different in each case. It is greater

than the still water value with wave crest at the ends, and less than the still water value with the wave crest amidship.

If the ship is now given an initial roll due to a small disturbance, it will roll at its natural period until the energy provided by the disturbing force is dissipated in damping. However, if the period of stability fluctuation and the natural rolling period of the ship have the right ratio, it is possible that the initial rolling angle will not only be sustained, but will build up. A qualitative explanation of this is as follows:

Suppose that the stability changes with a frequency twice the natural rolling frequency of the ship, and that the phase of the rolling and the stability changes are as shown in Figure 6.9.

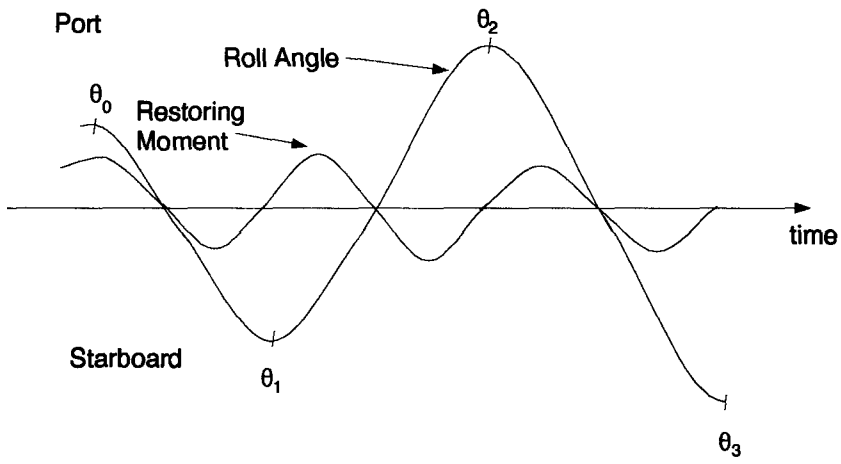

Figure 6.9: Stability changes with a frequency twice the natural roll frequency

Starting with the initial angle θ_0, during the swing back to an upright position the stability is higher than average, and the stability moment is in the direction of the motion. After crossing zero, the stability is now opposing the motion, but its value is now low. Therefore, θ_1 is greater than θ_0. Rolling back to zero again, the stability is now adding to the motion and its value is high. Thus the rolling motion builds up continuously. This

is known as low cycle resonance.

An example simulation for low cycle resonance is shown in Figure 6.10. In this simulation, the roll period is approximately equal to the natural roll period and the encounter period is half the period of roll. The wave length is approximately equal to the ship length.

$$\frac{L}{\lambda} = 0.975$$

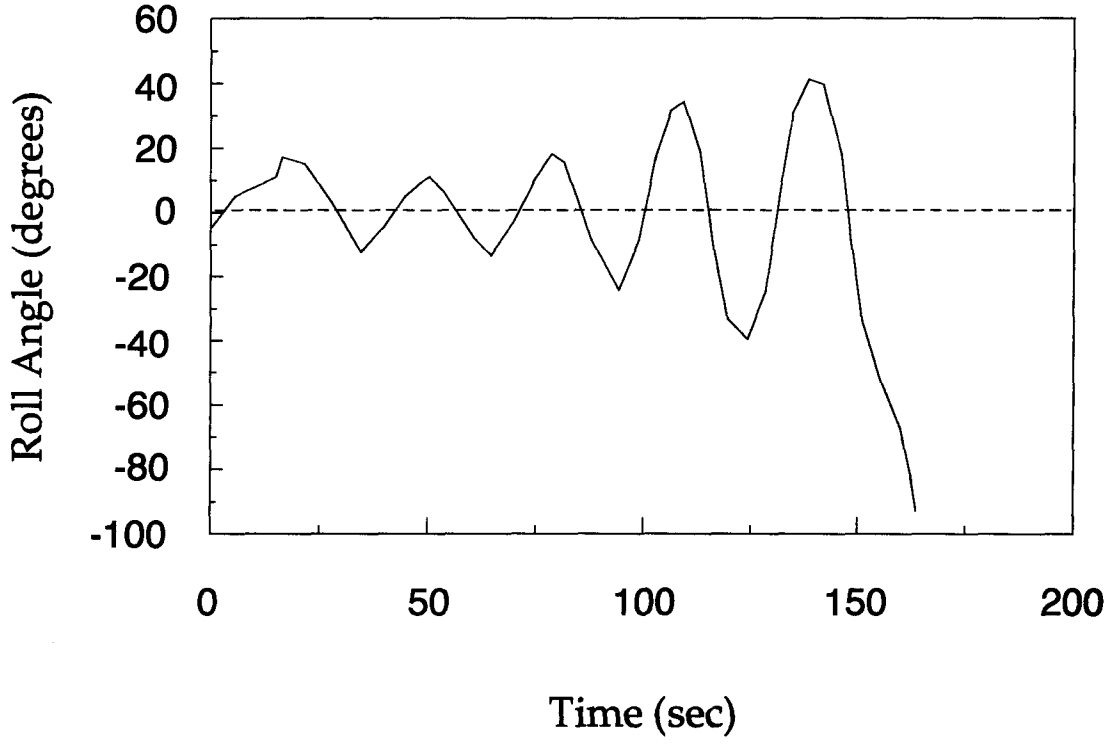

Figure 6.10: An experimental simulation for low cycle resonance

Rule 2 :

If Roll natural frequency **is** equal to g/8U

and Wave height **is** high

Then a) increase speed (if there is enough power)

b) Change speed.

From the previous works on the roll of a ship in astern regular waves [63, 69], it was found that the worst roll conditions exist when the roll natural frequency of the ship was one half the encounter frequency of the waves. On that basis, it is anticipated that a ship travelling in astern random sea would experience its greatest problem when the roll natural frequency is equal to one half the singular frequency in the metacenter height spectrum [63, 69].

$$\omega_n = g/8U$$

This condition could occur, for instance, if a ship with a 20 second roll periods were travelling at a speed of approximately 5 m/s (10 knots). If a ship found itself in such a situation, it would be beneficial to increase speed until the singular frequency in the spectrum was at least 20 percent below the roll natural frequency. If sufficient speed reserve exists for the ship to be able to increase speed by this amount, then the roll problem should dissipate. Otherwise, a decrease in speed may be necessary [63, 69].

Rule 3 :

If wave direction **is** beam seas

and wave height - ships beam is zero or negative

then change direction

This rule is found as a rule of thumb from statistical work called "Fishing vessels limits study" by SNAME [70]. In this research, surveys were sent to 12000 fishermen. The primary interest of this project was to identify wind and sea limits for fishing vessel. Statistical data and analysis can be found in [70].

Rule 4 :

If wave direction **is** beam or quartering seas

and wave height **is** high

and natural roll frequency **is** equal to encounter frequency

then change direction

This condition is called resonant excitation. It has been shown by experimental and numerical simulations [21, 71, 72] that if the vessel is excited at its natural roll frequency, it may result in very large roll angles if the wave amplitude is sufficiently large.

An example for this capsizing due to resonant excitation is shown in Figure 6.11 for the quartering sea condition [21]. It is seen that the vessel rolls at the encounter period, which is approximately equal to the natural roll period. The roll motion is 180° out of phase with the wave motion and has a negative mean; the roll angles are negative in the crests and positive in the troughs. There is no tendency for capsizing during the passage of the first wave group, while in the second wave group the roll amplitude is seen to increase after t=200 s until the vessel capsizes on the crest of a wave at t=265 s.

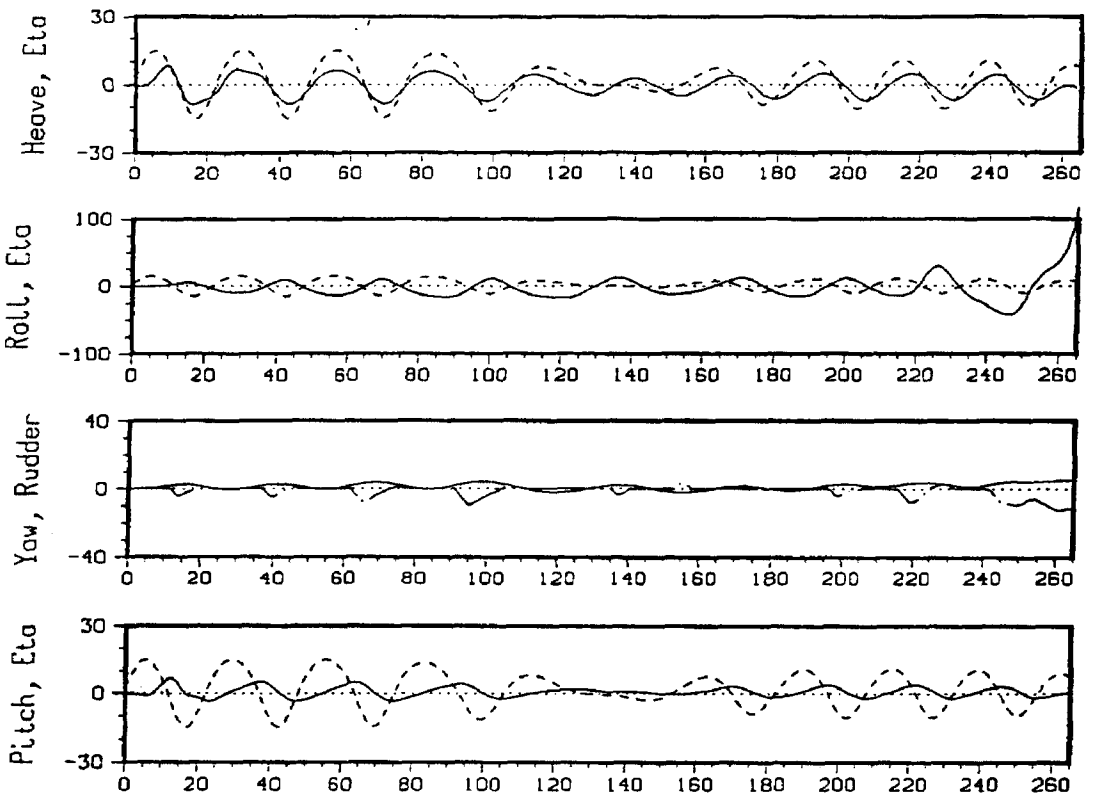

Figure 6.11: An example quartering seas motion data leading to capsizing

Rule 5 :

If wave direction **is** following seas

and wave height **is** high

and wave speed **is** approximately equal to the ship speed

then a) change direction

b) change speed

This capsizing mode is known as loss of transverse stability in following seas. An

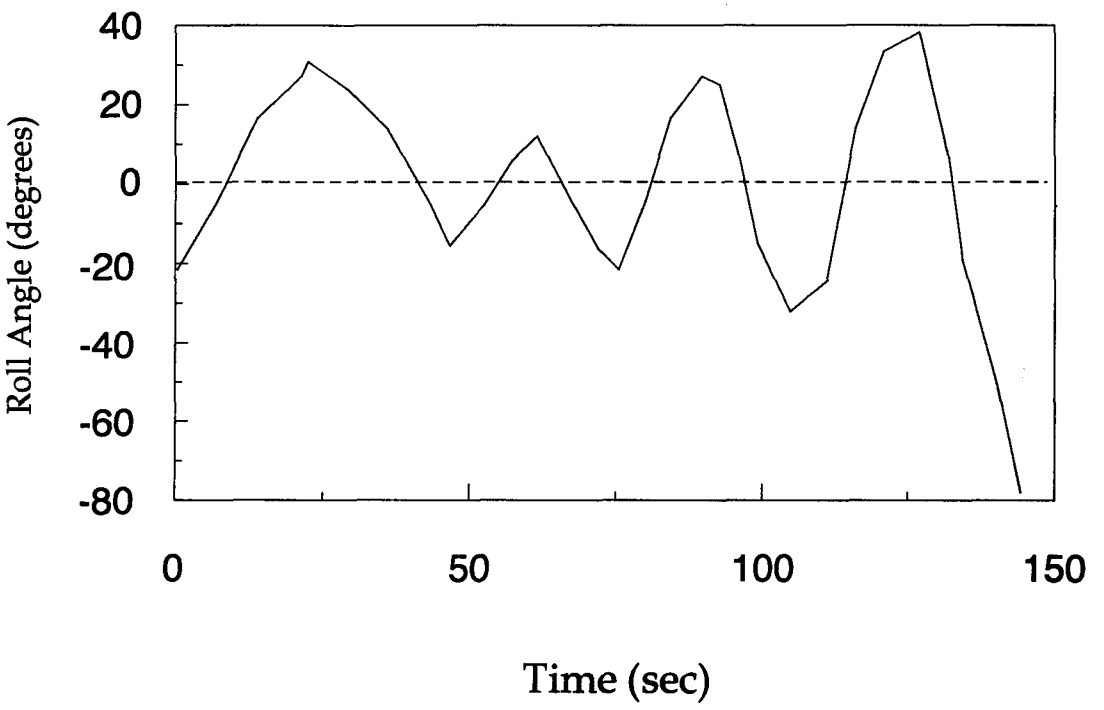

Figure 6.12: An example following seas motion data leading to capsizing due to loss of transverse stability

example motion record for this sort of capsizing is shown in Figure 6.12.

This capsize mode is characterized by the vessel being heeled over to one side for a prolonged period of time due to lack of sufficient restoring energy in the system and where roll period is not equal to the natural roll period. Typical conditions of this mode are steep, large amplitude waves, and a large enough ship speed so that the vessel stays in the wave crest for a relatively long period, during which static stability is reduced.

An example GZ curve for this condition is shown in Figure 6.13. As seen from this figure, when a wave crest is at the midship, the vessel does not have enough restoring

moment to upright herself. A small external force could capsize the vessel.

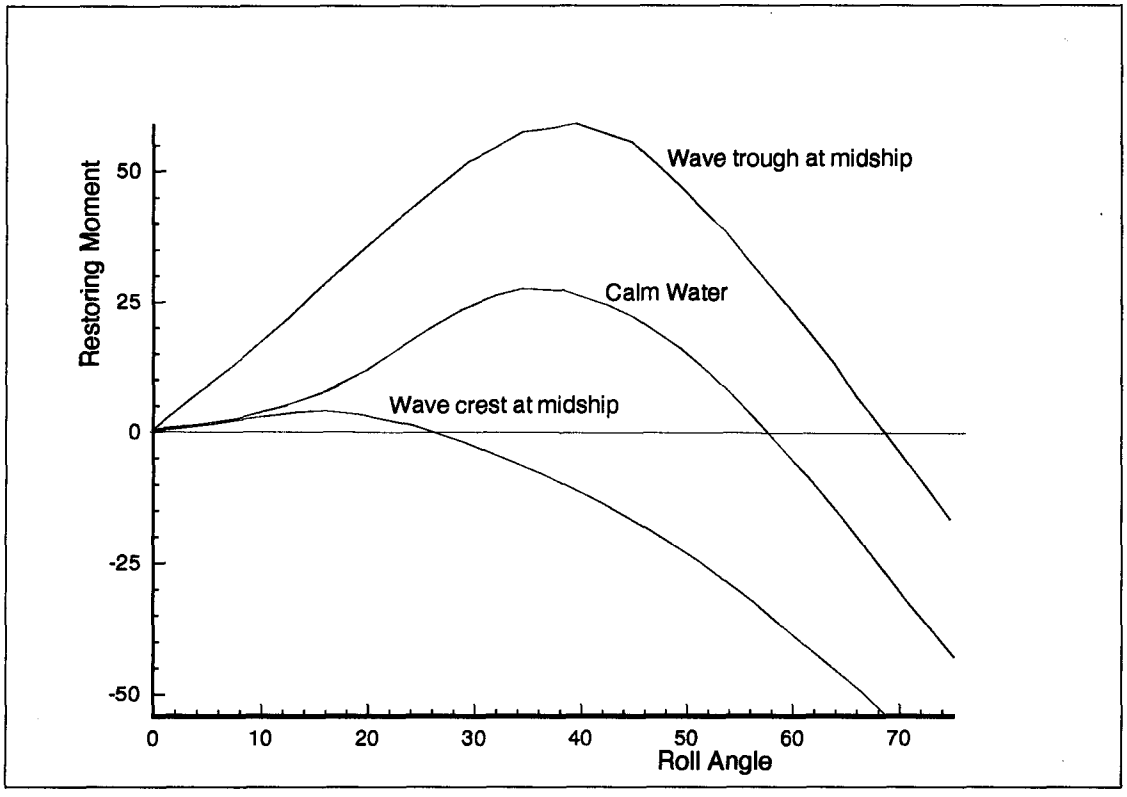

Figure 6.13: GZ curve of American Challenger for two different wave conditions

Rule 6 :

If wave direction **is** quartering seas

and wave height **is** high

and wave length **is** equal to 70% - 80% of the ship length

then a) change direction

b) change speed

The following example represents the mode of capsizing preceded by broaching [21]. In reference [21], capsizing is predicted to occur in steep, quartering seas and a wave

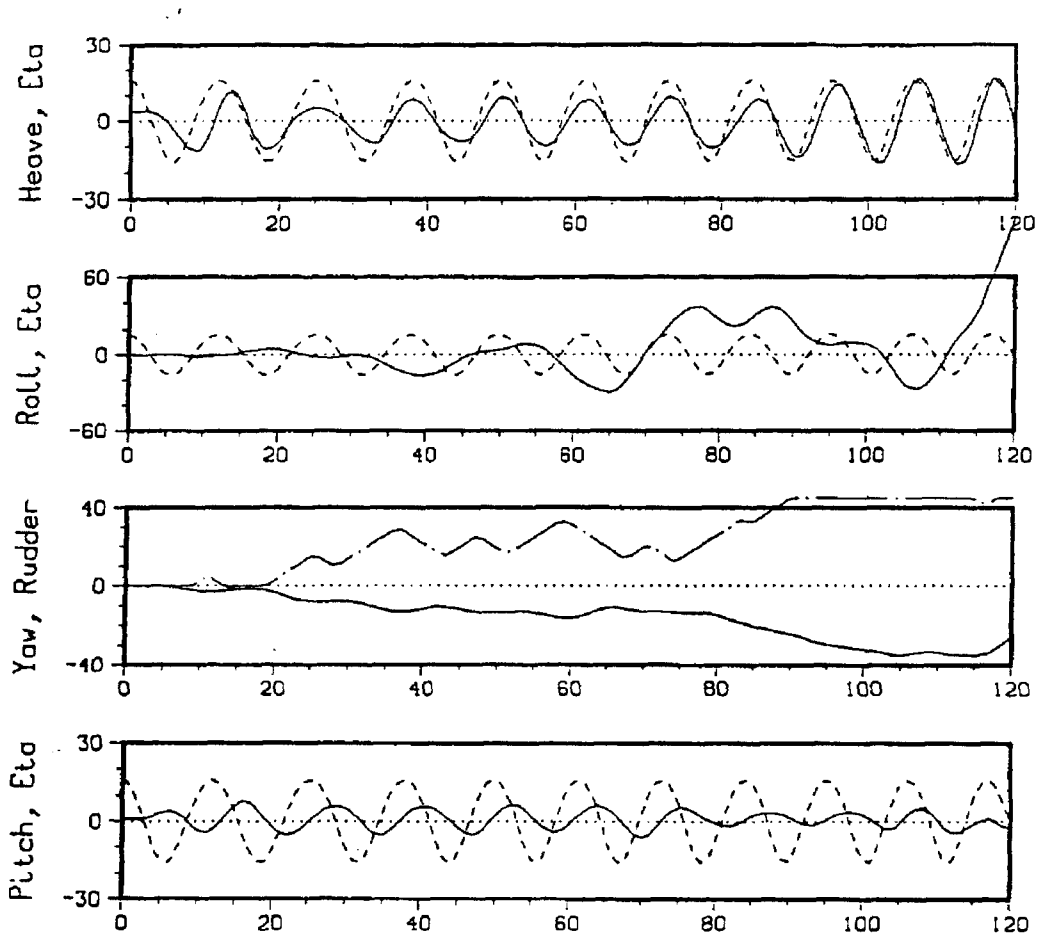

Figure 6.14: An example motion data leading to capsizing due to broaching

length of about 80 percent of the ship length. The motion records in Figure 6.14 show that up to about t=75 s, a steady yaw angle of $\phi = -12°$ is reached.

Subsequently, during the passage of four wave crest, the yaw angle monotonically increases to $-35°$ (despite the rudder being hard over), thereby putting the vessel in a position broadside to the waves, at an angle of 15° off the wave crest parallels. This part constitutes the broach. During the initial stage of the broach, the roll angle was quite large (40°), and once the vessel reached the broad side position to the waves, the angle of roll increased rapidly, and vessel capsized on the crest of a wave.

Chapter 7

Numerical Simulations

The capsizing modes mentioned above were simulated by using three different programs. These are SHIPMO4 [55], MOTION.FOR [28] and ROLL_DYN.C [63, 69]. Shipmo4 developed by DREA is a frequency domain ship motion program, while Motion.for and Roll_dyn.c developed at U.B.C. are time domain programs for regular and irregular following seas respectively.

All simulations were performed for 4 different types of vessels. Hydrostatic particular and body plan of those vessels are given in Table 7.1 and Figure 7.1.

	UBC #1	UBC #3	UBC #7	UBC #9
Length (ft)	70.00	91.00	70.00	70.00
Beam (ft)	22.86	22.86	22.64	22.64
Draft (ft)	9.25	9.25	9.17	9.17
Volume (tonnes)	271	308	196	160
C_b	0.566	0.5666	0.471	0.465
Natural frq.	0.448	0.448	0.453	0.414

Table 7.1: Hydrostatic particulars of UBC series

These simulations were performed in three different stages:

1. Low Cycle Resonance

2. Pure Loss of Stability

3. Resonant Excitation

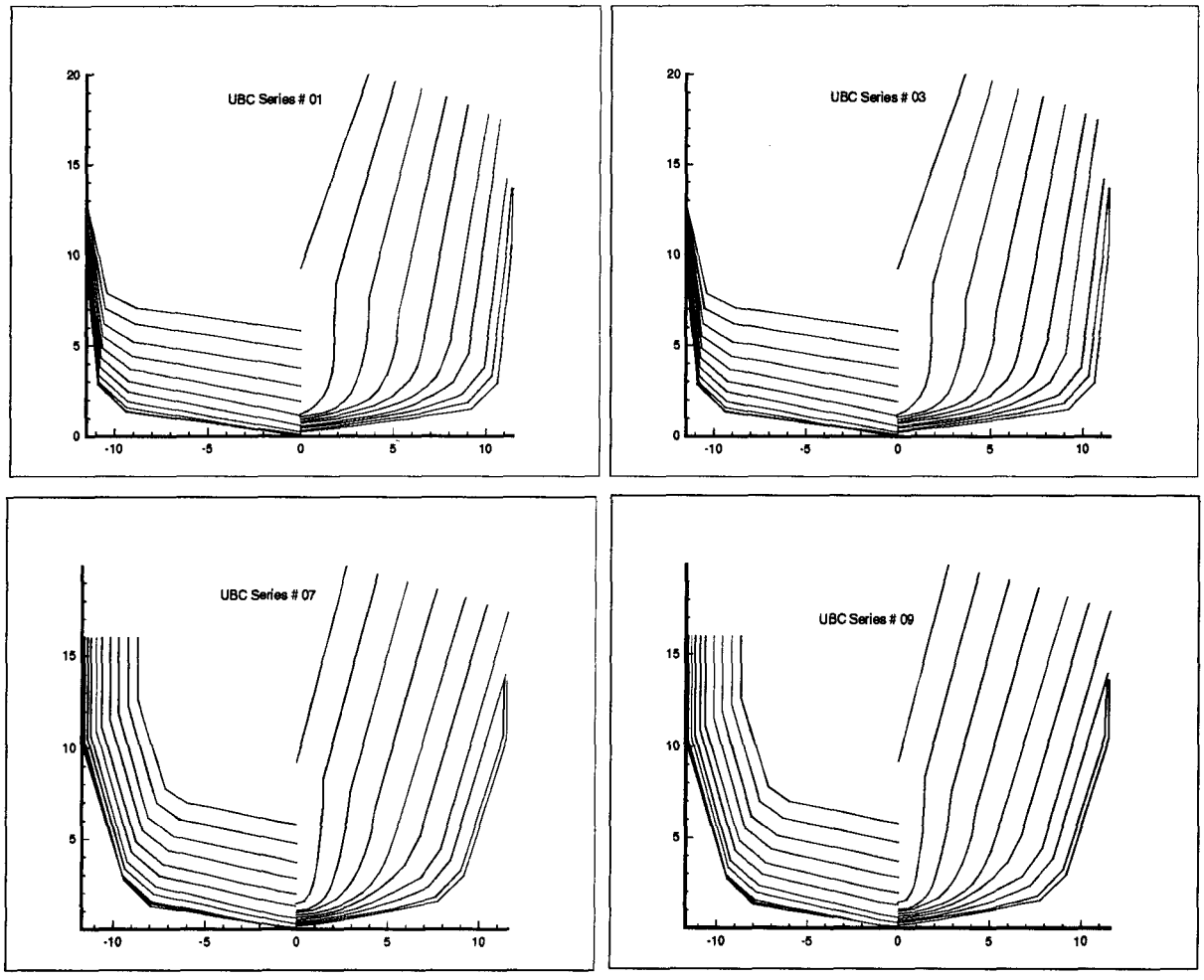

Figure 7.1: Body plans of UBC series

	UBC #1	UBC #3	UBC #7	UBC #9
Encounter frequency[1]	0.93	0.90	0.93	0.88
Wave length (ft)	65	85	65	65
Wave direction	following	following	following	following
Wave height (ft)	9.0	9.1	9.0	9.0
Ship speed (knots)	10	11.2	11.0	11.0

Table 7.2: Inputs for following seas low cycle resonance simulations

7.1 Low Cycle Resonance Simulations

These simulations were performed in regular and irregular waves. Inputs used in these simulations are given in the following table.

As seen from Figures 7.2, 7.3, 7.4, 7.5 a., the vessel capsized within 180 seconds, if no corrective action was taken. It should also be noted from this figure that capsizing occured in a very short time after the ship started rolling. This is in agreement with some reports [23] of accidents that happened in similar situations.

The same parameters were then used as inputs to the fuzzy expert system (advisory system) and the following two rules were fired in generating a suggested action :

IF wave_direction IS follow

AND Wave_height IS MEDIUM

AND WL_SL IS ZERO

AND WE_2WN IS ZERO

AND ship_speed IS HIGH

THEN change_speed IS NS

IF wave_direction IS follow

AND Wave_height IS HIGH

AND WL_SL IS ZERO

AND WE_2WN IS ZERO

AND ship_speed IS HIGH

THEN change_speed IS NM

The suggested action given by the fuzzy expert system was to reduce speed by 3 knots. Based on this change, the simulation program was again run to observe the effects of this change on the ship motion. In this run, all parameters were kept at the initial conditions, except the ship speed, which was reduced by 3 knots. Since the monitoring and advisory system takes about 1 minute to determine an action and 30 seconds were given for the ship to start to response, this run was initiated using the conditions at time 90 in the initial run that lead to capsizing. As seen from Figures 7.2, 7.3, 7.4, 7.5 b., the vessel did not capsize under the new conditions and the largest angle was between 5° and 15°.

Figure 7.2 shows low cycle resonance simulation runs for UBC series model # 01. As seen from Figure 7.2 a., the vessel rolls about 20° approximately at 60 seconds, then the roll decays rapidly. But at about time = 160 seconds, the ship starts rolling and capsizes at t=195 seconds. These results are in good agreement with the accidents reported under similar conditions [23, 64].

Figures 7.2, 7.3, 7.4, 7.5 also show similar patterns before capsizing. As seen from these figures, there is no clear indication of capsizing for a captain to recognize the danger, since the vessel rolls once or twice before actually capsizing.

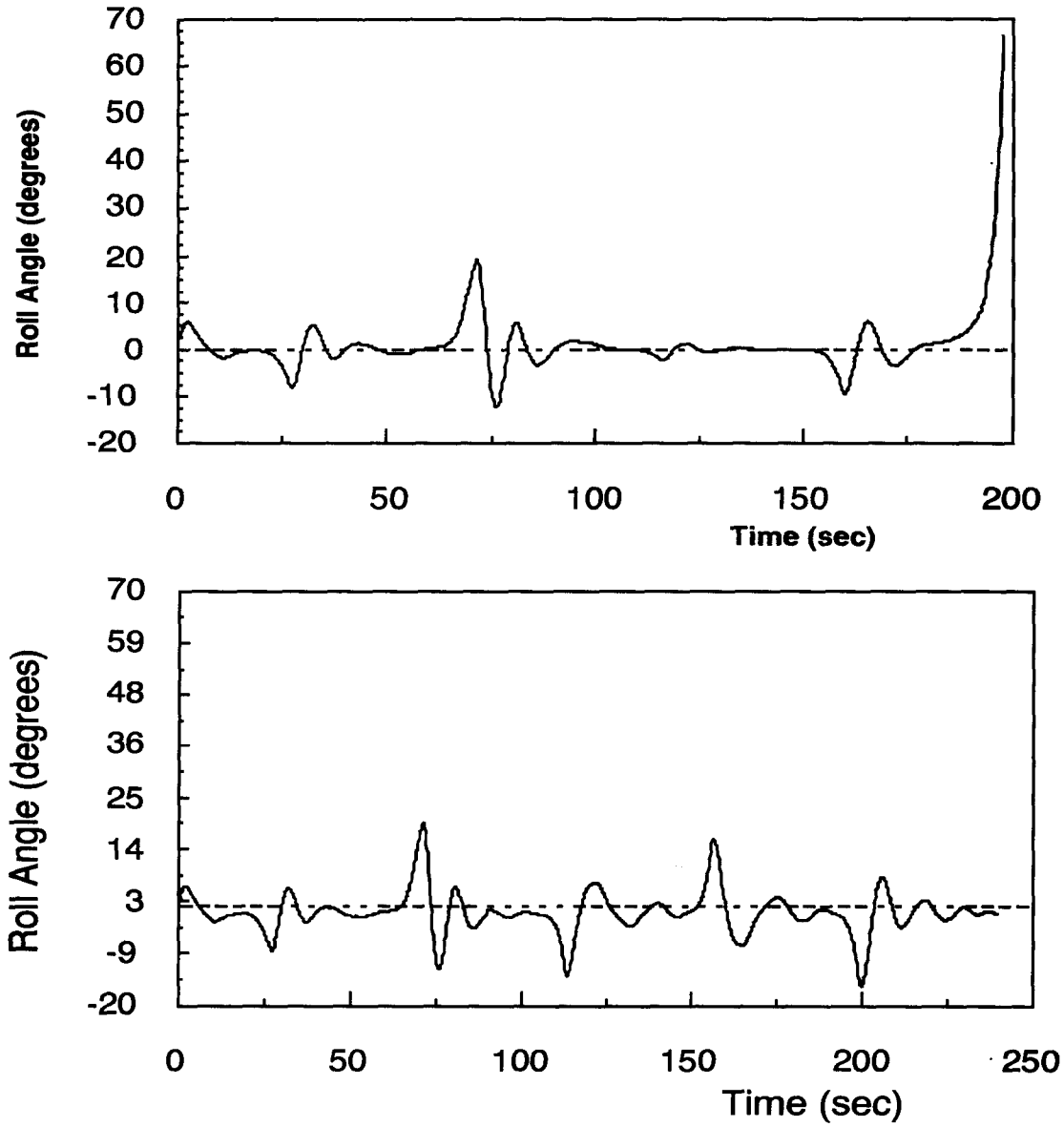

Figure 7.2: Low cycle resonance simulation in regular waves for UBC # 01

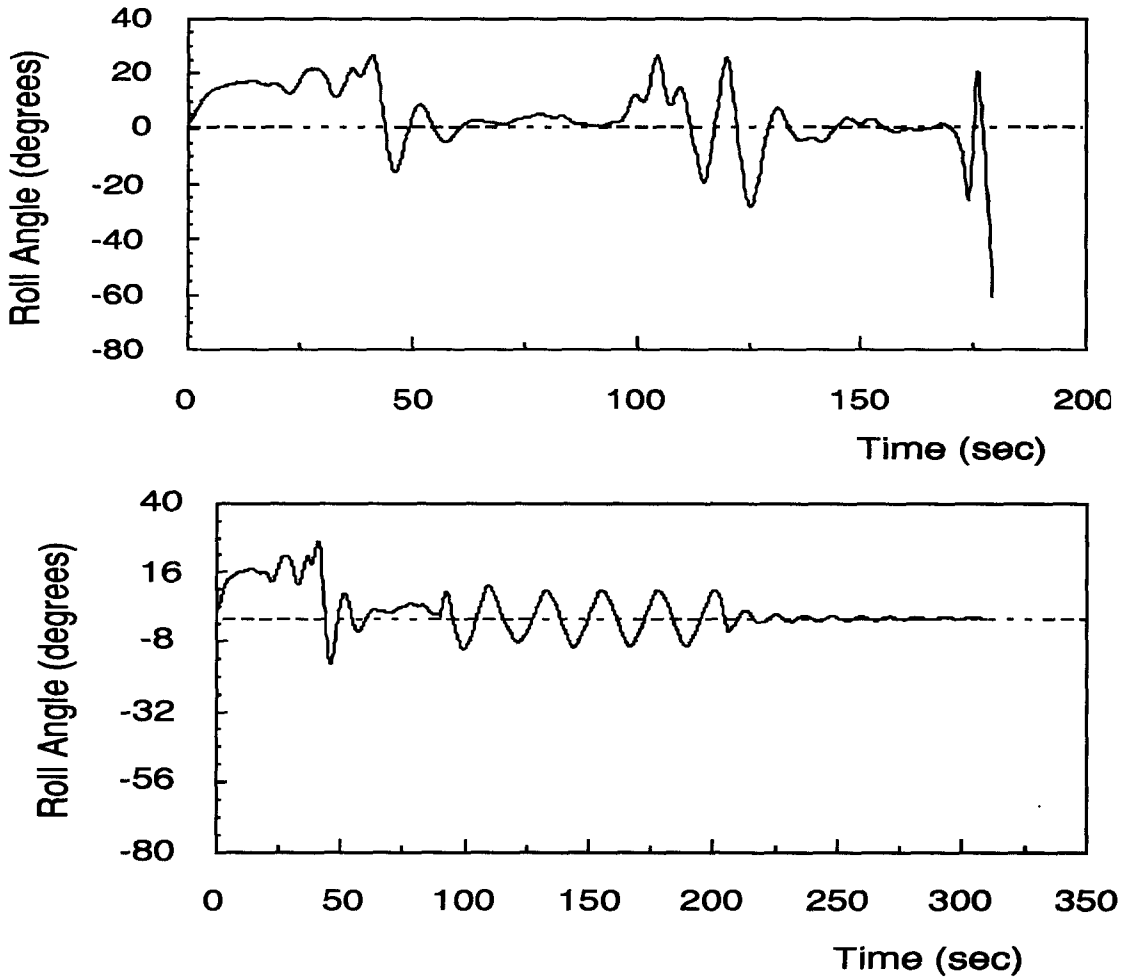

Figure 7.3: Low cycle resonance simulation in regular waves for UBC # 03

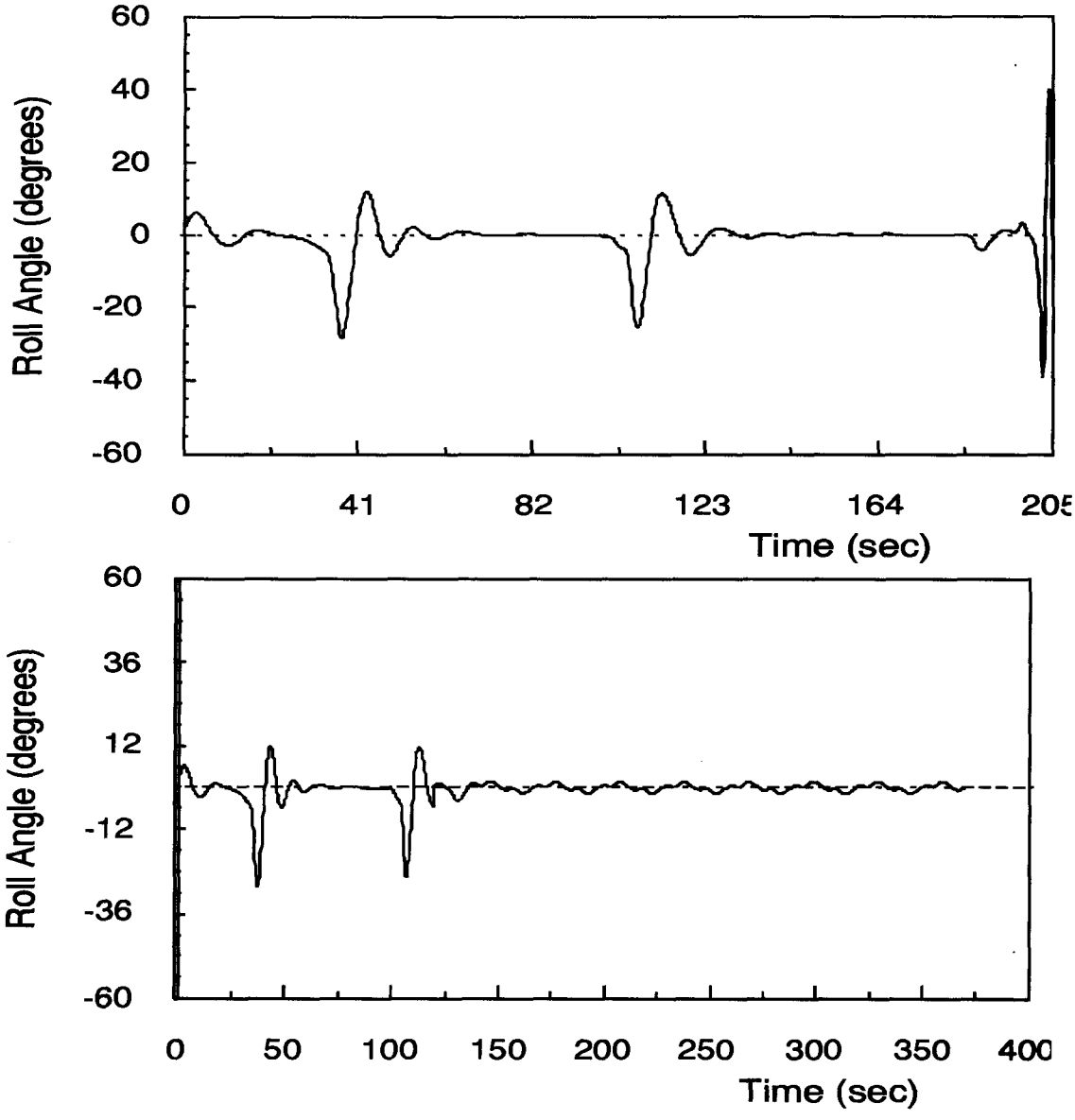

Figure 7.4: Low cycle resonance simulation in regular waves for UBC # 07

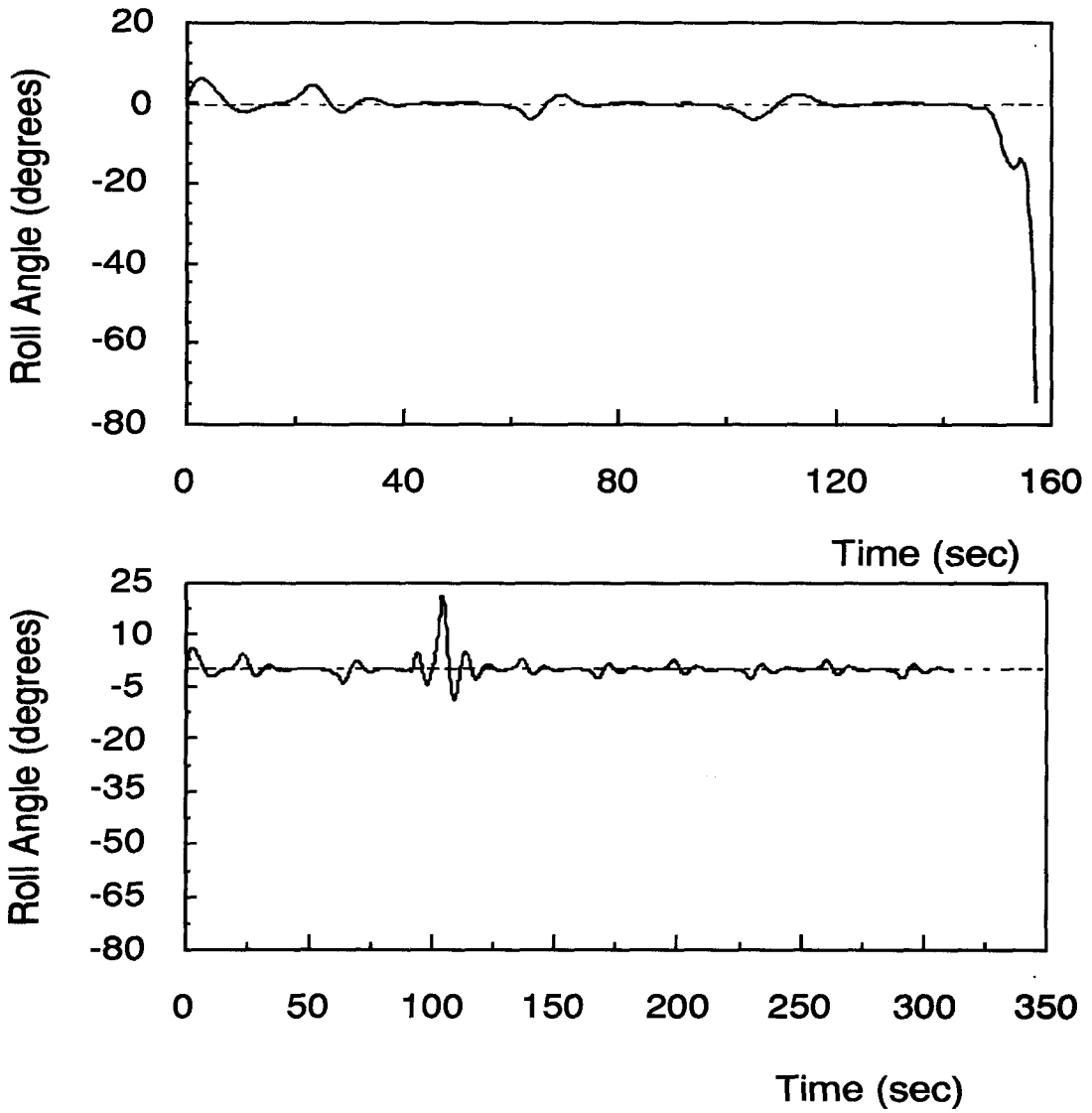

Figure 7.5: Low cycle resonance simulation in regular waves for UBC # 09

Figure 7.6 shows similar results for irregular following seas. A detailed explanation of these simulation techniques can be found in [28, 63, 69]

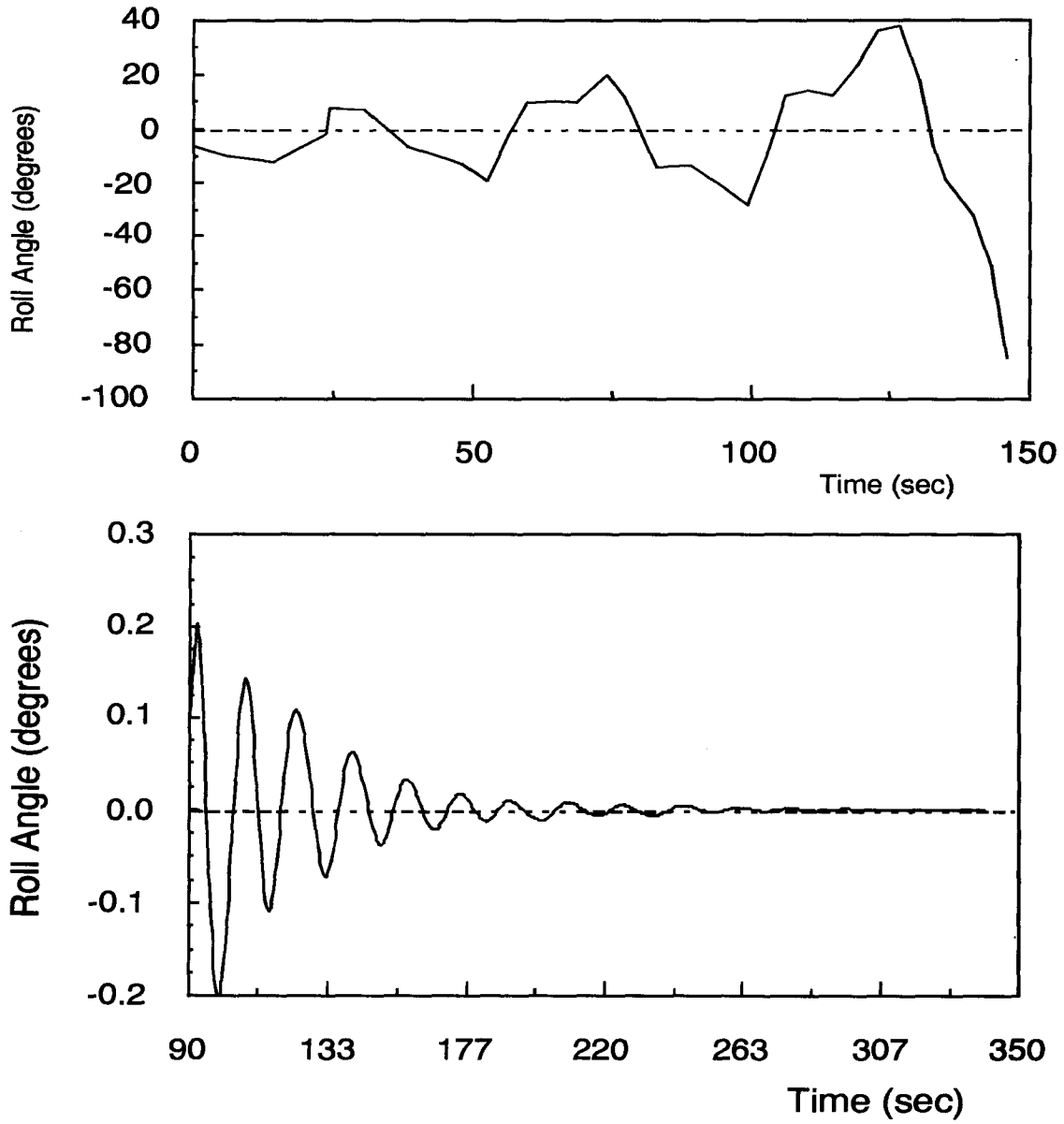

Figure 7.6: Low cycle resonance simulation in irregular waves

7.2 Pure Loss of Stability Simulations

This capsizing mode is characterized by the vessel being heeled over to one side for a prolonged period of time due to insufficient restoring energy in the system. Typical conditions for this mode are steep, large amplitude waves, and a large enough ship speed

so that the vessel stays in the wave crest for a relatively long period, during which static stability is reduced. The motion records for pure loss of stability in following seas are shown in Figure 7.7, 7.8, 7.9, 7.10. In this simulation the following inputs were used.

	UBC #1	UBC #3	UBC #7	UBC #9
Wave direction	180°	180°	180°	180°
Wave length (ft)	100 feet	110	100	100
Wave height (ft)	8.5 ft	8.7	8.7	8.6
Ship speed (knots)	12	12	12.2	12.5

Table 7.3: Inputs for pure loss of stability simulations in following seas

The following rule was selected by the advisory system to identify pure loss of stability.

IF wave_direction IS follow

AND WS_SS IS ZERO

AND Wave_height IS HIGH

AND ship_speed IS HIGH

THEN change_speed IS NM

Suggested action was to reduce speed by 3 knots. Following this suggestion, the simulation program was run again to observe the change in ship motion. Results after taking the suggested action are given in Figure 7.7, 7.8, 7.9, 7.10. As seen from Figure 7.7, 7.8, 7.9, 7.10, while the ship capsizes under those conditions, after the recommended action, the ship roll decays rapidly, and ship became stable.

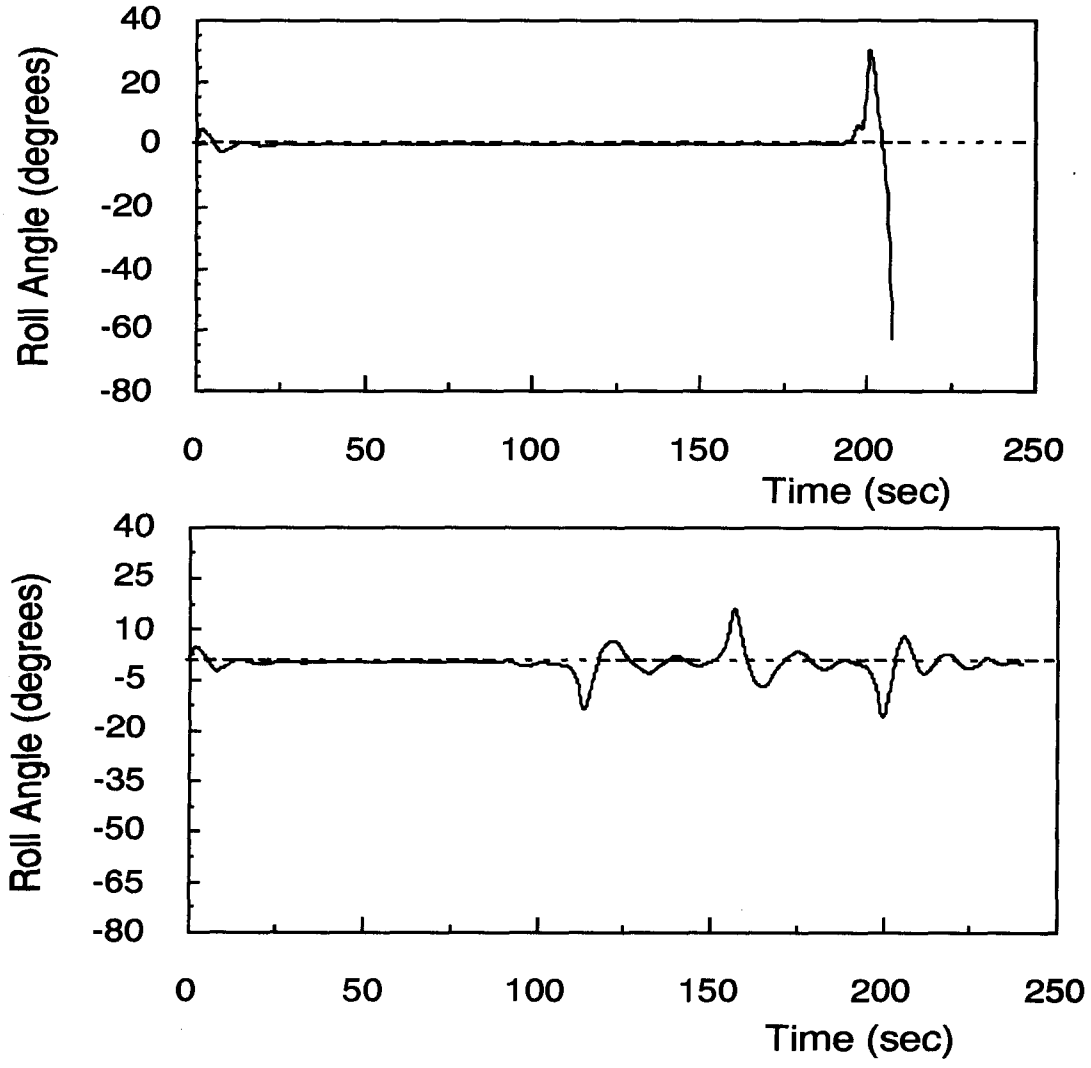

Figure 7.7: Pure loss of stability simulation for UBC #1

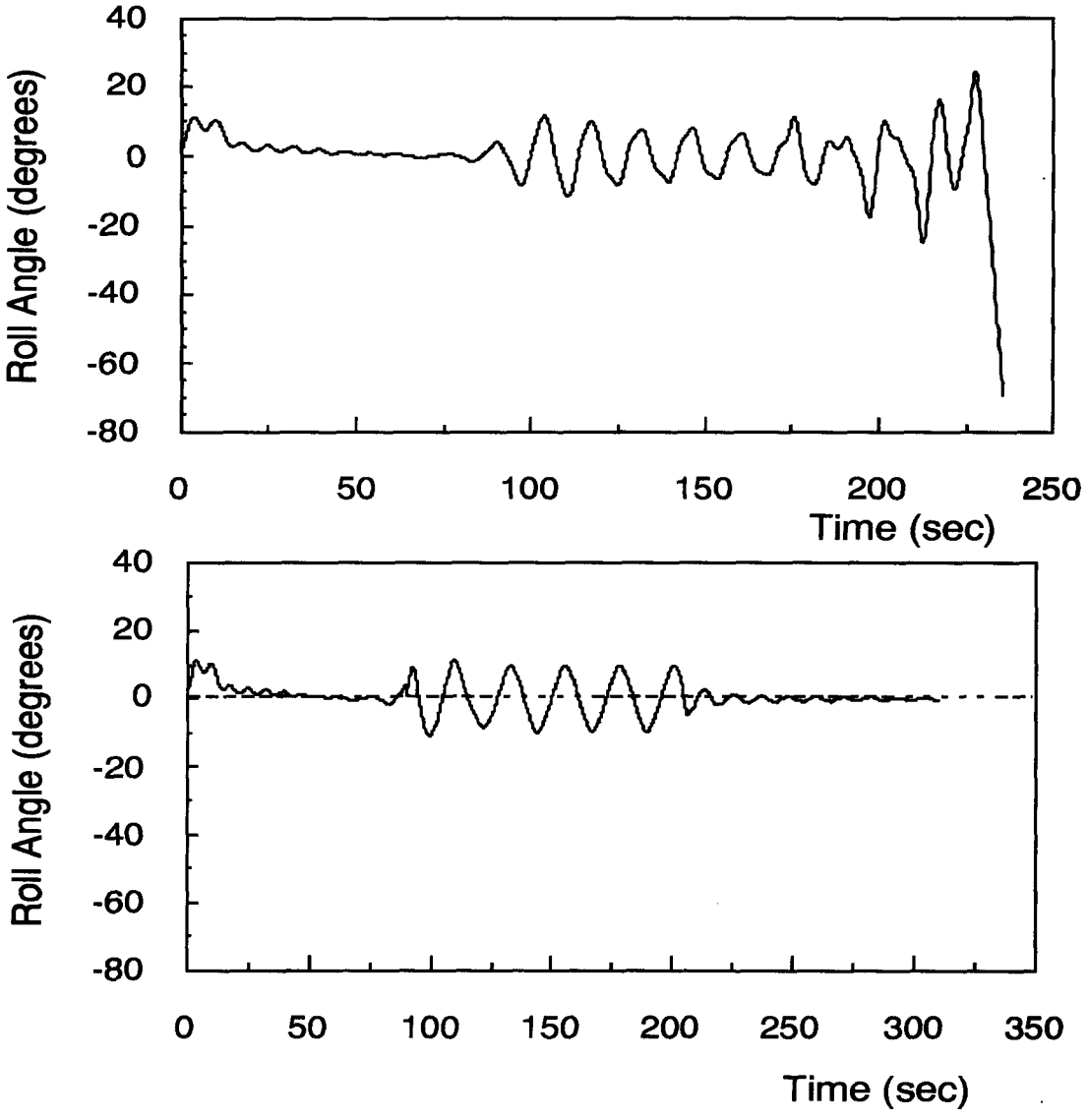

Figure 7.8: Pure loss of stability simulation for UBC #3

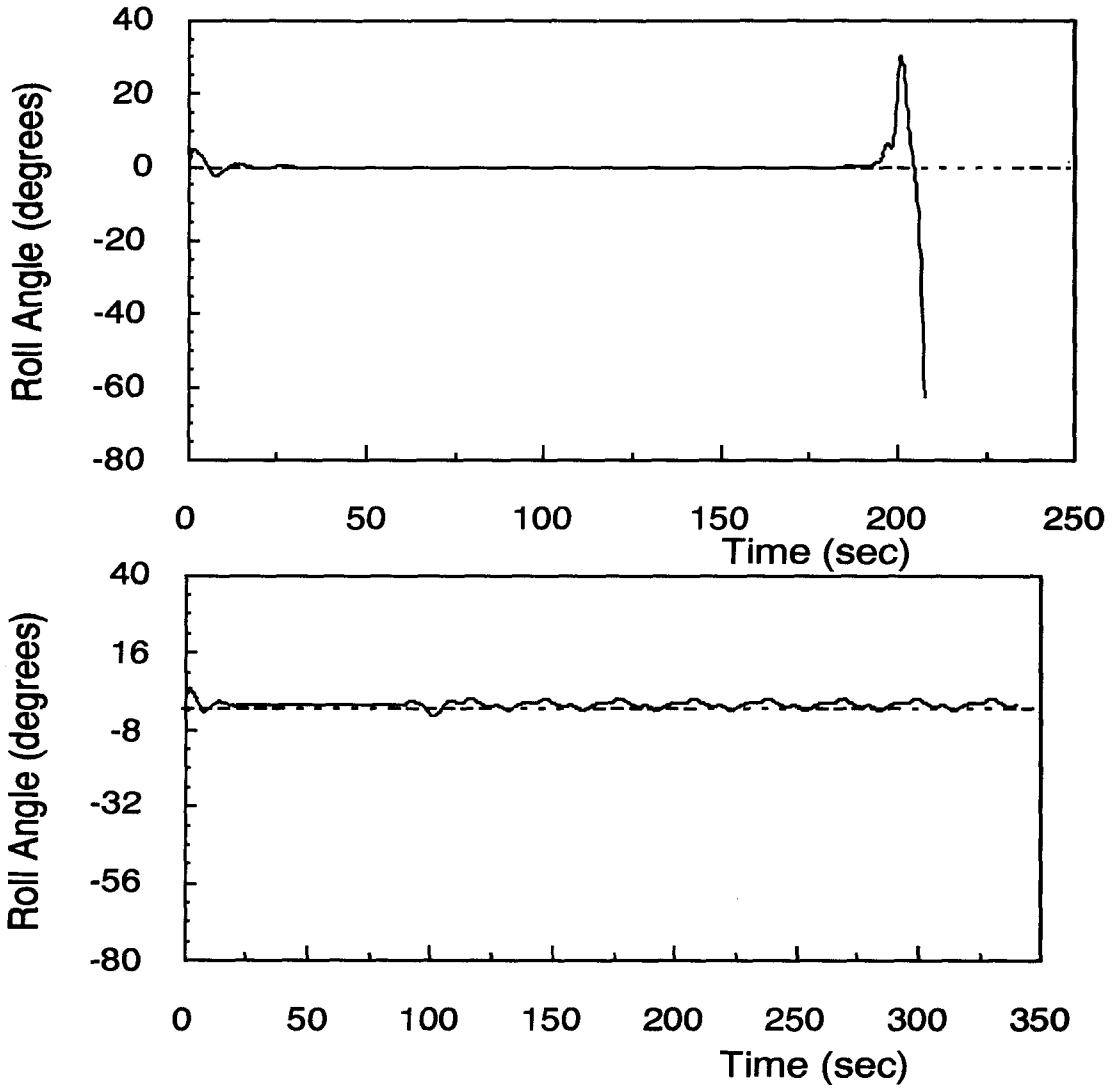

Figure 7.9: Pure loss of stability simulation for UBC #7

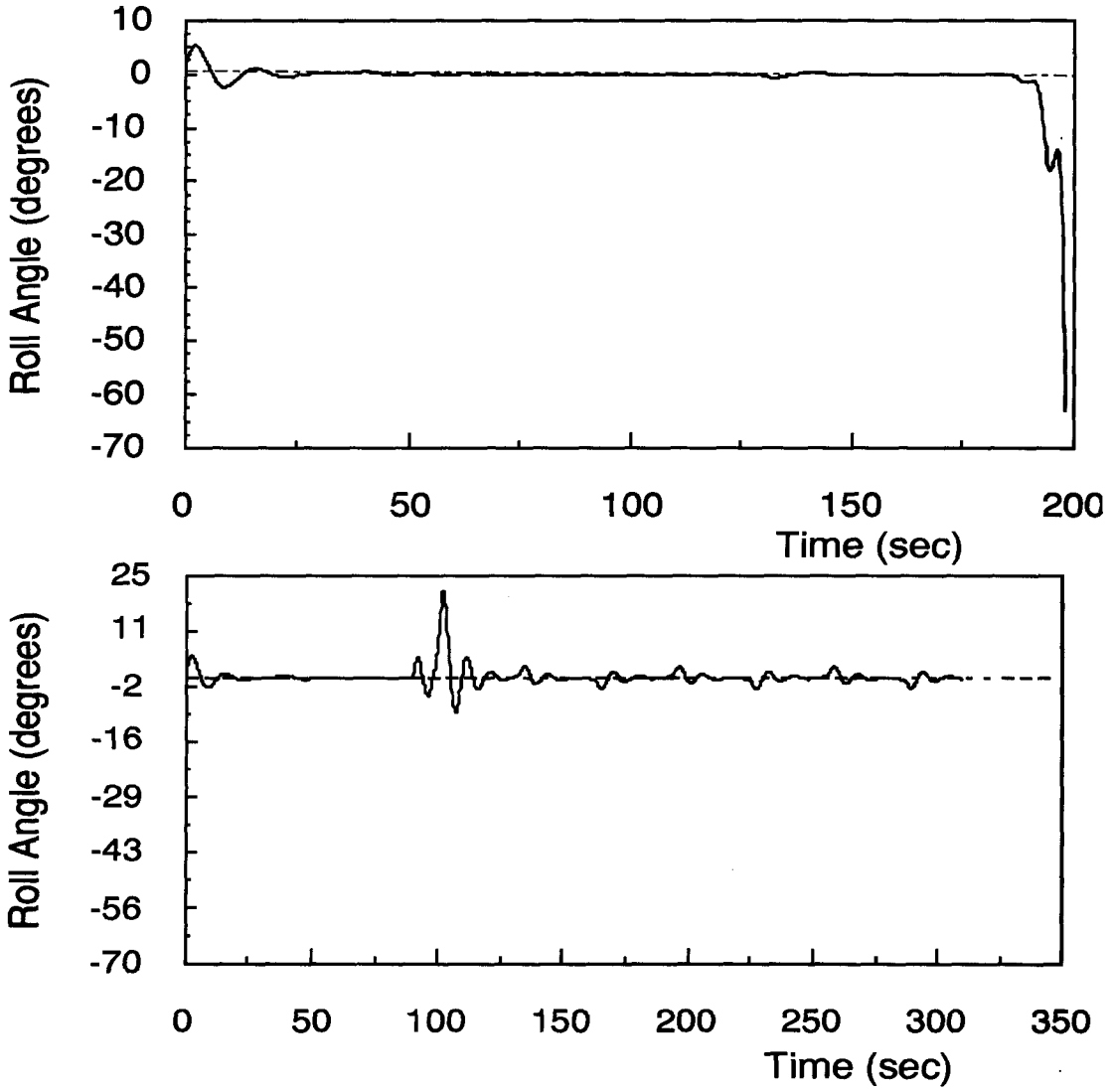

Figure 7.10: Pure loss of stability simulation for UBC #9

As seen from Figure 7.7, 7.8, 7.9, 7.10, the vessel capsizes in a relatively short time after it starts rolling (when captain may realise the danger), if the wave height is big enough. For this mode of capsizing, there is a certain critical amplitude, say A_{cr}. if $A < A_{cr}$, it was found that the roll motion (for a given initial roll angle) will decay to zero with increasing time, while for the case where $A > A_{cr}$, the vessel will lean over to either

side for a significant amount of time before capsizing. Although, numerical simulations show that A_{cr} is approximately equal to the draft of the ship, more simulations with different types of vessels are needed to confirm this.

7.3 Resonant Excitation Simulations

Resonant excitation simulations were done in two different seas : Quartering and beam seas. In these two different wave directions, a Bretschneider spectrum (see Appendix D) was used to simulate incoming waves.

RMS roll motion values were used to compare results before and after the suggestion. The RMS roll angle $\sigma_0$is given by :

$$\Sigma_0^2 = \int_0^\infty S(\omega_e) d\omega_e \tag{7.1}$$

where $S(\omega_e)$ is the roll motion spectrum and ω_e is encounter frequency.

Figure 7.11 shows the resonant excitation simulation for UBC # 01. In this simulation, the wave direction was 40° and ship speed was 9 knots. Using these inputs, the shipmo4.for program was run to obtain the RMS roll angle data. Then, the same conditions were used as inputs to the advisory system. The suggested action by the fuzzy expert system was to change direction by 30° towards following seas. These simulations were run for 6 different significant wave heights. The results of these two sets of runs are shown in Figure 7.11. Similarly, these runs were repeated for the other vessels.

As seen from Figure 7.11, 7.12, 7.13, 7.14, reductions in RMS roll motion are about 50 - 60 %.

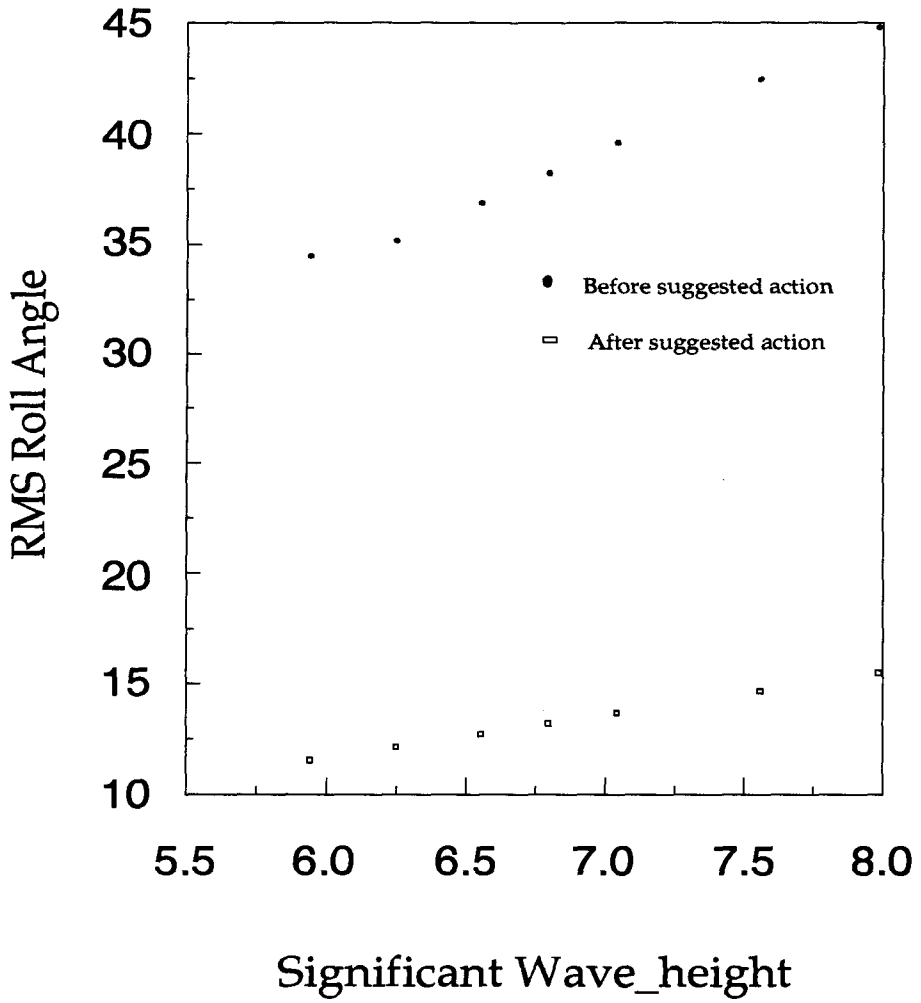

Figure 7.11: Quartering seas simulations for UBC # 01

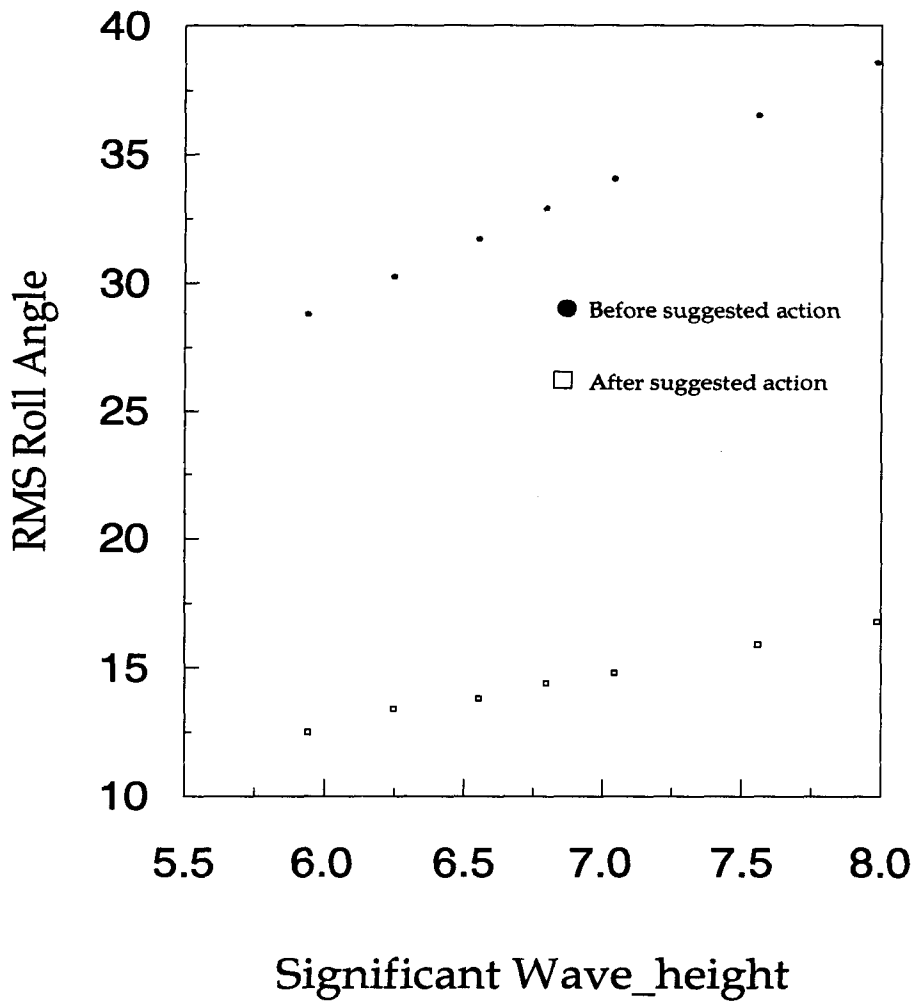

Figure 7.12: Quartering seas simulations for UBC # 03

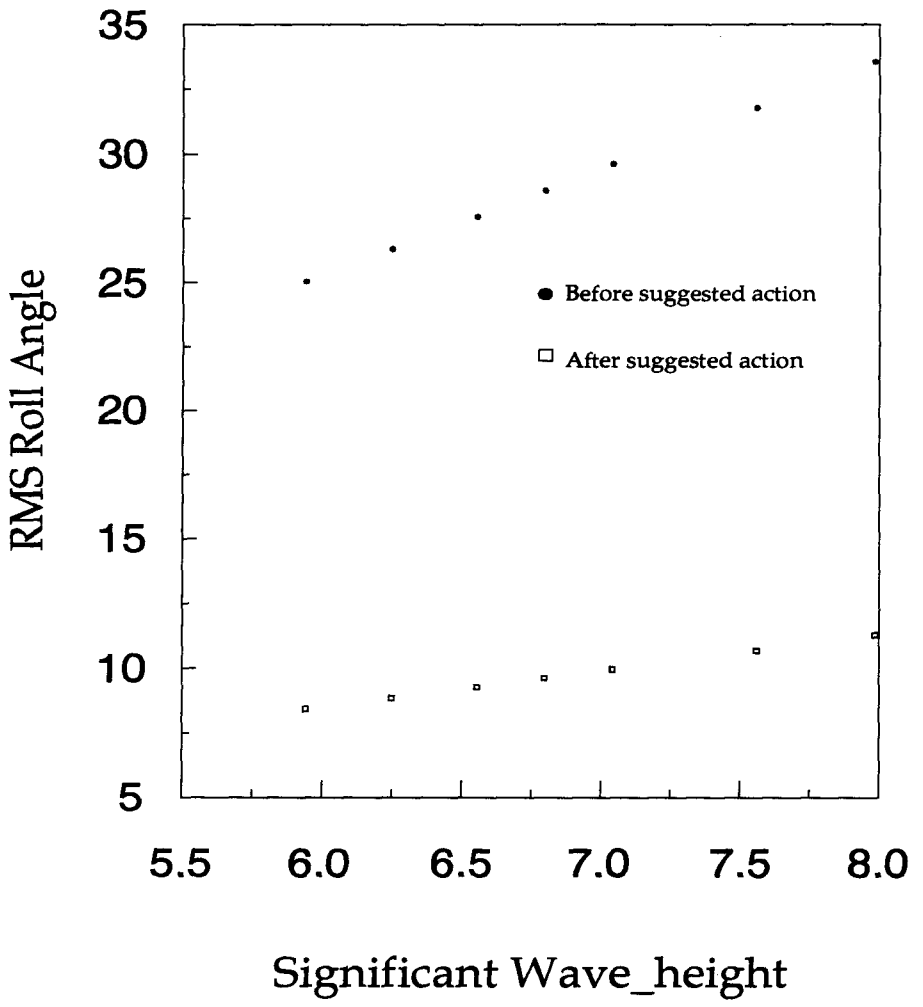

Figure 7.13: Quartering seas simulations for UBC # 07

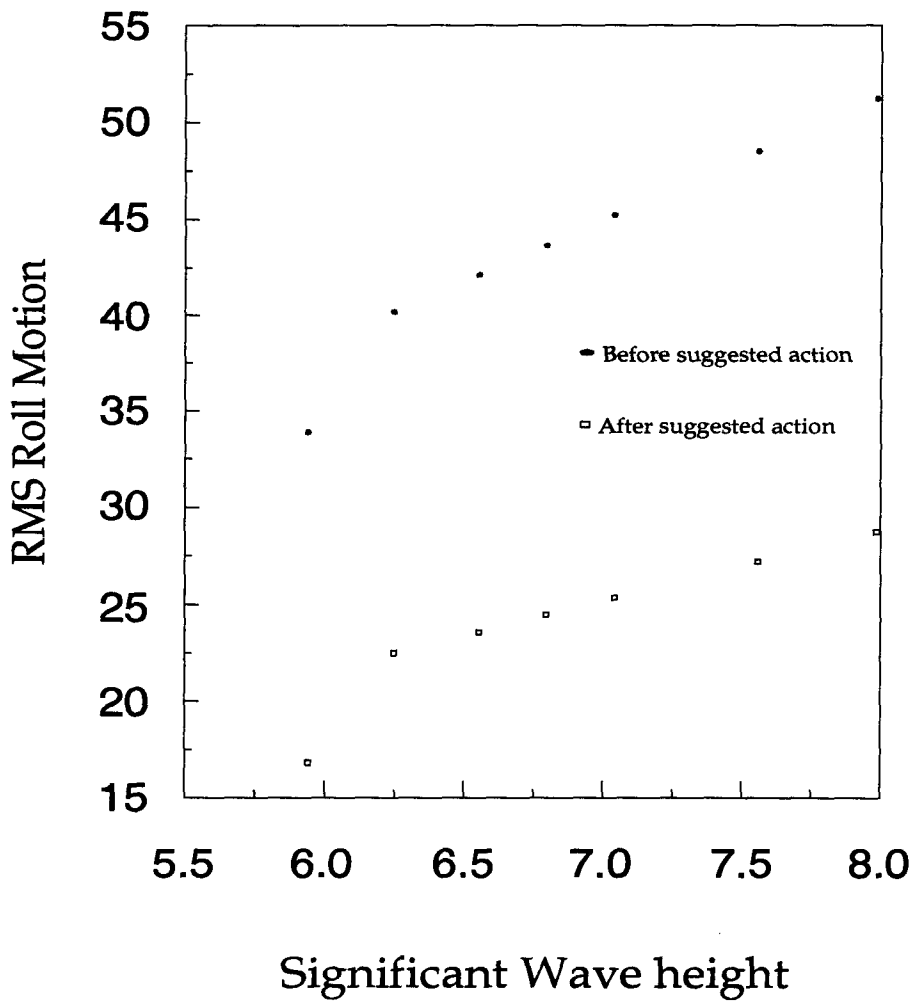

Figure 7.14: Quartering seas simulations for UBC # 09

Figures 7.11, 7.12, 7.13, 7.14 show the results for quartering seas resonant excitations. In this simulation, the wave direction is 40° and the suggested action by the fuzzy expert system is to change direction by 30° toward following seas. During the decision making, the expert system checks conditions after the estimated action before giving the advise to the captain. The reason for this is to make sure that the vessel would not face a low cycle resonance or a pure loss of stability after the suggested action. As seen from Figure 7.11, 7.12, 7.13, 7.14, reductions in RMS roll motion are about 40 - 70 %.

In these simulations, the feasibility of changing speed only is also investigated. These simulations were done for 7 different sea states. In order to investigate the effects of speed and direction , the simulation program was run by changing speed only, changing direction only and both. Tables 7.3, 7.3, 7.3, 7.3 show the results of these simulations. As seen from these tables, changing speed is not very effective for reducing roll motion under these conditions. From these results, it was decided to use only changing direction as a suggestion from the advisory system.

Sig. wave height	Sea State	UBC # 01			
		before	change direction	change speed	both
5.94	6	33.49	11.55	30.95	9.66
6.25	7	35.18	12.15	32.57	10.16
6.55	7	36.88	12.74	34.10	10.65
6.80	7	38.23	13.20	35.35	11.05
7.04	7	39.58	13.67	36.60	11.44
7.55	7	42.45	14.67	39.26	12.28
7.99	7	44.80	15.49	41.45	12.97

Table 7.4: Quartering seas simulation for UBC # 01

Sig. wave height	Sea State	UBC # 03			
		before	change direction	change speed	both
5.94	6	30.35	12.50	28.80	11.75
6.25	7	31.89	13.40	30.26	12.35
6.55	7	33.43	13.80	31.72	12.95
6.80	7	34.65	14.40	32.89	13.44
7.04	7	35.89	14.80	34.05	13.92
7.55	7	38.49	15.90	36.53	14.94
7.99	7	40.63	16.78	38.56	15.78

Table 7.5: Quartering seas simulation for UBC # 03

Sig. wave height	Sea State	UBC # 07			
		before	change direction	change speed	both
5.94	6	26.46	8.42	25.04	8.15
6.25	7	27.44	8.84	26.31	8.57
6.55	7	28.77	9.27	27.59	9.27
6.80	7	29.83	9.62	28.61	9.62
7.04	7	30.89	9.96	29.62	9.64
7.55	7	33.14	10.69	31.78	10.35
7.99	7	34.99	11.29	33.56	10.94

Table 7.6: Quartering seas simulation for UBC # 07

Sig. wave height	Sea State	UBC # 09			
		before	change direction	change speed	both
5.94	6	37.51	19.72	33.86	16.84
6.25	7	42.99	22.44	40.16	22.45
6.55	7	45.07	23.53	42.11	23.59
6.80	7	46.73	24.40	43.67	24.60
7.04	7	48.39	25.27	45.22	25.34
7.55	7	51.92	27.13	48.52	27.19
7.99	7	54.83	28.65	51.24	28.54

Table 7.7: Quartering seas simulation for UBC # 09

Similar results are found for resonant excitation at beam seas (see Figure 7.15, 7.16, 7.17, 7.18). In this case, wave direction is 80° . This was considered as mostly beam seas and partially quartering seas by the advisory system. The suggested action given is to change direction by 30° towards head seas. Reduction in RMS roll motion was about 40 - 60 %.

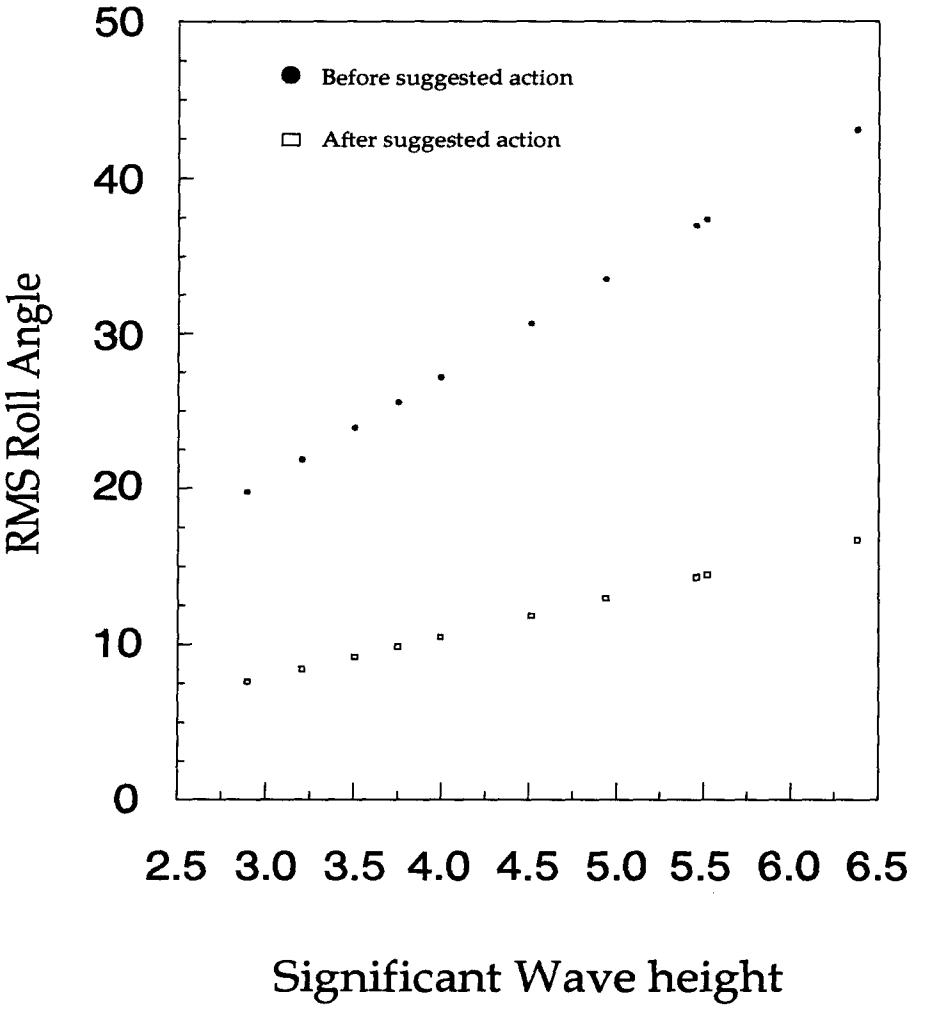

Figure 7.15: Beam seas simulations for UBC # 01

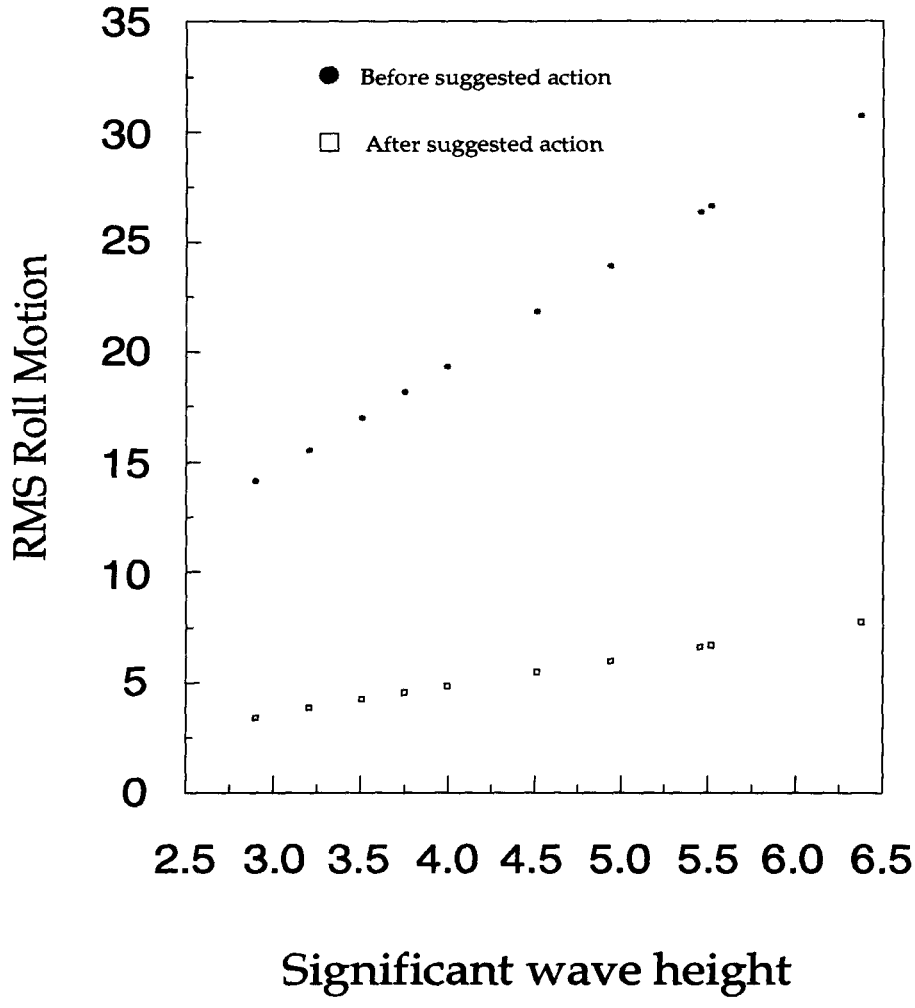

Figure 7.16: Beam seas simulations for UBC # 03

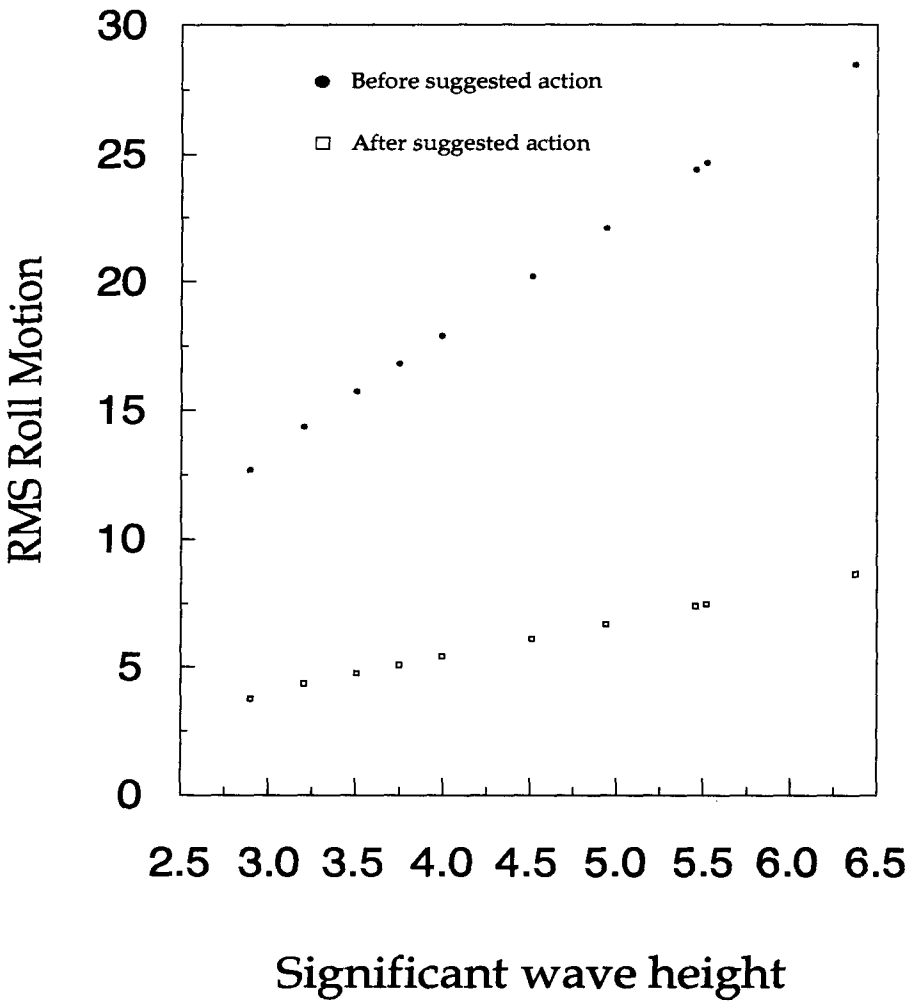

Figure 7.17: Beam seas simulations for UBC # 07

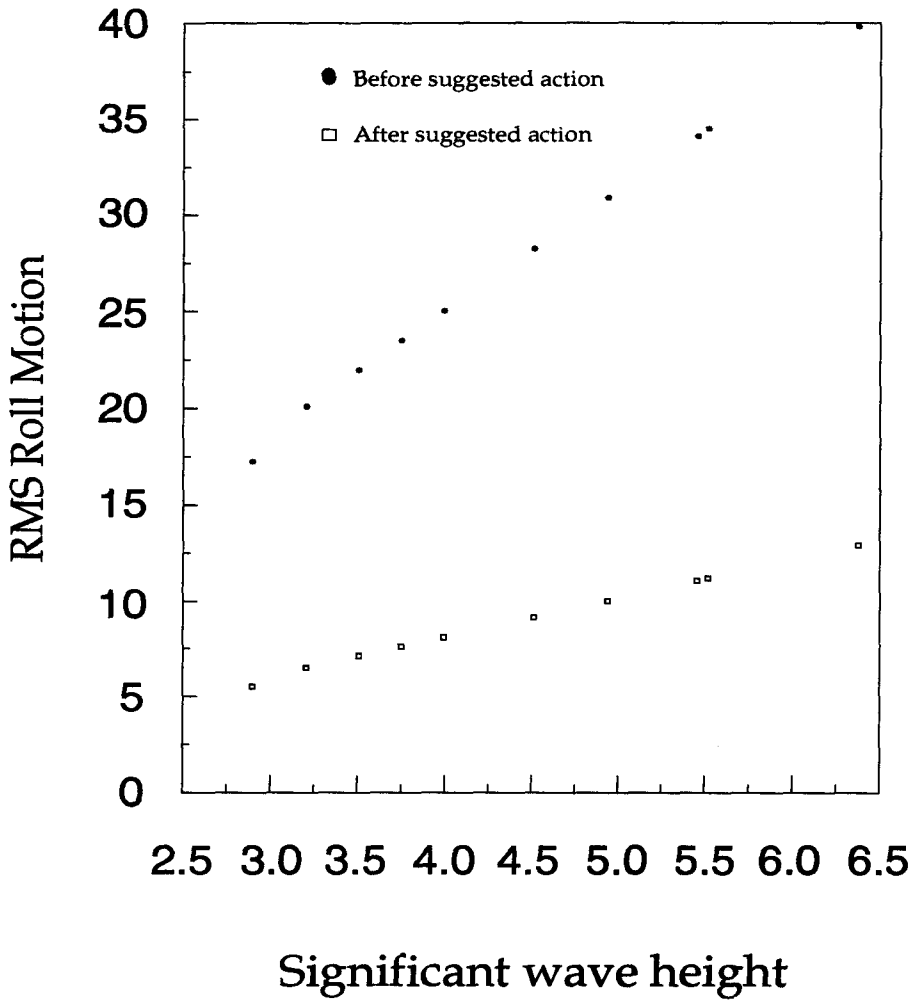

Figure 7.18: Beam seas simulations for UBC # 09

7.4 Simulation of Soehae (Korean) Ferry Accident

A tragic accident struck the Korean people on the 10th of October 1993, when the Soehae Ferry capsized and sank. This accident claimed 270 lives. Figure 7.19 shows the Soehae ferry, when it was brought to the surface to retrieve more bodies trapped inside the vessel (The Korean Herald Newspaper).

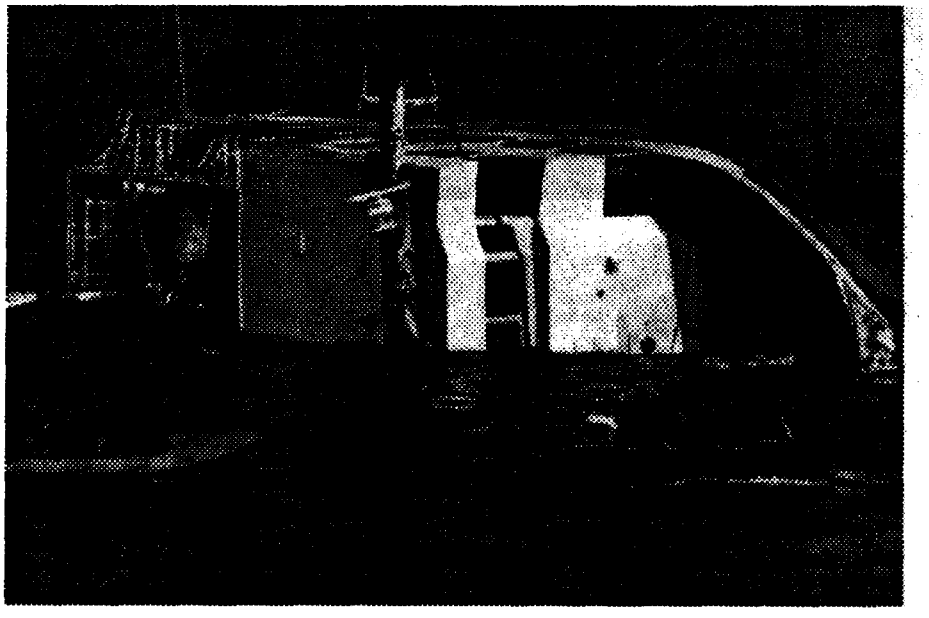

Figure 7.19: The Seohae Ferry after it was brought to surface

According to eyewitnesses, the accident occurred very quickly. After turning to starboard, the vessel rolled two or three times and capsized.

In this section, possible use of the monitoring and advisory system for this kind of accidents is discussed.

The first step is to analyse the static stability of the vessel and check if it meets the rules, such as IMO or Coast Guard rules. These analyses were done just after the accident by Prof. K. P. Rhee of Seoul National University. A body plan of the vessel

and the results from these analyses are given in Figure 7.20 and Table 7.4.

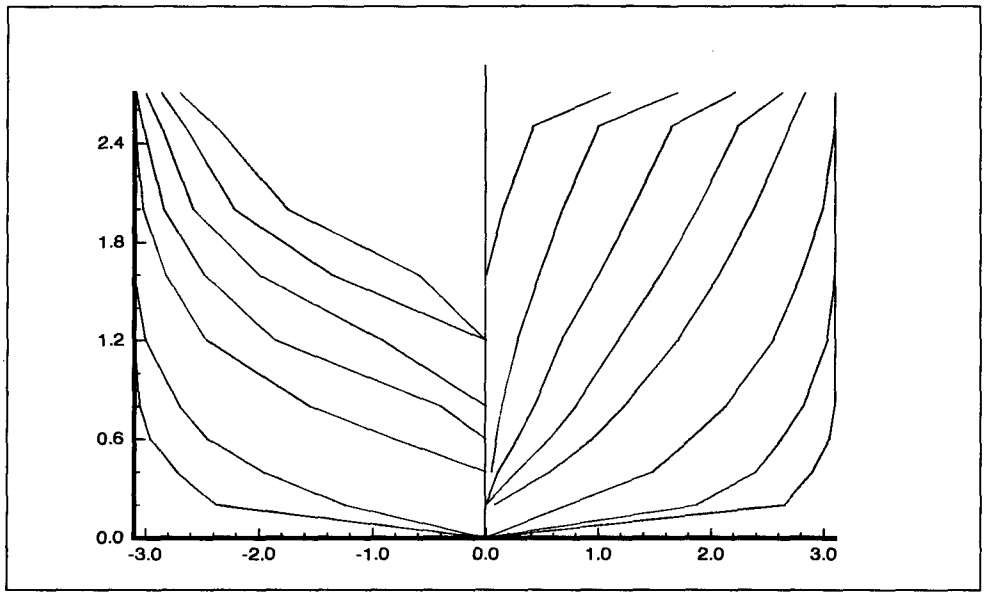

Figure 7.20: Body Plan of the Seohae Ferry

	Loading Conditions			
	Light ship	Light load departure	light load arrival	Full load departure
Overall Length (m)	37.40	-	-	-
LBP (m)	33.0	-	-	-
Breadth (m)	6.20	-	-	-
Depth mld. (m)	2.70	-	-	-
Displacement (Ton)	188.0	205.2	199.9	231.7
Draft (m)	1.628	1.715	1.686	1.886
MTC (t-m)	3.035	3.352	3.267	3.754
KG (m)	2.576	2.518	2.558	2.508
GM (m)	0.605	0.623	0.594	0.592
LCB (Aft -) (m)	-0.926	-0.972	-0.957	-1.044
LCG (Aft -) (m)	-2.054	-2.516	-2.470	- 1.858

Table 7.8: Results From Static Stability Calculation of the Seohae

According to the International Maritime Organization (IMO) stability rules, the minimum GM should be bigger than 0.15 m. As seen from Table 7.4, the Seohae met this criteria under all conditions.

The second step is to analyse the dynamic conditions. When the accident occurred, the ship was navigating at about 10 knots, estimated wave height was about 2.0 m, and the wave direction was following seas. There is no information available about wave frequencies or length.

The following data is used to simulate the accident conditions.

Ship Speed	10 Knots
LBP	33.0 m
Draft	1.90
Wave Height	2.0 m
Wave Length	32.0 m

Table 7.9: Input Data for Dynamic Stability Simulations

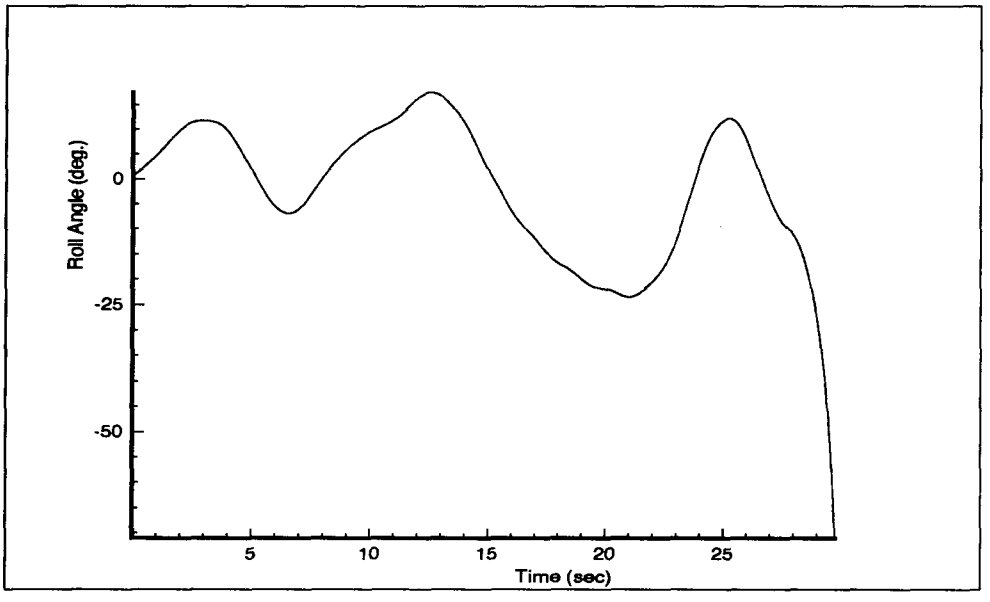

Figure 7.21: Capsizing Simulations of the Seohae

As seen from Figure 7.21, the vessel was capsized within 28 seconds, after 3 rolls.

This result is in agreement with the eyewitness reports.

After the above simulation, the same conditions were input to the monitoring and advisory system. The recommended action was to reduce speed 3 knots. In this simulation, it is assumed that the captain had an option to analyse the situation before turning. That is, the captain input new heading and speed. Since the other information such as wave direction, frequencies and estimated height are available from the monitoring system, the advisory system only needs these two pieces of information to analyse the new condition. Figure 7.22 shows roll motion data of the vessel after suggested action.

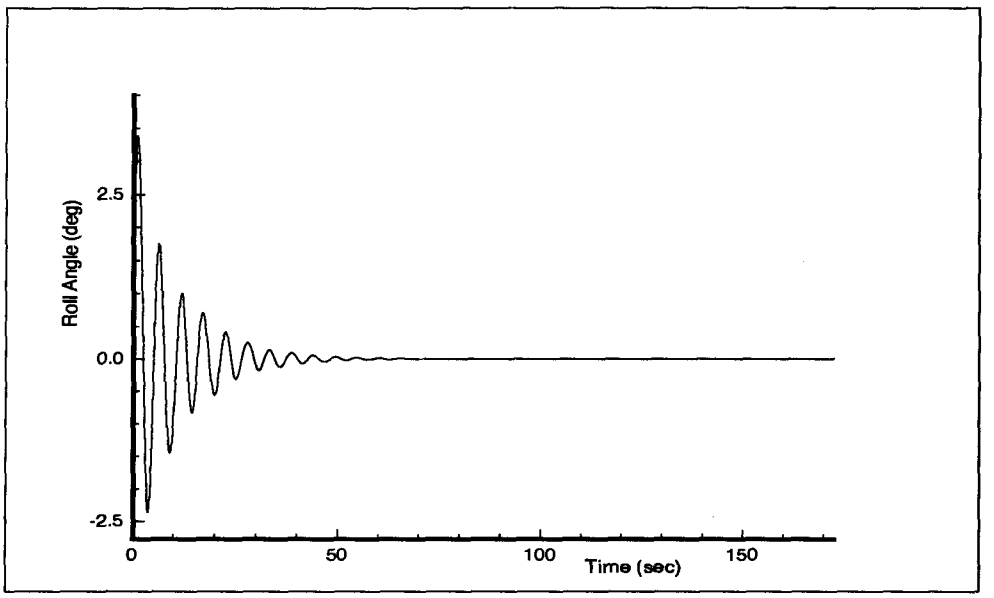

Figure 7.22: Capsizing Simulations of the Seohae

These simulations show the possible use of a monitoring and advisory system. Because these simulations do not take some factors, such as shift of cargo, sloshing etc. into account, these results should only be considered as preliminary. But it is clear that a captain would have a better understanding of the vessel and environment conditions and more help to make a reliable decision.

Chapter 8

Conclusions and Future work

8.1 Conclusions

In this research, the architecture of an intelligent monitoring and advisory system has been developed. This system uses environmental information obtained from a number of sensors and proposes corrective action based on a rule-base derived from human expertise, experiments and theoretical research. This system has two primary advantages for practical application :

- The system uses the available on-board equipment such as Loran-c, radar and computer, (most ships have nowadays) making the system less costly.
- The system does not interfere with the operation of the vessel.

Contrary to the previous work on this area, this system also monitors the static stability of the vessel. The importance of this can easily be seen from statistics on accidents. In this part, two different methods (dynamic inclining experiments) are developed for estimating metacentric height (GM) of the vessel. These are *Estimating the coefficients of GZ curve* and *Spectral analysis.* Reasonable agreements were found between predicted and experimental values.

Monitoring the dynamic stability of the system is divided into two steps :

1. monitoring environment parameters
2. measurement and analysis of ship motions

As a part of the monitoring system, processing of radar images is used as a method for extracting wave properties.

Three-dimensional spectral analysis of a series of radar images has been previously demonstrated as a method for determining the orientation and direction of ocean waves. Unfortunately, this technique is very costly in terms of processing time which is in the order of 12 minutes on a dedicated HP Workstation [51, 52]. In view of the need for the wave parameters at a much faster rate (see Appendix F), in the order of 30-60 seconds, for input into the intelligent advisory system, alternative techniques based on image processing methods have been developed.

Two techniques, the *boxing technique* and the *thinning technique*, have been developed to provide the required wave parameter data at an acceptable rate. The *boxing technique* finds the wave orientation by fitting thin rectangular boxes to wave regions in a binary radar image.

The success of the *boxing technique* depends on the initial placement of the rectangular box. The radar images tend to have limited regions in which the wave directions are obvious. There is considerable noise in the images and much of the wave information is obscured. The *boxing technique* works well if the box is placed in the vicinity of an obvious wave, reliable automatic placement of the box still remains as a problem. In order to overcome the local nature of the boxing technique, a more global *thinning technique* has been developed.

The *thinning technique* transforms a binary radar image by eroding all objects until only the skeleton or spine of each object remains. A histogram of wave orientations is maintained, and the goodness-of-fit and the length of each segment are used to bias the histogram entries. The wave orientation corresponding to the peak in the histogram is selected as the dominant wave direction. Since the wave orientation is known, comparisons between the initial image region and regions in successive images is restricted to

shifts along the line normal to the wave orientation. The least-squares error between the regions is used as the basis for selecting the wave direction. Finally, the maximum entropy method is used to determine the wave frequency in a direction normal to the wave orientation. This technique has been tested on typical radar images and the resulting parameters are in agreement with both the 3-D spectral analysis technique and the simpler *boxing technique*. The primary advantage of the *thinning technique* over the *boxing technique* is the global nature of the orientation phase.

A fuzzy expert system has been developed as a decision making process for the monitoring and advisory system. Rules forming the basis for the advisory system are presented. An advantage of this structure is that new rules may be easily appended to the existing rule base in view of further knowledge gained through interview with experts, experiments or theoretical developments.

Finally, the feasibility of the approach has been demonstrated through simulations of various sea conditions on a range of ship forms. Simulations show that the vessel considered capsizes very quickly, in the order of 2 - 2.5 minutes and usually after only a few rolls. As seen from Figures 7.2, 7.3, 7.4, 7.5, 7.7, 7.8, 7.9, 7.10, the maximum roll angle before capsizing is about 20°. Therefore, it is difficult for a captain can realise the danger under these conditions, since the captain cannot estimate the wave frequency and wave length. But having a system described in this thesis would help the captain to see the danger very quickly and take preventive action in time. This would prevent accidents and loss of lives.

8.2 Contributions of this research

The main contribution of this research is to show the feasibility of obtaining environmetal data in a short time and the development of a suitable monitoring and advisory system

for safety of vessels. Using a fuzzy expert system based monitoring and advisory system to help to combine the knowledge already available from experts and experience with the knowledge gained from theoretical and experimental analysis to enhance the reliability of the system is another contribution.

This research provides image processing techniques to find wave parameters from radar images in 30 - 60 second. This technique is also suitable for automated processing which is needed for this work.

Other contributions include: Showing the need for monitoring static stability and providing a methodology for it. Using the ship as a sensor to estimate the wave height.

8.3 Future Work

Further developments on this area may be suggested as :

In static stability : More experiments with different kinds of ships to test the estimation methods for GM is needed.

In the fuzzy expert system : Since the membership values for each variable have to be set manually, a methodology for making this process automatic would be useful in developing a general system. Including the rules to warn a captain before any maneuvering would be beneficial. For these rules, a user interface unit can be added to the system. The captain, before maneuvering in heavy weather, can input the ship's new heading and/or speed. Then the system could analyse these new conditions with the information gathered from radar and other sensors and give the captain advice such as to continue a particular action or not to.

In general : On-board testing of the system is necessary to learn more about the system's behaviour under operational conditions. A hardware version of this method needs to be developed and tested.

Bibliography

[1] E. A. Dahle and O Kjaerland. The capsizing of m/s helland-hansen. *Transactions of RINA*, pages 51 – 73, 1979.

[2] E. A. Dahle and N Gunnar. Intact and demaged stability of small crafts with emphasis on design. *Design consideration for small craft, London*, 1, 1984.

[3] A Morrall. The gaul disaster: An investigation into the loss of a large stern trawler. *Transactions of RINA*, 1980.

[4] A Morrall and A. R. MacNaughton. Fishing vessel stability and safety- a cautionary note when considering possible changes in imo standards. *Design Considerations for Small Crafts, London*, 1984.

[5] H Bird and A. Morrall. Research towards realistic stability criteria. *Transactions of RINA*, 1985.

[6] Y. S. Yang. *Marine Hazard Assessment.* PhD thesis, U. of Newcastle Upon Tyne, 1985.

[7] Transport Canada. *Statistical Summary of Marine Accidents.*

[8] E. Köse. Risk assessment of fishing vessels. Master's thesis, University of Newcastle Upon Tyne, U.K., 1991.

[9] K. Lindemann and N. Nordenstrø m. A system for ship handling in rough waether. In *4th Ship Control System Symposium*, 1975.

[10] D. Hoffman. The impact of seakeeping on ship operatoions. *Marine Technology*, 13:241 – 292, 1976.

[11] Ff-1052 class heavy weather operator guidance catalog. Technical report, Naval Sea Systems Command, 1979.

[12] D. Hoffman. The integration of shipboard and shore based systems for operation in heavy weather. *Ship Operation Automation*, pages 159 – 168, 1980.

[13] D. Hoffman. Wave measurements and implementation on board ship. Technical report, National Maritime Research Center NMRC-KP-141, 1977.

[14] Great lake carriers hull monitoring system. Technical report, U.S. Department of Commerce / Maritime Administration, Office of Maritime Technology, 1978.

[15] K. Lindemann, J. Odland, and J. Strenghangen. On the application of the hull surveillance system for increased safety and improved utilization in rough weather. In *SNAME*, volume 85, 1977.

[16] Proposal for 1979 - norwegian so3. Technical report, Det Norske Veritas, 1979.

[17] Hull surveillance. *Marine Week*, page 10, 1979.

[18] M. schofield. Unique heavy lift monitoring system computerizes offshore construction. *Offshore Magazine*, 1977.

[19] T. Koyama, Susumu. H., and K. Okumoto. On a micro - computer based capsize alarm system. In *Second Int. Conf. on Stability of Ship and Ocean Vehicles*, pages 329 – 339, 1982.

[20] J. R. Paulling. The transverse stability of a ship in a longitudinal seaway. *Journal of Ship Research*, pages 37 – 49, 1961.

[21] J. O. de Kat. *Large amplitude ship motions and capsizing in severe sea conditions.* PhD thesis, U. of Berkeley USA, 1988.

[22] O. H. Oakley, J Paulling, and P. D. Wood. Ship motions and capsizing in astern seas. In *10th Symposium of Naval Hydrodynamics*, pages 297 – 337, 1974.

[23] *Accident investigation reports.* no : 476 and 479.

[24] E. V. Lewis. *Principle of Naval Architecture.* Society of Naval Architecture And Marine Engineers, 1989.

[25] C. R. Martin. Rudder roll reduction for small ships. Master's thesis, University of British Columbia, Vancouver, Canada, 1993.

[26] H. Himeno. Prediction of roll damping. Technical report, The University of Michigan, 1981.

[27] K. J. Rawson and E. C. Tupper. *Basic Ship Theory.* Longman Scientific & Technical, 1988.

[28] A. Allievi. Experimental and numerical analysis of a fishing vessel motions and stability in longitudinal seaway. Master's thesis, University of British Columbia, 1987.

[29] H. Kato. On the approximate calculation of ship's rolling period. *SNAJ*, 1956.

[30] R. Bhattarcharyya. *Dynamics of Marine Vehicles.* John Wiley & Sons, 1978.

[31] P. S. DeLeonibus, J. F. Boogaard, Sheil R. J., and B. E. Olson. Shipboard observations of wave spectra with a bow - mounted wave height sensor. *Journal of Geophysical Resarch*, 78, 1973.

[32] A. G. Voronovich, A. D. Rozenberg, and P. V. Sakov. Instrument and methods : Application of a wire wave - gauge for wave state measurements from a driffting ship. *Oceanology*, 26, 1986.

[33] D. Crombie. Doppler spectrum of sea echoes at 13.56 mc/s. *Nature*, 175:681 – 682, 1955.

[34] T. T. Ijima and H Sasaki. Application of radars to wave observation. In *11th Coastal Engineering*, volume 30, pages 10 – 22, 1967.

[35] F. F. Wright. Wave observations by shipboard radar. *Ocean science Ocean Eng.*, 1:506 – 514, 1965.

[36] H. M. Oudshoorn. The use of radar in hydrodynamic surveying. In *7th Coastal Eng.*, pages 59 – 76, 1960.

[37] T. G. Willis and H. Beaumont. Wave direction measurements using sea surveillance radars. Technical report, Tech. memo. TR 118. R. Aircraft Establishment Farnbough U.K., 1971.

[38] V. F. Evmenov. Test of the radar method of defining ocean waves elements. *Fluid Mech. Sov. Res.*, 2:141 – 145, 1973.

[39] M. G. Mattie and D. L. Harris. A system for using radar to record wave direction. Technical report, US Army Corps of eng. Coast Eng Res. Ctr.79-1, 1979.

[40] P. Hoogeboom and Rosenthal W. Directional wave spectra images. *International Geoscience and Remote sensing symposium, IEEE Geoscience and Remote sensing Soc. Munich*, 1982.

[41] F. Ziemer and A. D. Rosenthal. Measurments of the directional wave spectra by ship radar. *IAPSO symposium PS-11, IUGG XVIII General Assembly*, 11, 1983.

[42] M. G. Mattie, V. S. Hsiao, and D. D. Evans. Wave direction measured by four different systems. *IEEE, Oceanic Eng. OE-6*, 6:87 – 93, 1981.

[43] A. Braun. Critical analysis of dsa5 and expected improvments. In *Int. conf. on Wave and Wind Directionality, Paris*, 1981.

[44] P. Wadhams. Wave decay in the marginal ice zone measured from a submarine. *Journal of Deep Sea Research*, 25:23 – 40, 1978.

[45] R. B. Long. Scattering of surface waves by irregular bottom. *Geophysical Resarch*, 78:7861 – 7870, 1973.

[46] V. Atanasov, W Rosenthal, and Ziemer F. Removal of ambiquity of the two-dimensional power spectra obtained by processing ship radar images of ocean waves. *Geophysical Resarch*, 90:1061 – 1067, 1985.

[47] I. R. Young and W. Rosenthal. A three dimensional analysis of marine radar images for the determination of ocean wave directionality and surface currents. *Journal of Geophysical Research*, 90 C1:1049 – 1059, 1985.

[48] F. Ziemer and W. Rosenthal. On the transfer function of a shipborn radar for imaging ocean waves. In *IGARSS'87 Ann Arbor*, pages 18 – 21, 1987.

[49] R Watson-watt. *The use of radar at sea.* Hollis and Carter, London, 1978.

[50] R. B. Blackman and J.W. Tukey. *The measurement of power spectra.* Dover, New York, 1958.

[51] M. Allingham. Directional spectra of the sea surface using marine radar. Master's thesis, Royal Road Military College, Victoria, Canada, 1992.

[52] J. Buckley, R., Allingham M., and R. Michaud. On the determination of directional sea surface spectra from marine radar imagery. In *Oceans'93*, Victoria B.C, 1993.

[53] F. Dobson and P. Vachon. Ers-1 calibration / validation experimental plan. Technical report, Bedford Institute of Oceanography, Fisheries and Oceans Canada, 1991.

[54] M. J. Tucker. A shipborne wave recorder. *TINA*, pages 7861 – 7870, 1956.

[55] Defence Research Establisment Atlanta. *Shipmo Manual.*

[56] Autoregressive spectrum estimation. Statistical approach in computer control of cement totary kilns. In *3rd conference on Probability and Atmospheric Sciences*, 1973.

[57] J. P Burg. Maximum entropy spectral analysis. *37th Annual International Meetings Soc. of Explor. Geophysics, Oklahoma City*, 1967.

[58] J. P Burg. A new analysis technique for time series data. *Advanced study Institute on Signal processing NATO Enschede Netherlands*, 1968.

[59] T. J Ulrych and Bishop N.T. Maximum entropy spectral analysis and autoregressive decomposition. *Reviews of Geophysics and Space Physics*, 13:183 – 200, 1975.

[60] T. E. Barnard. Analytical studies of techniques for the computation of high resolution wave number spectra. Technical report, Spec. ref . 9, Texas Instrument Advanced Array Res., 1969.

[61] J. A. Edward and M. M. Fitelson. Notes on maximum entropy processing. In *IEEE Trans. Information Theory IT-19*, pages 232 – 242, 1973.

[62] D. E. Symlie and K. C. Clarke. Analysis of irregularities in the earth's rotation. In *Methods in Computational Physics*, volume 13, pages 391 – 430, 1973.

[63] A. B. Dunwoody. Roll of a ship in astern seas - metacentric height spectra. *Ship Research*, 33 – 3, 1989.

[64] R. Haddara, M., S. Kastner, and F. Magel, L. Capsizing experiments with a model of a fast cargoliner in san francisco bay. Technical report, Department of Naval Architecture and Offshore Eng. University of California Berkeley, 1972.

[65] S. H. Crandall and W. D. Mark. *Random Vibration in Engineering.* Academic Press, 1963.

[66] S. O. Rice. Mathematical analysis of random noise. *Selected Papers on Noise and Stochastic Processes*, 1954.

[67] A. B. Dunwoody. Random processing in engineering. 1991.

[68] L. Zadeh. Fuzzy sets. volume 8, pages 338 – 353, 1965.

[69] A. B. Dunwoody. Roll of a ship in astern seas - response to gm fluctuations. *Ship Research*, 33 – 4, 1989.

[70] K. Keays. Fishing vessel limits study. Technical report, Society of Naval Architecture and Marine Engineers, 1990.

[71] Haddara M. R. and Suimin Zhang. Experimental study of roll damping of fishing vessels moving with forward speed. *Proceedings of The OMAE 93, Glasgow*, 1993.

[72] S. J. Chou, J. R. Paulling, and P. D. Van Slyke, R. Wood. Ship motions and capsizing in astern seas final report for period august 1970 - december 1974. Technical report, Dept. of Naval Architecture and Ocean Engineering, University of California, Berkeley, 1974.

[73] H Levinson. The wiener rms (root mean square) error criterion in filter design and prediction. *Journal of Math. Physics*, 25:261 – 278, 1947.

[74] J Durbin. The fitting of the time series models. *Rev. Int. Inst. Statistics*, 28:233 – 244, 1960.

[75] G. E Box and G. H. Jenkins. *Time series analysis : Forcasting and Control.* Holden day, San francisco, 1970.

[76] J. P Burg. The relationship between maximum entropy spectra and maximum likelihood spectra. *Journal Geophysics*, pages 375 – 376, 1972.

[77] H Akaike. Fitting autoregressive model for prediction. In *Ann. Inst. Statist. Math.*, volume 21, pages 243 – 247, 1969.

[78] H Akaike. Power spectrum estimation through autoregressive model fitting. In *Ann. Inst. Statist. Math.*, volume 21, pages 407 – 419, 1969.

[79] H Akaike. Autoregressive model fitting for control. In *Ann. Inst. Statist. Math.*, volume 23, pages 163 – 180, 1971.

[80] W. Gersch and D. R. Sharpe. Estimation of power spectra with finite order autoregressive models. In *IEEE Trans. Automatic control AC-18*, volume 18, pages 367 – 369, 1974.

[81] G. J. Fryer, M. E. Odegard, and G. H. Sutton. Deconvolution and spectral estimation using final prediction error. In *Journal of Geophysics*, volume 40, pages 411 – 425, 1974.

[82] T Otomo, T Nakagawa, and H. Akaike. Statistical approach in computer control of cement totary kilns. *Journal of Automatica*, 8:35 – 43, 1972.

[83] H Akaike. Statistical predictor identification. In *Ann. Inst. Statist. Math.*, volume 22, pages 203 – 217, 1970.

[84] H Akaike. A new look at the statistical model identification. In *IEEE Trans. Automatic control AC-18*, volume 19, pages 716 – 723, 1974.

[85] R. H. Janes. Identification and autoregressive spectrum estimation. In *IEEE Trans. Automatic control AC-19*, volume 19, pages 894 – 898, 1975.

[86] G. Klir and T. Folger. *Fuzzy Sets, Uncertainty and Information.* Prentice Hall, Englewood Cliffs:USA, 1988.

[87] Togai Infralogic Inc. Irvine:USA. *Fuzzy-C Development System: User's Manual.*

[88] E. Dougherty and C. R., Giardina. *Image Processing - Continuous to Discrete*, volume 1. Prentice-Hall, 1987.

[89] J. Serra. *Image Analysis and Mathematical Morphology.* Academic Press, 1988.

[90] E. Dougherty. *Mathematical Morphology in Image Processing.* Marcel Dekker Inc., 1991.

[91] V. Atanasov, W. Rosenthal, and Ziemer F. Removal of ambiguity of two-dimensional power spectra obtained by processing ship radar images of ocean waves. *Journal of Geophysical Research*, 90 C1:1061 – 1067, 1985.

[92] Barrick E. D. Extraction of wave parameters from measured hf radar sea-echo doppler spectra. *Radio Science*, 12:415 – 424, 1977.

[93] Belinda L. Derivation of directional ocean wave spectra by integral inversion of second order radar echoes. *Radio Science*, 12:425 – 434, 1977.

[94] E. Köse, R. Gosine, and S. M. Calisal. Toward a real -time system for monitoring the safety of fishing vessel. In *Marsim'93*, St. John's Newfoundland, Canada, 1993.

[95] A. C. Lindley. *Practical Image Processing In C.* John Wiley & Sons, Inc, 1991.

[96] D. Hoffman and W.H. Jr. Grazke. Heavy weather monitoring and guidance system on the s.s. lash italia (second phase of test and evaluation). Technical report, National Maritime Research Center NMRC-KP-197, 1980.

[97] A. Nafarieh. A fuzzy logic rule-based automatic target recognizer. *Intelligient system*, 6:295 – 312, 1991.

[98] D. W. Bass, Haddara M. R., and B. Zou. A comparison of the roll damping characteristics of five small fishing vessels at zero speed. *Proceedings of The Marine Dynamics Conference St. John's Newfoundland*, pages 1 – 8, 1991.

[99] Haddara M. R. and D. W. Bass. On the form of roll damping moment for small fishing vessels. *Ocean Engineering*, 17:525 – 539, 1990.

[100] Haddara M. R. and P. Bennett. A study of the angle dependence of roll damping moment. *Ocean Engineering*, 16:411 – 427, 1989.

[101] R. C. Gonzalez and P. Wintz. *Digital Image Processing.* Addison Wesley Publishing Company, 1987.

[102] B. K. P. Horn. *Robot Vision.* McGraw-Hill Book Company, 1986.

Appendix A

Encounter Frequency

The time history of waves encountered by a moving point (a ship under way, for example) is significantly modified by the *Doppler shift* in the component frequencies of the wave system. Suppose an x_0, y_0 coordinate system, fixed in relation to the earth, and a regular progressive wave of amplitude $\overline{\zeta}$ and wave number k, propagating in a direction μ relative to the x_0 axis. In the fixed coordinate system the free surface of the wave field is described by A.1 [24] :

$$\zeta(x_0, y_0, t) = \overline{\zeta}\cos[k(x_0\cos\mu + y_0\sin\mu) - \omega t + \epsilon] \tag{A.1}$$

Now suppose further that a ship proceeds in the direction of the x_0 axis at constant velocity U_0, and we wish to describe the wave field as would be observed from the moving ship. We assume a moving, $x - y$ coordinate system with origin in the ship and whose x axis is aligned with the fixed x axis. Since the location of the ship at any instant time t, is $U_0 t$, the relation between the two coordinate sytems is :

$$x_0 = x + U_0 t \tag{A.2}$$

$$y_0 = y \tag{A.3}$$

$$\tag{A.4}$$

Substituting in Equation A.1 the expression for the wave field as seen from the moving ship becomes:

$$\zeta(x_0, y_0, t) = \overline{\zeta}\cos[kx\cos\mu + ky\sin\mu - (\omega - kU_0\cos\mu)t + \epsilon] \tag{A.5}$$

The coefficient of t in equation A.5 defines a frequency of encounter, ω_e, and noting that $k = \omega^2/g$ for deep water :

$$\omega_e = \omega_w - \frac{\omega_w^2 U}{g}\cos(\phi) \tag{A.6}$$

where

ω_e :Encounter Frequency

ω_w :Wave frequency

U : Ship speed

ϕ : Angle between wave direction and ship direction

Appendix B

FFT Algorithm

Young et al.[1983] present a concise explanation of how a time series of two dimensional maps of sea surface height (or radar backscatter) can be transformed into a directionally unambiguous wave spectrum (or radar images spectrum).

Starting with sea surface height $\eta(\xi)$ where ξ is a three dimensional vector (x, y, t), the three dimensional Fourier series can be written as

$$F(\Omega) = \sum_{j=1}^{3} \eta(\xi)_j \exp(-i\Omega\xi) \tag{B.1}$$

where $\Omega\xi = k_x x + k_y y - \omega t$. Now since $\eta(\xi)$ is real valued, the complex conjugate of Equation B.1 is

$$F^*(\Omega) = \sum_{j=1}^{3} \eta(\xi)_j \exp(-i\Omega\xi) \tag{B.2}$$

It is clear from B.1 and B.2 that

$$F(\Omega) = F^*(-\Omega) \tag{B.3}$$

The variance spectrum is defined as

$$E(\Omega) = \frac{1}{L_x L_y T} |F(\Omega)|^2 \tag{B.4}$$

where L_x and L_y are the spatial length of the data vector and T is the temporal length. The factor $\frac{1}{L_x L_y T}$ is chosen to normalize the variance so that

$$\int_{-\Omega_N}^{\Omega_N} E(\Omega)d\Omega = \sigma^2 \tag{B.5}$$

where Ω_N is the Nyquist limit and σ^2 is the variance of the data set. From Equation B.3 and B.4 it follows that

$$E(\Omega) = E(-\Omega) \tag{B.6}$$

Equation B.6 shows that the variance spectrum is reflection symmetric about the point $\Omega = 0$ in wave number frequency space. Now in the case of a single sea surface height field ($\eta = \eta(x, y)$, the two dimensional case). Equation B.6 simplifies to

$$E(k_x, k_y) = E(-k_x, -k_y) \tag{B.7}$$

Thus any wave spectrum calculated from a single 'image' will be ambiguous as to the propagation direction. In the three dimensional data case, Equation B.6 can be rewritten as

$$E(k_x, k_y, \omega) = E(-k_x, -k_y, -\omega) \tag{B.8}$$

Each point in wave number frequency space corresponds to a plane wave in physical space, the phase speed of which is given by the time development of a fixed phase plane

$$\Omega\xi = (k_x x + k_y y - \omega t) = \text{constant} \tag{B.9}$$

So it can be seen that two points in wave number frequency space mirrored about $\Omega = 0$ will have phase speed of opposite sign, and will represent counter propagating waves.

To obtain the two dimensional spectrum $E(\Omega)$ can be integrated with respect to ω

$$E(k_x, k_y) = \int_{\omega_N}^{\omega_N} E(\Omega) d\omega \tag{B.10}$$

However using this procedure the phase speed direction information is lost. Now if instead the integration is limited to only one-half of the ω space, say $\omega > 0$

$$\tilde{E}(k_x, k_y) = \int_{\omega > 0} E(\Omega) d\omega \tag{B.11}$$

then $\tilde{E}$ will be asymmetrical. The phase speed direction for a given wave will then be that of its wavenumber $k = (k_x, k_y)$. Conversely, if the integration is limited to the negative ω space the wave propagation direction will be $(-k_x, k_y)$. Thus a series of sea surface height images can be processed into a directionally unambiguous wave spectrum.

Appendix C

MEM Spectrum

Estimation of AR coefficients

In order to compute the MEM power spectrum using 5.21, we must determine first of all the length of the required prediction filter M (or equivalently the order of the AR process) and second, the coefficients themselves. Since the method of determining M assumes knowledge of the coefficients, estimation of these parameters will be discussed first.

Burg Estimates

Burg[1967,1968] suggested a method of estimating the AR parameters (or equivalently the prediction error filter coefficients) that does not require prior estimate of the autocovariance function.

The YW equations can be written as

$$\begin{bmatrix} \hat{\rho}(0) & \hat{\rho}(1) & \cdots & \hat{\rho}(M-1) \\ \hat{\rho}(1) & \hat{\rho}(0) & \cdots & \hat{\rho}(M-2) \\ \vdots & \vdots & \ddots & \vdots \\ \hat{\rho}(M-1) & \hat{\rho}(M-2) & \cdots & \hat{\rho}(1) \end{bmatrix} \begin{bmatrix} \hat{\alpha}_{M1} \\ \hat{\alpha}_{M2} \\ \vdots \\ \hat{\alpha}_{MM} \end{bmatrix} = \begin{bmatrix} \hat{\rho}_1 \\ \hat{\rho}_2 \\ \vdots \\ \hat{\rho}_M \end{bmatrix} \tag{C.1}$$

where $\hat{\alpha}_{Mj}$ is the jth coefficient of the Mth order AR process.

A recursive solution may be obtained by using the Levinson [73] and Durbin [74] procedure. The recursion obtains the estimates $\hat{\alpha}_{3j}$, $j = 1, 2, 3$ from the estimates $\hat{\alpha}_{2j}$,

$j = 1, 2$ [75]. By using the first two equation of (C.1) with M=3 the estimates $\hat{\alpha}_{31}$ and $\hat{\alpha}_{32}$ may be expressed in terms of $\hat{\alpha}_{33}$ in the form

$$\begin{bmatrix} \hat{\rho}(0) & \hat{\rho}(1) \\ \hat{\rho}(1) & \hat{\rho}(0) \end{bmatrix} \begin{bmatrix} \hat{\alpha}_{31} \\ \hat{\alpha}_{32} \end{bmatrix} = \begin{bmatrix} \hat{\rho}(1) \\ \hat{\rho}(2) \end{bmatrix} - \hat{\alpha}_{33} \begin{bmatrix} \hat{\rho}(2) \\ \hat{\rho}(1) \end{bmatrix} \tag{C.2}$$

$$\hat{C}(1) = \begin{bmatrix} \hat{\rho}(0) & \hat{\rho}(1) \\ \hat{\rho}(1) & \hat{\rho}(0) \end{bmatrix} \tag{C.3}$$

The above equation can be written as

$$\begin{bmatrix} \hat{\alpha}_{31} \\ \hat{\alpha}_{32} \end{bmatrix} = \hat{C}(1)^{-1} \begin{bmatrix} \hat{\rho}(1) \\ \hat{\rho}(2) \end{bmatrix} - \hat{C}(1)^{-1} \hat{\alpha}_{33} \begin{bmatrix} \hat{\rho}(2) \\ \hat{\rho}(1) \end{bmatrix} \tag{C.4}$$

However, since substituting M = 2 in (C.1) gives

$$\begin{bmatrix} \hat{\alpha}_{21} \\ \hat{\alpha}_{22} \end{bmatrix} = \hat{C}(1)^{-1} \begin{bmatrix} \hat{\rho}(1) \\ \hat{\rho}(2) \end{bmatrix} \tag{C.5}$$

it follows that

$$\begin{bmatrix} \hat{\alpha}_{31} \\ \hat{\alpha}_{32} \end{bmatrix} = \begin{bmatrix} \hat{\alpha}_{21} \\ \hat{\alpha}_{22} \end{bmatrix} - \hat{\alpha}_{33} \begin{bmatrix} \hat{\alpha}_{22} \\ \hat{\alpha}_{21} \end{bmatrix} \tag{C.6}$$

It is convenient at this stage to obtain an alternate form of the YW formulation expressed by C.1. This alternate form, which is suggested by (C.6), will allow us to express the recursion for the Burg [57, 58, 76] estimates of AR coefficients in a very elegant form. In deriving (C.7) $E(x_{t-k}a - t) = 0$ for $k > 0$. When k=0, however, $E(x_{t-k}a_t) = E(x_t a_t) = E(a_t^2) = \sigma_a^2$. Hence when k=0

$$\rho(0) = \alpha_1 \rho(1) + \alpha_2 \rho(2) + \cdots + \alpha_M \rho(M) + \sigma_a^2 \tag{C.7}$$

C.7 allows us to write

$$\begin{bmatrix} \rho(0) & \rho(1) & \cdots & \rho(M) \\ \rho(1) & \rho(0) & \cdots & \rho(M-1) \\ \vdots & \vdots & \ddots & \vdots \\ \rho(M) & \rho(M-1) & \cdots & \rho(0) \end{bmatrix} \begin{bmatrix} 1 \\ -\alpha_1 \\ \vdots \\ -\alpha_M \end{bmatrix} = \begin{bmatrix} \sigma_a^2 \\ 0 \\ \vdots \\ 0 \end{bmatrix} = \begin{bmatrix} P_{M+1} \\ 0 \\ \vdots \\ 0 \end{bmatrix} \tag{C.8}$$

The correspondence between the AR process and the prediction of x_t from a knowledge of its past values identifies the constant P_{M+1} as the prediction error power resulting from convolution of x_t with the M+1 point prediction error filter γ_t.

Burg [76] expressed the recursion in (C.6) using the formulation in (C.8) in the following manner

$$\hat{C}(3) = \begin{bmatrix} 1 \\ -\hat{\alpha}_{31} \\ -\hat{\alpha}_{32} \\ -\hat{\alpha}_{33} \end{bmatrix} = \hat{C}(3) \left[\begin{Bmatrix} 1 \\ -\hat{\alpha}_{21} \\ -\hat{\alpha}_{22} \\ 0 \end{Bmatrix} - \hat{\alpha}_{33} \begin{Bmatrix} 0 \\ -\hat{\alpha}_{22} \\ -\hat{\alpha}_{21} \\ 1 \end{Bmatrix} \right] \tag{C.9}$$

Clearly, since (C.6) is independent of $\hat{\rho}(k)$, it can be used to relate $\hat{\alpha}_{31}$ and $\hat{\alpha}_{32}$ to $\tilde{\alpha}_{21}$ and $\hat{\alpha}_{22}$, therefore the recursion of these coefficients is contained in (C.9). The $\hat{\rho}(k)$ in this equation represents some as yet undetermined estimates of the autocovariance function.

To determine $\hat{\rho}(k)$, we can minimize $\sum a_t^2$ (following the principle of least squares) with respect to $\hat{\alpha}_{33}$. This procedure is equivalent to minimizing the prediction error power with respect to $\hat{\alpha}_{33}$. Thus $\hat{\alpha}_{33}$ may be obtained

$$\frac{\partial S(\alpha_{33})}{\partial \alpha_{33}} = 0 \tag{C.10}$$

where $S(\alpha_{33})$ is the residual sum of squares for the third order AR process and is given by

$$S(\alpha_{33}) = \sum_{i=4}^{N}(x_t - \hat{\alpha}_{31}x_{t-1} - \hat{\alpha}_{32}x_{t-2} - \hat{\alpha}_{33}x_{t-3})^2 \tag{C.11}$$

Actually, the solution of (C.10) for $\hat{\alpha}_{33}$ using estimates of $\hat{\alpha}_{31}$ and $\hat{\alpha}_{32}$ obtained from the recursion given by (C.6) in fact corresponds to an approximate maximum likelihood estimation of these coefficients [75].

An important extension to (C.11) was proposed by Burg[1968] on the basis of the predictive interpretation of the AR process. Thus Burg suggested that the prediction error power be calculated by running the prediction error filter over the data in a forward and backward direction. The expression for the error power for the third order AR process is

$$\begin{aligned} P_4 &= \frac{1}{2(N-3)}\sum_{i=4}^{N}\{(x_t - \hat{\alpha}_{31}x_{t-1} - \hat{\alpha}_{32}x_{t-2} - \hat{\alpha}_{33}x_{t-3})^2 + \\ &\qquad (x_{t-3} - \hat{\alpha}_{31}x_{t-2} - \hat{\alpha}_{32}x_{t-1} - \hat{\alpha}_{33}x_t)^2\} \end{aligned} \tag{C.12}$$

and $\hat{\alpha}_{33}$ is determined from $\partial P_4/\partial\hat{\alpha}_{33} = 0$. The important point to notice about (C.12) is that P_4 is determined by running the filter over the data, not off the data. In the other words, no assumptions are made concerning the extension of the data outside the parameter space, and estimation of the AR coefficients is consistent with the principle of maximum entropy.

If the estimate of $\hat{\rho}(0)$ is computed in the usual manner:

$$\hat{\rho}(0) = \frac{1}{N}\sum_{t=1}^{N} x_t^2 \tag{C.13}$$

then the remaining autocovariance estimates may be determined recursively. It easily shown from (C.9) that

$$\hat{\rho}(\tau) = \sum_{k=1}^{\tau} \hat{\rho}(\tau - k)\hat{\alpha}_{\tau k} \qquad \tau = 1, 2, \cdots, M \tag{C.14}$$

Determination of the order of the AR process

An issue which must be dealt with in the course of computing MEM spectral estimates is the selection of the order which best matches the MEM spectrum to the true spectrum.

The estimation of the order of the AR model from a realization of the process has been treated by a number of author [Anderson, 1963; Jones, 1964; Jenkins and Watts, 1969; Galbraith, 1971], but all these techniques lack to some extent the objective basis that is required . Akaike [77, 78, 79] proposed an estimating procedure which gives excellent results, and its application to MEM spectral analysis removes the chief shortcoming of these techniques. The Akaike criterion, which is called the final prediction error FPE, has been investigated by Gersch and Sharpe [80] with respect to the estimation of power spectra of finite order AR models and by Fryer et al. [81], who investigated the application of the FPE to multichannel time series [77, 78, 79, 82].

The Akaike [83] criterion minimizes the prediction error when the error is considered as the sum of the innovation and the error in estimating the AR parameters. For an Mth order fit:

$$(FPE)_M = \frac{N + (M+1)}{N - (M+1)} S_M^2 \tag{C.15}$$

where S_M^2 is the residual sum of squares.

Akaike [84] has extended this criterion through the application of the principle of maximum likelihood. The new criterion is called an information theoretic criterion (AIC) and allows the specification of the probability density function for the observation:

$$(AIC)_k = -2log(maximized\ likelihood\ function) + 2k \tag{C.16}$$

where k is the number of independent parameters estimated.

When the process is AR of order M with Gaussian errors the above expression reduces to:

$$(AIC)_M = NlogS_M^2 + 2(M+1) \tag{C.17}$$

Since the 1 in eq. (C.17) is only an additive constant which reflects subtraction of the mean eq. (C.17) is usually written as:

$$(AIC)_M = NlogS_M^2 + 2M \tag{C.18}$$

Gercsh and Sharpe [80], Akaike [84] and Jones [56, 85] have used the AIC successfully in a number of different applications. Generally, it has been found that the AR order given by the FPE and AIC criteria is the same.

Appendix D

Sea Spectrums

D.1 I.T.T.C. Sea Spectrum

Recommended by the 16th I.T.T.C. Sea Keeping Committee to be used as a standard for open ocean conditions, the spectrum is available as either a one parameter (Sig. Wv. Ht. (Hs)) or two parameter (Sig. Wv. Ht. (Hs) and Av. Period (T1)) formulation. The general form for the spectral formulation is

$$S(w) = (A/w^5)e^{(-B/w^4)} \qquad m^2 - sec \tag{D.1}$$

where w = wave frequency (rad/sec) and A and B are constants dependent upon whether one or two parameter formulation is required. The one parameter form relates to the case of fully developed sea conditions and is derived from data collected in the North Atlantic Ocean. The formulation is a modification of the Pierson-Moskowitz Spectrum using the relationship between Sig. Wv. Ht. and Wind speed at 19.5m above sea level for fully developed seas (i.e. that have an unlimited fetch). Therefore to define a number of spectra using this formulation, for each spectra required, a value for Hs is input usually in the range 1.0 to 10.0 m. The constants A and B are defined in this formulation as

$$A = 0.0081g^2 \qquad B = \frac{3.11}{H_s^2} \tag{D.2}$$

The two parameter spectrum is to be used for open ocean conditions and is again derived from wave data collected in the North Atlantic Ocean. The formulation requires values to be input for both Hs and T1. Therefore this formulation is to be used when a relationship

between Hs and T1 is known for the sea area in question or the Hs and T1 combinations that can occur (e.g. scatter diagrams) are available. Usual values for Hs are in the range 1.0 to 10.0 m.

Scatter diagram data may be for observed sea conditions so the relationship between these and the parameters used in the spectrum formulation must be determined. The constants A and B are defined as follows

$$A = 173\frac{H_s^2}{T_1^4} \qquad B = \frac{691}{T_1^4} \tag{D.3}$$

D.2 Bretschneider Sea Spectrum

This spectrum is for a fully developed sea with the formulation being derived on the premise that the wave period follows a Rayleigh distribution, as does the wave height. The spectrum is available as a two parameter formulation (Sig. Wv. Ht. (Hs) and Av. Period (T1)) and is of the following form,

$$S(w) = \frac{A}{w^5}e^{\frac{-B}{w^4}} \qquad m^2 - sec \tag{D.4}$$

where

$$A = 263\frac{Hs^2}{T1^4} \tag{D.5}$$

$$B = \frac{1052}{T1^4} \tag{D.6}$$

$$\tag{D.7}$$

This spectrum is to be used for open ocean conditions and is derived from wave data collected in the North Atlantic Ocean. To define a number of spectra using this formulation requires values for both Hs and T1 for each required sea spectra Therefore this formulation is to be used in the case either when a relationship between Hs and T1

is known for the sea area in question or the Hs and T1 combinations that can occur (eg from scatter diagrams) are available. Usual values for Hs are in the range 1.0 to 10.0 m.

Appendix E

Catalogue of Radar Image series

The following information is reproduced from [51] for convenience.

RRMC X-Band Radar

ERS-1 Cal/Val Cruise November 1991

The wave directions are described using numbered octans relative to ship's heading. Octan 1 is directly forward, 3 is starboard, 5 is aft, and 7 is to port. Wave direction is ambiguous.

Times are UT. Ship speed is in knots.

Date	Time	Wave Image Description	Heading	Speed
12	09:38	Swell 8-4. Wind waves 2-6		
12	14:46	Rain showers	119	1.2
14	11:42	Clear image 7-3 swell and 2-6 wind wave	119	11.6
14	11:57	Good wave signal	87	1.4
14	12:12	Rain reduce signal/noise but waves still visible	94	0.5
14	12:42	Strong wave signal but considerable radar interference	99	2.1
20	11:30	7-3 wind wave. 8-4 swell		
20	13:00	Wind wave 6-2. Swell 8-4 Possible additional swell		

Date	Time	Wave Image Description	Heading	Speed
20	13:30	Wind wave 6-2. Swell 8-4	270	1.3
		Possible additional swell		
20	14:00	Swell 8-4 becoming clearer	280	1.3
20	14:14	Crossed wind and wave swell	272	1.5
20	15:30	Crossed wind and wave swell	297	3.0
20	16:00	Crossed wind and wave swell	285	1.8
20	16:30	Crossed wind and wave swell	276	2.0
20	23:30	Crossed wind and wave swell	273	1.5
		Wind wave 8-4.		
21	18:51	Wind wave 7-3. Wind 40 kt		
21	19:42	Wind wave 8-4. Fairly monochromatic	267	3.4
21	20:35	Wind wave 8-4 Building sea	272	1.6
21	21:32	Wind wave 8-4 Building sea	91	13.1
		High speed		
21	22:00	Wind wave and swell 8-4	276	2.8
21	22:30	Wind wave and swell 8-4	271	1.9
21	23:00	Wind wave and swell 8-4	282	0.9
21	23:30	Wind wave and swell 2-6	11	4.0
21	24:00	Wind wave and swell 2-6	255	1.6
		Possible upwind / downwind test series		
22	00:32	Wind wave and swell 2-6	272	1.8
		Possible upwind / downwind test series		
23	15:30	Swell 6-2. Wind wave 7-3	336	1.7
		Possible swell 1-5		
23	19:02	Wind wave and swell 8-4, Swell 1-5	356	0.6
23	19:40	Swell 8-4 and 7-3	84	2.3
23	20:08	Swell 1-5	180	0.3
23	20:33	Swell 7-3 and 6-2	259	1.5
23	23:30	Swell 1-5 and 2-6	313	2.5
23	24:00	Swell 1-5 and 2-6	293	2.1
24	01:30	Swell 1-5. Very much reduced	304	0.4
		signal strength		

Appendix F

Capsizing Times

The following Table is reproduced from [64] to show capsizing times. These experiments were done in San Fransisco Bay.

Date	Heading	Duration (sec.)	Capsize
9-2-1971	following	75	port
9-13-1971	quartering	164	port
9-16-1971	quartering	375	starbord
" " "	following	147	port
" " "	following	100	port
" " "	following	360	starboard
" " "	following	213	port
" " "	quartering	351	starboard
9-21-1971	quartering	228	starboard
" " "	quartering	235	starboard
" " "	quartering	280	starboard
" " "	quartering	365	starboard
" " "	quartering	52	starboard
" " "	following	254	port
9-28-1971	following	121	port

Table F.1: Capsizing times obtained from model tests in San Francisco Bay

Appendix G

Rules

1.

IF Wave_Height IS MED
AND Wave_Direction IS MED
AND WL_SL IS Z
AND WE_2WN IS Z
AND Ship_Speed IS HIGH
THEN Change_Speed = NB

2.

IF Wave_Height IS HIGH
AND Wave_Direction IS MED
AND WL_SL IS Z
AND WE_2WN IS Z
AND Ship_Speed IS HIGH
THEN Change_Speed = NB

3.

IF Wave_Height IS MED
AND Wave_Direction IS MED
AND WL_SL IS Z
AND WE_2WN IS Z
AND Ship_Speed IS MED
THEN Change_Direction = PS

4.

IF Wave_Height IS HIGH
AND Wave_Direction IS MED
AND WL_SL IS Z
AND WE_2WN IS Z
AND Ship_Speed IS MED
THEN Change_Direction = PS

5.

IF Wave_Height IS MED
AND Wave_Direction IS MED
AND GM_Singular IS Z
AND Ship_Speed IS HIGH
THEN Change_Speed = NB

6.

IF Wave_Height IS HIGH
AND Wave_Direction IS HIGH
AND GM_Singular IS Z
AND Ship_Speed IS HIGH
THEN Change_Speed = NB

7.

IF Wave_Height IS MED

AND Wave_Direction IS MED

AND GM_Singular IS Z

AND Ship_Speed IS MED

THEN Change_Direction = PB

8.

IF Wave_Height IS MED

AND Wave_Direction IS HIGH

AND GM_Singular IS Z

AND Ship_Speed IS MED

THEN Change_Direction = NB

9.

IF Wave_Direction IS VL

AND WH_Beam IS Z

THEN Change_Direction = PB

Return_Port = HIGH

10.

AND Wave_Direction IS VL

AND WH_Beam IS Z

THEN Change_Direction = PB

Return_Port = HIGH

11.

IF Wave_Direction IS VL

AND WH_Beam IS NB

THEN Change_Direction = PB

Return_Port = HIGH

12.

AND Wave_Direction IS VH

AND WH_Beam IS Z

THEN Change_Direction = NB

Return_Port = HIGH

13.

IF Wave_Direction IS VH

AND WH_Beam IS NS

THEN Change_Direction = NB

Return_Port = HIGH

14.

AND Wave_Direction IS VH

AND WH_Beam IS NB

THEN Change_Direction = NB

Return_Port = HIGH

15.

IF Wave_Direction IS VH

AND WH_Beam IS NB

THEN Change_Direction = NB

Return_Port = HIGH

16.

AND Wave_Direction IS MED

AND WH_Beam IS MED

WE_WN IS Z

THEN Change_Direction = PB

17.

IF Wave_Height IS MED

AND Wave_Direction IS MED

AND WE_WN IS Z

THEN Change_Direction = PB

18.

IF Wave_Height IS MED

AND Wave_Direction IS HIGH

AND WE_WN IS Z

THEN Change_Direction = PS

19.

IF Wave_Height IS HIGH

AND Wave_Direction IS HIGH

AND WE_WN IS Z

AND WH_Beam IS Z

THEN Change_Direction = PS

20.

IF Wave_Height IS HIGH

AND Wave_Direction IS HIGH

AND WE_WN IS Z

AND WH_Beam IS NS

THEN Change_Direction = PS

21.

IF Wave_Height IS HIGH

AND Wave_Direction IS HIGH

AND WE_WN IS Z

AND WH_Beam IS NB

THEN Change_Direction = PS

22.

IF Wave_Height IS MED

AND Wave_Direction IS LOW

AND WE_WN IS Z

AND WH_Beam IS Z

THEN Change_Direction = NS

25.

IF Wave_Height IS MED

AND Wave_Direction IS MED

AND WE_WN IS Z

AND WH_Beam IS NS

THEN Change_Direction = NS

26.

IF Wave_Height IS MED

AND Wave_Direction IS LOW

AND WE_WN IS Z

AND WH_Beam IS Z

THEN Change_Direction = NS

27.

IF Wave_Height IS HIGH

AND Wave_Direction IS LOW

AND WE_WN IS Z

AND WH_Beam IS Z

THEN Change_Direction = NS

28.

IF Wave_Height IS MED

AND Wave_Direction IS HIGH

AND WE_WN IS Z

AND WH_Beam IS HIGH

THEN Change_Direction = NB

29.

IF Wave_Height IS HIGH

AND Wave_Direction IS MED

AND WS_SS IS Z

AND Ship_Speed IS HIGH

THEN Change_Speed = NB

30.

IF Wave_Height IS HIGH

AND Wave_Direction IS MED

AND WS_SS IS Z

AND Ship_Speed IS MED

THEN Change_Direction = PB

Change_Speed = PS

31.

IF Wave_Height IS HIGH
AND Wave_Direction IS LOW
AND WL_SL IS Z
AND Ship_Speed IS HIGH
THEN Change_Direction = PS
Change_Speed = NS

32.

IF Wave_Height IS HIGH
AND Wave_Direction IS LOW
AND WL_SL IS Z
AND Ship_Speed IS HIGH
THEN Change_Direction = PS
Change_Speed = NS

33.

IF Wave_Height IS HIGH
AND Wave_Direction IS LOW
AND WL_SL IS Z
AND Ship_Speed IS MED
THEN Change_Direction = PS

34.

IF Wave_Height IS HIGH
AND Wave_Direction IS HIGH
AND WL_SL IS Z
AND Ship_Speed IS HIGH
THEN Change_Direction = NS
Change_Speed = NS

35.

IF Wave_Height IS HIGH
AND Wave_Direction IS LOW
AND WL_SL IS Z
AND Ship_Speed IS MED
THEN Change_Direction = NS

36.

IF Wave_Height IS HIGH
AND Wave_Direction IS HIGH
AND WL_SL IS Z
AND Ship_Speed IS LOW
THEN Change_Speed = PB

Appendix H

Membership Functions

H.1 Setting the values of membership functions

Two methods are used to obtain the values of each member :

1. By definition : The values for wave direction with respect to ship is set by using the definition shown in Figure 2.4.

2. Theoretical calculations.

Values of the some membership functions such as WL_SL, WE_2WN and ship speed are found by using simulation programs. These programs were run for different combinations of the membership functions to see their effect on ship behaviour. Then, membership values were obtained from these results to give suggestions if the vessel is in danger. For example, say when WL_SL is 1 m, the vessel capsizes, but when WL_SL is 2 m, vessel does not capsize, then this membership value is set to say 1.5 to accommodate the gray area in between values. Although, the values try to cover most ships, this is impossible for some variables such as ship speed and wave direction. For example, membership values for ship speed depend on maximum ship speed and available power on the ship. Therefore membership values for some variables such as ship speed and wave height have to be changed for series of ship e.g. series 60, UBC series.

Membership	Meaning
HIGH	: High
LOW	: Low
MED	: Medium
NB	: Negative big
NS	: Negative small
PB	: Positive big
PS	: Positive small
VH	: Very high
VL	: Very low
VVH	: Very very high
VVL	: Very very low
Z	: Zero

Membership functions for wave Direction :

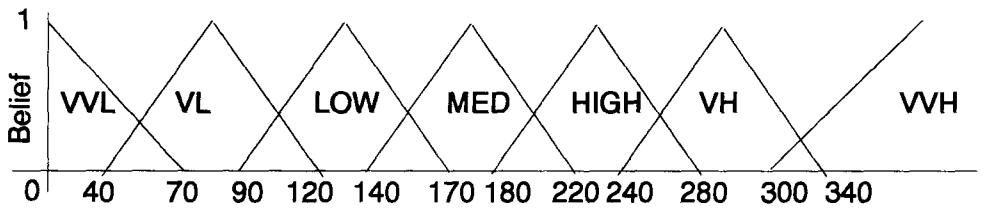

Membership function for wave height :

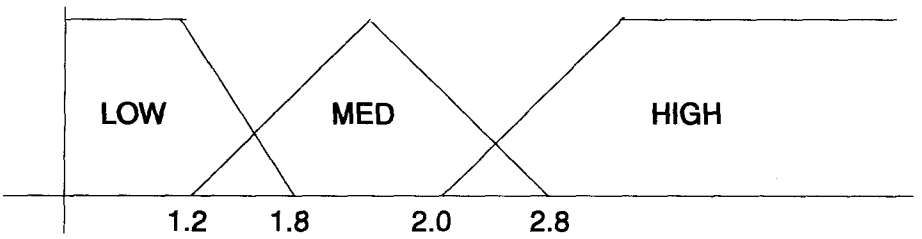

Membership function for Wave speed - Ship speed (WS_SS)

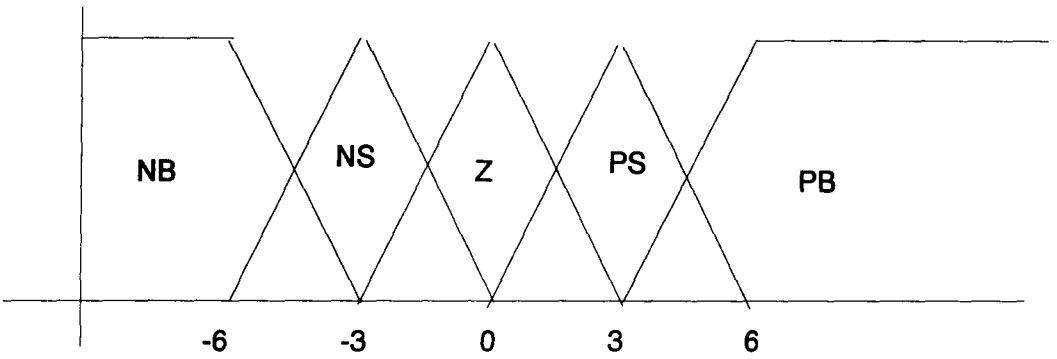

Membership functions for Wave length - Ship length (WL_SL) :

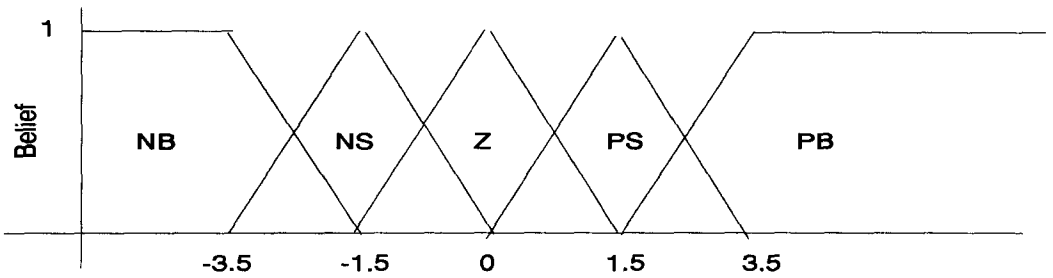

Membership function for Encounter frequency - twice roll natural frequency (WE-2WN) :

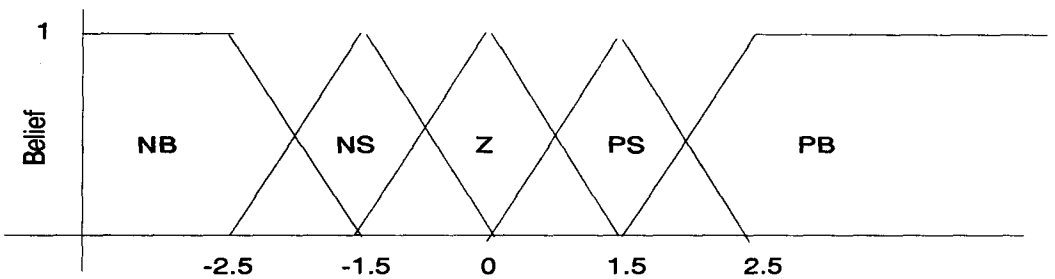

Membership function for Ship speed :

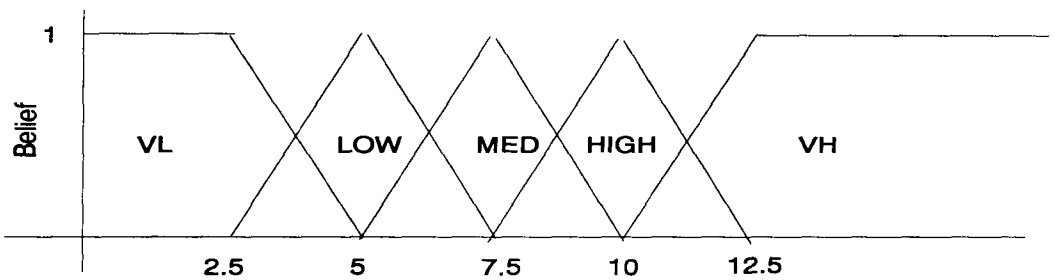

Appendix I

Glossary

Some ship related terminologies :

Baseline Suppose a ship's basic hull shape is placed in an imaginary rectangular box whose bottom and sides just touch the ship's surface. The bottom of the this box may be used as a reference base and is called the baseline.

Block coefficient (C_b) The ratio of the volume of displacement to the volume of rectangular block having a length appropriate to the type of ship and a beam and draft equal to that of the maximum section area.

$$C_B = \frac{\Delta}{LBT} \tag{I.1}$$

Center of Buoyancy The center of bouyancy is the line of action of the resultant of all bouyant forces on the immersed portion of the ship's hull. It passes through the geometric center of the underwater form, at which point, it is called center of bouyancy. The height of the center of bouyancy above the keel is designated KB and determined by

$$\mathrm{KB} = \frac{1}{\Delta}\int A_w z dz \tag{I.2}$$

where A_w is the area of waterplane at height z above the keel.

Designed Waterline (DWL) : Specially designated waterline is the designed waterline (DWL), where the ship is designed to float at a predetermined load (see Figure I

Displacement The weight of the water that the ship displaces when floating freely is called displacement. The symbol Δ is used for displacement.

Drafts The forward and after draft are those vertical distances from the baseline to the waterline of reference measured at the forward and after perpendicular.

Length Between Perpendicular (LBP) ; The length between perpendicular is customarily coincident with the designed waterline (DWL). For the merhant ship practice, the location of the after perpendicular most frequently is coincident with the vertical rudder post (Figure I). In all cases, the forward perpendicular is coincident with the forward extremity of the DWL (Figure I).

List, Heel and Roll Ships are designed to and normally do, float upright. However, because of unsymmetrical loading conditions or other unbalanced forces, they may incline transversely with respect to their normal upright positions. Such transverse inclinations are described as list, heel or roll depending on the nature of the situation. List describes a definite attitude of transverse inclination of a static nature. Heel describes a temporary inclination, generally involving motion, whereas roll involves recurrent inclination from side to side.

The Metacenter (M) The intersection of the vertical through the center of bouyancy of an inclined body or ship with the upright vertical when the angle of inclination approaches zero as a limit.

Metacentric Height (GM) The metacentric height is the vertical distance measured on the vertical centerline between the metacenter and the center of gravity.

Metacentric Radius (BM) The metacentric radius is the distance between the center of bouyancy B and the metacenter M.

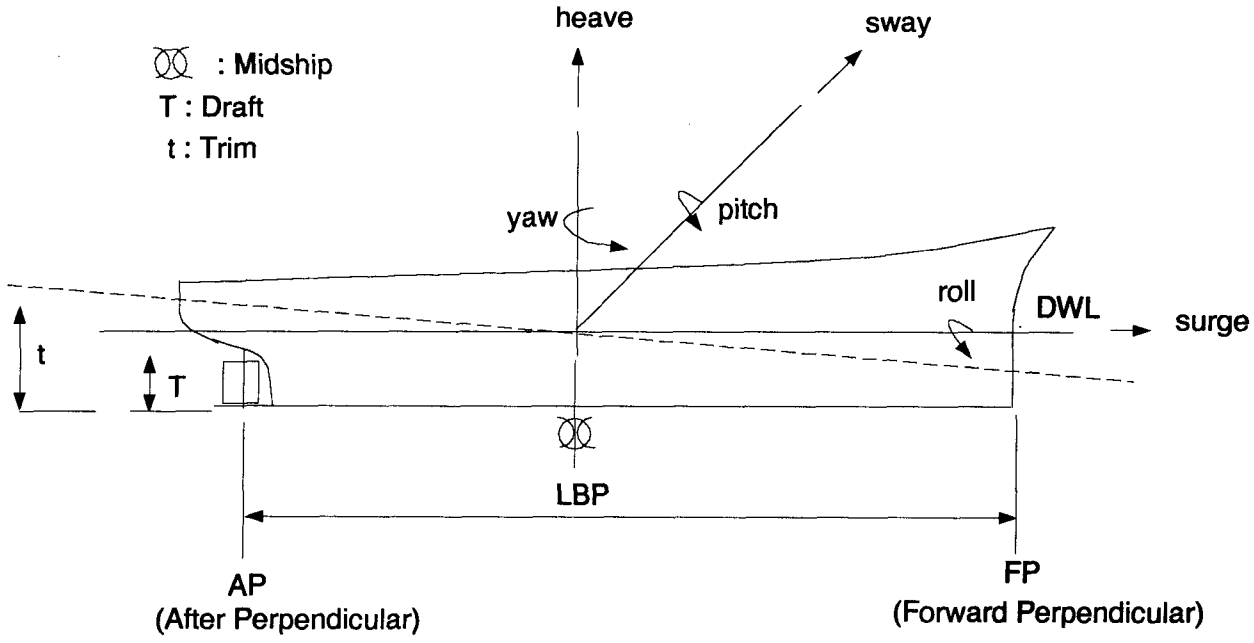

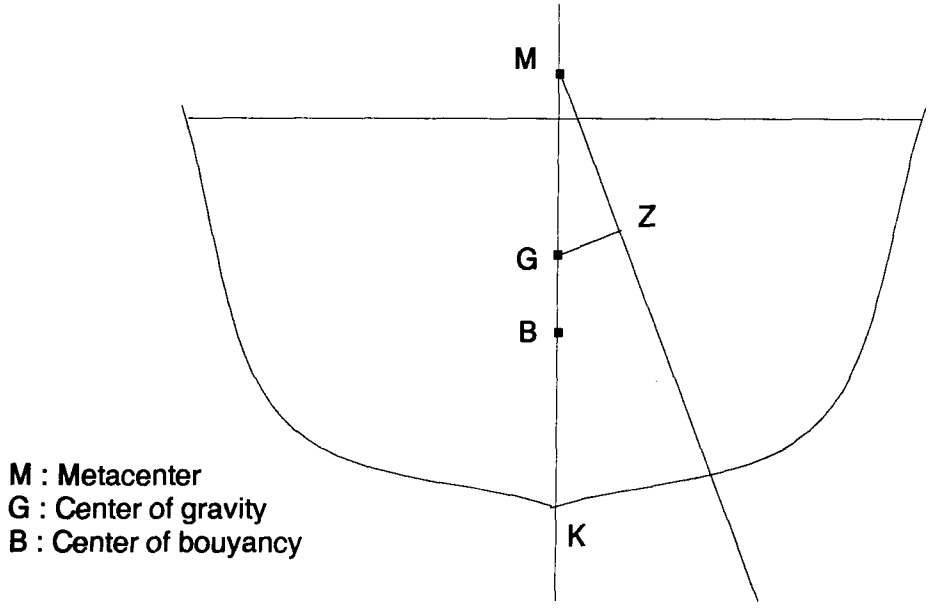

Image processing related terminology:

Bi-modal histogram A characteristic histogram pattern showing that image is pixels partition into two distinct classes.

Convolution : Filtering a data series by integration or summation of data series with a kernel.

Dilation A morphological operation during which an object is incresed in size by the addition of pixels from around its boundary.

Erosion A morphological operation during which an object is decreased in size by the removal of pixels from around its boundary.

Segmentation The division of an image into regions corresponding to objects or parts of objects.

Thinning One technique for retrieving the medial axis of an object based on removing pixels from the object boundary whilst retaining connectivity.

Threshold A pixel value at which a decision is made about the value assigned to the output.